From the Department of Clinical Neuroscience
Karolinska Institutet, Stockholm, Sweden

MRI QUANTIFICATION OF MULTIPLE SCLEROSIS PATHOLOGY

Russell Ouellette

Karolinska Institutet

Stockholm 2021

All previously published papers were reproduced with permission from the publisher.
Published by Karolinska Institutet.
Printed by Universitetsservice US-AB, 2021
© Russell Alexander Ouellette IV, 2021
ISBN 978-91-8016-089-6
Cover illustration: An illustration characterizing the translational efforts of the *in vivo* and *ex vivo* elucidation of multiple sclerosis pathology through MRI quantification.

MRI quantification of multiple sclerosis pathology

THESIS FOR DOCTORAL DEGREE (Ph.D.)

By

Russell Ouellette

The thesis will be defended in public at Lecture hall Erna Möllersalen, Neo Building, Blickagången 16, Karolinska Institutet, Huddinge, on Thursday February 25th, 2021 at 1:00 pm.

Principal Supervisor:
Doctor Tobias Granberg
Karolinska Institutet
Department of Clinical Neuroscience

Co-supervisor(s):
Professor Fredrik Piehl
Karolinska Institutet
Department of Clinical Neuroscience

Professor Maria Kristoffersen Wiberg
Linköping University
Department of Health, Medicine and Caring Sciences
Karolinska Institutet
Department of Clinical Neuroscience

Associate Professor Caterina Mainero
Harvard Medical School,
A.A. Martinos Center for Biomedical Imaging,
Massachusetts General Hospital

Opponent:
Associate Professor Srinivasan Mukundan Jr.
Harvard Medical School
Department of Radiology,
Brigham and Women's Hospital

Examination Board:
Professor Johan Wikström
Uppsala University
Department of Surgical Sciences, Radiology

Professor Pia Maly Sundgren
Lund University
Department of Diagnostic Radiology, Lund

Associate Professor Christina Sjöstrand
Karolinska Institutet
Department of Clinical Neuroscience

"*If I have seen further than others,*
it is only by standing upon the shoulders of giants."

– Sir Isaac Newton (1675, 1643–1727)

To my beloved wife Asia and our amazing daughter Adeline,

for your daily support and unconditional love.

To my inspirational parents Russ and Susan,

for your loving patience in nurturing a hyperactive mediocre boy.

Forever and always.

All that I am, and hope to yet become, is because of you.

ABSTRACT

Background: Multiple sclerosis (MS) is a chronic neuroinflammatory and neurodegenerative disease and a common cause of neurologic disability. MS pathology is characterized by demyelination, neuroaxonal loss and atrophy. Magnetic Resonance Imaging (MRI) is an essential tool in diagnosing and monitoring MS, but its clinical value could be even further expanded by more advanced and quantitative MRI methods, which may also provide additional pathophysiological insights.

Purpose: The overall aim of this thesis was to quantify MS pathology using volumetric brain MRI, ultra-high field brain and cervical spinal cord MRI as well as a newly developed rapid myelin imaging technique in relation to cognitive and physical MS disability.

Study I, a prospective 17-year longitudinal study of 37 MS participants with 23 age/sex-matched healthy controls for comparison at the last follow-up. Longitudinal volumetric brain 1.5 Tesla MRI during the second half of the study showed that lesion accumulation and corpus callosum atrophy were the most strongly associated neuroanatomical correlates of cognitive disability, with the lesion fraction being an independent predictor of cognitive performance 8.5 years later.

Study II, a prospective cross-sectional study of 35 MS participants and 11 age-matched healthy controls using 3 and 7 Tesla MRI. The study demonstrated involvement of both grey and white matter in MS, not only the brain but also the cervical spinal cord, associated with MS disability. Lesions appeared in proximity to the cerebrospinal fluid (CSF), with special predilection to the periventricular and grey matter surrounding the central canal in secondary progressive MS.

Study III, a prospective *in vivo* (71 MS participants and 21 age/sex-matched healthy controls) and *ex vivo* (brain tissue from 3 MS donors) study at 3 Tesla, showed that a new clinically approved and feasible rapid myelin imaging technique correlates well with myelin stainings and produces robust *in vivo* myelin quantification that is related to both current and future cognitive and physical disability in MS.

Study IV, an in-depth topographical analysis based on Study III, mapped the distribution of demyelination, both *in vivo* and *ex vivo*, in the periventricular and perilesional regions of the brain. A gradient of demyelination with predominance near the CSF spaces was seen. Measures of clinical disability were consistently and more strongly associated with the myelin content in normal-appearing tissue compared to the intralesional myelin content.

Conclusions: Lesions and atrophy contribute to cognitive and physical disability in MS but to a varying degree, likely dependent on the relative involvement of white vs. grey matter. Both focal lesions/demyelination as well as diffuse demyelination in normal-appearing white matter shows an apparent gradient from the CSF, which differ between relapsing-remitting and progressive MS subtypes/phases. The growing utility and clinical availability of advanced and quantitative MRI techniques holds promise for improved monitoring of MS pathology and likely represents a vital tool for assessing the efficacy of potential remyelinating/reparative therapies in MS.

SAMMANFATTNING

Bakgrund: Multipel skleros (MS) är en kronisk inflammatorisk sjukdom som drabbar hjärna och ryggmärg. MS är en vanlig orsak till neurologisk funktionsnedsättning och kännetecknas av skador på isoleringen kring nervtrådar, myelin, samt vävnadsförlust. Magnetkamera (MR) har en central roll för att kunna diagnosticera MS samt följa sjukdomsförloppet och behandlingssvaret. Det kliniska värdet av MR skulle dock kunna förbättras ytterligare genom mer avancerade MR-tekniker, vilket också kan leda till ökad förståelse för sjukdomsmekanismerna vid MS.

Syfte: Det övergripande syftet med denna doktorsavhandling var att objektivt mäta omfattningen av vävnadsskador vid MS med nya MR-tekniker (automatiska 3D-volymmätningar, MR med ultrahög fältstyrka och en nyutvecklad MR-teknik som gör det möjligt att mäta halten av myelin i hjärnan) samt ställa dessa nya mätvärden i relation till klinisk funktionsförmåga och utfall.

Studie I, en 17-årsuppföljning av 37 personer med MS samt 23 friska kontrollpersoner. Långtidsuppföljning med 3D-volymmått av hjärnan vid 1,5 Tesla visade att det främst var mängden av MS-plack och vävnadsförlust i hjärnbalken som var kopplat till nedsatt tankeförmåga vid MS och att framtida funktionsnedsättning delvis kunde förutspås av MR.

Studie II, en jämförelse av 35 personer med MS och 11 kontrollpersoner som undersöktes med två MR-kameror av högsta kliniskt tillgängliga fältstyrka (3 och 7 Tesla). Studien påvisade att inte bara den vita substansen (där det finns mycket nervtrådar och myelin), utan även den gråa substansen (där nervcellskropparna finns) drabbas vid MS, såväl i hjärnan som i ryggmärgen. MS-skadorna uppstår främst i områden som står i nära kontakt med ryggmärgsvätskan.

Studie III, en studie av 71 personer med MS och 21 kontrollpersoner samt hjärnvävnad från 3 donatorer som avlidit med MS, utförd med 3 Tesla MR. Studien visade att en nyutvecklad kliniskt godkänd MR-teknik för att mäta myelinhalten i hjärnan har god överensstämmelse med mätning av myelinhalten med mikroskopi. Tekniken är robust, relativt snabb och ger mätvärden som är kopplade till både nuvarande och framtida funktionsnedsättningar vid MS.

Studie IV, utgör en mer fördjupad analys där den nya MR-tekniken i Studie III, som har en tydligare känslighet för just myelin, användes för att bekräfta fynden från Studie II; nämligen att MS-skadorna är mer utbredda i områden i hjärnan nära ryggmärgsvätskan. Dessutom påvisade tekniken utbredd förlust av myelin i områden av hjärnan som såg frisk ut på vanlig MR och att myelinhalten var starkare kopplade till funktionsnedsättning än vanliga 3D-volymmått.

Slutsatser: MS-skador till följd av inflammationshärdar och vävnadsförlust bidrar i varierande grad till funktionsnedsättning beroende på det relativa engagemanget av den vita/gråa substansen i hjärnan och ryggmärgen. MS-skadorna är mest utbredda i områden nära ryggmärgsvätska. Nya avancerade MR-tekniker möjliggör förbättrad kartläggning av MS-skador och kommer sannolikt vara ett viktigt verktyg för utvärdering av nya behandlingar som syftar till att stimulera läkning av skadad vävnad vid MS.

LIST OF SCIENTIFIC PAPERS

This thesis is primarily composed of the following four papers, which will be referred to in the text by their corresponding roman numerals.

I. **Lesion accumulation is predictive of long-term cognitive decline in multiple sclerosis**

Ouellette R, Bergendal Å, Shams S, Juha Martola J, Mainero C, Kristoffersen Wiberg M, Fredrikson S, and Granberg T.

Multiple Sclerosis and Related Disorders. 2018;21:110-116. doi: 10.1016/j.msard.2018.03.002.

II. **7 T imaging reveals a gradient in spinal cord lesion distribution in multiple sclerosis**

Ouellette R, Treaba CA, Granberg T, Herranz E, Barletta V, Mehndiratta A, De Leener B, Tauhid S, Yousuf F, Dupont SM, Klawiter EC, Sloane JA, Bakshi R, Cohen-Adad J, Mainero C.

Brain. 2020;143(10):2973-2987. doi: 10.1093/brain/awaa249

III. **Validation of rapid magnetic resonance myelin imaging in multiple sclerosis**

Ouellette R, Mangeat G, Polyak I, Warntjes M, Forslin Y, Bergendal Å, Plattén M, Uppman M, Treaba CA, Cohen-Adad J, Piehl F, Kristoffersen Wiberg M, Fredrikson S, Mainero C, Granberg T.

Annals of Neurology. 2020;87(5):710-724. doi: 10.1002/ana.25705.

IV. **Multiple sclerosis demyelination beyond lesions: an *in vivo* and *ex vivo* study**

Ouellette R, Mangeat G, Plattén M, Forslin Y, Bergendal Å, Andrada Treaba C, Barletta V, Warntjes M, Cohen-Adad J, Fredrikson S, Kristoffersen Wiberg M, Piehl F, Mainero C, and Granberg T.

In Manuscript.

LIST OF RELATED WORKS

This thesis has been influenced by other related studies that have impacted the student's scientific development, in particular the following publications that the student contributed to.

Neuroinflammatory component of gray matter pathology in multiple sclerosis

Herranz E, Giannì C, Louapre C, Treaba CA, Govindarajan ST, **Ouellette R**, Loggia ML, Sloane JA, Madigan N, Izquierdo-Garcia D, Ward N, Mangeat G, Granberg T, Klawiter EC, Catana C, Hooker JM, Taylor N, Ionete C, Kinkel RP, Mainero C.

Annals of Neurology. 2016;80(5):776-790. doi: 10.1002/ana.24791.

***In vivo* characterization of cortical and white matter neuroaxonal pathology in early multiple sclerosis**

Granberg T, Fan Q, Treaba CA, **Ouellette R**, Herranz E, Mangeat G, Louapre C, Cohen-Adad J, Klawiter EC, Sloane JA, Mainero C.

Brain. 2017;140(11):2912-2926. doi: 10.1093/brain/awx247.

Spatial distribution of multiple sclerosis lesions in the cervical spinal cord

Eden D, Gros C, Badji A, Dupont SM, De Leener B, Maranzano J, Zhuoquiong R, Liu Y, Granberg T, **Ouellette R**, Stawiarz L, Hillert J, Talbott J, Bannier E, Kerbrat A, Edan G, Labauge P, Callot V, Pelletier J, Audoin B, Rasoanandrianina H, Brisset JC, Valsasina P, Rocca MA, Filippi M, Bakshi R, Tauhid S, Prados F, Yiannakas M, Kearney H, Ciccarelli O, Smith SA, Andrada Treaba C, Mainero C, Lefeuvre J, Reich DS, Nair G, Shepherd TM, Charlson E, Tachibana Y, Hori M, Kamiya K, Chougar L, Narayanan S, Cohen-Adad J.

Brain. 2019;142(3):633-646. doi: 10.1093/brain/awy352.

Multiple sclerosis lesions in motor tracts from brain to cervical cord: spatial distribution and correlation with disability

Kerbrat A, Gros C, Badji A, Bannier E, Galassi F, Combès B, Chouteau R, Labauge P, Ayrignac X, Carra-Dalliere C, Maranzano J, Granberg T, **Ouellette R**, Stawiarz L, Hillert J, Talbott J, Tachibana Y, Hori M, Kamiya K, Chougar L, Lefeuvre J, Reich DS, Nair G, Valsasina P, Rocca MA, Filippi M, Chu R, Bakshi R, Callot V, Pelletier J, Audoin B, Maarouf A, Collongues N, De Seze J, Edan G, Cohen-Adad J.

Brain. 2020;143(7):2089-2105. doi: 10.1093/brain/awaa162.

Longitudinal characterization of cortical lesion development and evolution in multiple sclerosis with 7.0-T MRI

Treaba CA, Granberg T, Sormani MP, Herranz E, **Ouellette R**, Louapre C, Sloane JA, Kinkel RP, Mainero C.

Radiology. 2019;291(3):740-749. doi: 10.1148/radiol.2019181719.

Automatic segmentation of the spinal cord and intramedullary multiple sclerosis lesions with convolutional neural networks

Gros C, De Leener B, Badji A, Maranzano J, Eden D, Dupont SM, Talbott J, Zhuoquiong R, Liu Y, Granberg T, **Ouellette R**, Tachibana Y, Hori M, Kamiya K, Chougar L, Stawiarz L, Hillert J, Bannier E, Kerbrat A, Edan G, Labauge P, Callot V, Pelletier J, Audoin B, Rasoanandrianina H, Brisset JC, Valsasina P, Rocca MA, Filippi M, Bakshi R, Tauhid S, Prados F, Yiannakas M, Kearney H, Ciccarelli O, Smith S, Treaba CA, Mainero C, Lefeuvre J, Reich DS, Nair G, Auclair V, McLaren DG, Martin AR, Fehlings MG, Vahdat S, Khatibi A, Doyon J, Shepherd T, Charlson E, Narayanan S, Cohen-Adad J.

Neuroimage. 2019;184:901-915. doi: 10.1016/j.neuroimage.2018.09.081.

Changes in structural network are associated with cortical demyelination in early multiple sclerosis

Mangeat G, Badji A, **Ouellette R**, Treaba CA, Herranz E, Granberg T, Louapre C, Stikov N, Sloane JA, Bellec P, Mainero C, Cohen-Adad J.

Human Brain Mapping. 2018;39(5):2133-2146. doi: 10.1002/hbm.23993.

Evidence of diffuse cerebellar neuroinflammation in multiple sclerosis by ^{11}C-PBR28 MR-PET

Barletta VT, Herranz E, Treaba CA, **Ouellette R**, Mehndiratta A, Loggia ML, Klawiter EC, Ionete C, Jacob SA, Mainero C.

Multiple Sclerosis Journal. 2020;26(6):668-678. doi: 10.1177/1352458519843048.

Profiles of cortical inflammation in multiple sclerosis by ^{11}C-PBR28 MR-PET and 7 tesla imaging

Herranz E, Louapre C, Treaba CA, Govindarajan ST, **Ouellette R**, Mangeat G, Loggia ML, Cohen-Adad J, Klawiter EC, Sloane JA, Mainero C.

Multiple Sclerosis Journal. 2020;26(12):1497-1509. doi: 10.1177/1352458519867320.

Evidence of early microstructural white matter abnormalities in multiple sclerosis from multi-shell diffusion MRI

De Santis S, Granberg T, **Ouellette R**, Treaba CA, Herranz E, Fan Q, Mainero C, Toschi N.

Neuroimage Clinical. 2019;22:101699. doi: 10.1016/j.nicl.2019.101699.

MRI-based manual versus automated corpus callosum volumetric measurements in multiple sclerosis

Platten M, Martola J, Fink K, **Ouellette R**, Piehl F, Granberg T.

Journal of Neuroimaging. 2020;30(2):198-204. doi: 10.1111/jon.12676.

Evidence for progressive microstructural damage in early multiple sclerosis by multi-shell diffusion magnetic resonance imaging

Toschi N, De Santis S, Granberg T, **Ouellette R**, Treaba CA, Herranz E, Mainero C.

Neuroscience. 2019;403:27-34. doi: 10.1016/j.neuroscience.2019.01.022.

Characterization of thalamic lesions and their correlates in multiple sclerosis by ultra-high-field MRI

Mehndiratta A, Treaba CA, Barletta V, Herranz E, **Ouellette R**, Sloane JA, Klawiter EC, Kinkel RP, Mainero C.

Multiple Sclerosis Journal. 2020;25:1352458520932804. doi: 10.1177/1352458520932804.

Nervous system involvement in COVID-19: results from a retrospective consecutive neuroimaging cohort

Klironomos S, Tzortzakakis A, Kits A, Öhberg C, Kollia E, Ahoromazdae A, Almqvist H, Aspelin Å, Martin H, **Ouellette R**, Al-Saadi J, Hasselberg M, Haghgou M, Pedersen M, Petersson S, Finnsson J, Lundberg J, Falk Delgado A, Granberg T.

Radiology. 2020;30:202791. doi: 10.1148/radiol.2020202791.

Neurological manifestations of coronavirus infections - a systematic review

Almqvist J, Granberg T, Tzortzakakis A, Klironomos S, Kollia E, Öhberg C, Martin R, Piehl F, **Ouellette R**, Ineichen BV.

Annals of Clinical Translational Neurology. 2020;7(10):2057-2071.
doi: 10.1002/acn3.51166.

Deep learning corpus callosum segmentation as a neurodegenerative marker in multiple sclerosis

Platten M, Brusini I, Andersson O, **Ouellette R**, Piehl F, Wang C, Granberg T.

Journal of Neuroimaging. Accepted on January 14th, 2021. doi: 10.1111/jon.12838

CONTENTS

LIST OF ABBREVIATIONS

2D	Two-dimensional
3D	Three-dimensional
CHARMED	Composite hindered and restricted model of diffusion
CIS	Clinically isolated syndrome
CNS	Central nervous system
CoV	Coefficient of variance
COVID-19	Coronavirus disease 2019
CSF	Cerebrospinal fluid
DIS	Dissemination in space
DIT	Dissemination in time
DMT	Disease-modulatory therapy
EDSS	Expanded disability status scale
EQ-5D	EuroQol-5D
FAS	F-A-S verbal fluency test
FLAIR	Fluid attenuated inversion recovery
FSL	FMRI software library
HLA	Human leukocyte antigen
LST	Lesion segmentation toolbox
MHC	Major histocompatibility complex
MPRAGE	Magnetization-prepared rapid acquisition gradient echo
MRI	Magnetic resonance imaging
MS	Multiple sclerosis
MSIS	Multiple sclerosis impact scale
MTR	Magnetization transfer ratio
MWF	Myelin water fraction
NAGM	Normal-appearing grey matter
NAWM	Normal-appearing white matter
NODDI	Neurite orientation dispersion and density imaging
PET	Positron emission tomography
PMS	Progressive multiple sclerosis
PPMS	Primary progressive multiple sclerosis
REMyDI	Rapid estimation of myelin for diagnostic imaging
RIS	Radiologically isolated syndrome
RAVLT	Rey auditory verbal learning test
ROCFT	Rey–osterrieth complex figure test
RRMS	Relapsing–remitting multiple sclerosis
SCT	Spinal cord toolbox
SDMT	Symbol digit modalities test
SPMS	Secondary progressive multiple sclerosis
T	Tesla
QSM	Quantitative susceptibility mapping
SPM	Statistical parametric mapping

1. INTRODUCTION

1.1 MULTIPLE SCLEROSIS

1.1.1 Overview and historical background

Multiple sclerosis (MS) is a chronic and progressive inflammatory, demyelinating, and degenerative autoimmune disease of the brain and spinal cord (Filippi *et al.*, 2018; Reich *et al.*, 2018; Rovira and Barkhof, 2018). MS is the leading cause of non-traumatic neurological disability in young adults aged 30-40 years (Dutta and Trapp, 2011; Ahlgren *et al.*, 2014). Approximately 2.5 million people worldwide suffer from MS, with the largest prevalence in North America and Europe (Rovira and Barkhof, 2018). The etiology of MS remains uncertain; however, studies indicate the importance of genetic, lifestyle and environmental risks, highlighted in the observation of twice as many women diagnosed with MS as compared to men (Figure 1, Olsson *et al.*, 2017; Rovira and Barkhof, 2018). MS is the cause of a significant loss of health-related quality of life for those diagnosed, particularly in those in the more advanced disease stages (Rovira and Barkhof, 2018). Moreover, there is a substantial economic burden due to MS, with an associated annual estimated cost in Sweden of €600 million (Berg *et al.*, 2006). Notably, there currently is no verified cure for MS, nor do any of the current disease-modifying treatments fully arrest disease activity (Reich *et al.*, 2018).

Clinically, MS is classified into three subtypes: relapsing-remitting (RRMS), secondary progressive (SPMS) and primary progressive (PPMS) (Lublin *et al.*, 2014), with RRMS being the most prevalent at diagnosis of approximately 85-90% (Brownlee *et al.*, 2017). Since MS can affect any part of the central nervous system (CNS), there is a wide range of clinical presentations with a variety of affected neurological functions; these include vision, sensation, mobility, balance, sphincter, and cognition (Kister *et al.*, 2013). Over time and with increasing disease duration, more progressive physical and cognitive dysfunction will typically become evident (Rovira and Barkhof, 2018).

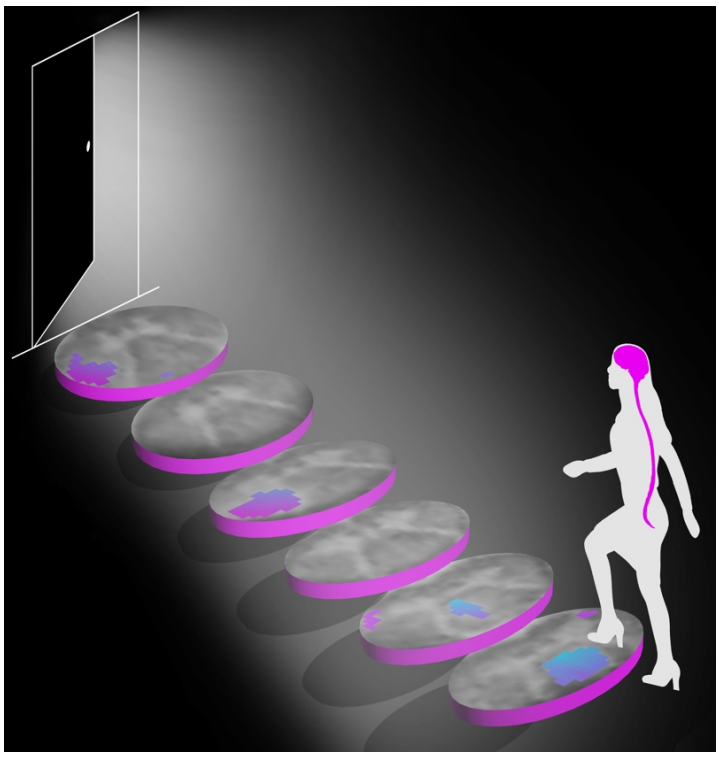

Figure 1. The climb.
A representation the daily challenges that those affected by MS must overcome and the pursuit of the research community in broadening our understanding of MS to better raise all those affected by the disease.

The diagnosis of MS is based on the presence of clinical symptoms, MRI findings and analysis of the cerebrospinal fluid according to the McDonald criteria, which have been revised based on scientific findings, most recently as of 2017, as illustrated in Figure 2 and Table 1 (Thompson *et al.*, 2018). The fundamental element of the MS diagnosis is demonstrating an inflammatory attack in the CNS in at least two different locations (Dissemination In Space, DIS) at two different periods of time (Dissemination In Time, DIT) (Table 1, Thompson *et al.*, 2018). While it was previously necessary for a patient to be affected by two clinical relapses to be diagnosed with RRMS, MRI provides the means to substitute DIS and DIT without waiting for another clinical inflammatory attack. This ability to provide an early and accurate diagnosis with appropriate initiation of treatment has been shown to be essential for the patient since it slows the progression of cognitive and physical disability (Giovannoni *et al.*, 2015).

Up until the 1990s, there was no effective disease-modifying therapy for MS. Today, there are several increasingly effective treatments, including modulators of inflammatory mediators, immune cell migration inhibitors, cell depleting or induction therapies, immunomodulators with intracellular mechanisms of action, tolerization therapies, regenerative and neuroprotective strategies. However, due to the emphasis of therapies addressing the inflammatory component of the disease, the treatment options for those in the progressive phase of the disease remain minimal with limited success and require further attention moving forward. More therapies are undergoing clinical trials, and of particular interest are those that may enhance the remyelinating potential of axons.

1.1.2 Genetic, lifestyle and environmental risk factors

The risk of developing MS is a complex balance between genetic, lifestyle and environmental interaction (Olsson *et al.*, 2017). The convoluted relationship of these multifactorial interactions is most well evidenced by the clinical heterogeneity observed across those who develop MS (Piehl, 2021). The factors affecting disease severity and prognosis at diagnosis remain undetermined, nevertheless, progress is ongoing by large-scale multi-center consortium studies with diverse cohorts (IMSGC, 2019).

Genetic factors: The genetic predisposition in developing MS is classically exemplified through familial studies, where the heritability for MS was estimated to be 64% and the likelihood of developing MS was approximately 7-times greater for those with a sibling with MS, as compared to the general population of Sweden (Westerlind *et al.*, 2014). The more clearly defined linkage between genes and modifying risk factors for developing MS are the relationships found within the major histocompatibility complex (MHC) molecule (the human leukocyte antigen [HLA] in animals). Located on the surface of nucleated cells, the major histocompatibility complex presents endogenous and exogenous antigens found within the cell to passing screening T-lymphocytes (Esiri and Gay, 1990; IMSGC, 2019). The genetic variants coding for products comprising the molecular machinery of the MHC have varying degrees of affecting one's likelihood for the development MS. For example, The HLA class I HLA-A*02:01 is associated with protection against developing MS, whereas HLA class II HLA-

DRB1*15:01 increases one's likelihood of developing the disease (Olsson *et al.*, 2017). A large-scale extensive effort to extract MS heritability via a genome-wide association study of 47,429 MS participants and 68,374 control participants found that genome-wide and suggestive effects contribute to 48% of the MS heritability (IMSGC, 2019). Genome-wide mapping also indicated microglia, several peripheral immune pathways and an *X*-linked locus (IMSGC, 2019).

Lifestyle factors: One of the more commonly associated lifestyle-risk contributors to the development of MS, and many other diseases, is smoking (Olsson *et al.*, 2017). This is believed to be compounded by a genetic-lifestyle interaction with the HLA MS risk variants (Hedström *et al.*, 2011*c*). Adolescence has been implicated as a critical time for heightened risk in developing MS, particularly concerning obesity and night shift work (Olsson *et al.*, 2017). An increased likelihood for women developing MS was associated with obesity early in life, independent of one's body mass index at the time of diagnosis (Munger *et al.*, 2013). Shift work, working throughout the evening and night, has also been associated with an increase in developing MS, not only in adolescence (before age 20) but to a lesser degree later in life (Hedström *et al.*, 2011*a*, 2015). The observed greater proportion of women diagnosed with MS, while classically defined chromosomally, has been increasing at a rate that remains unexplained by changing population gender ratios alone (Koch-Henriksen and Sørensen, 2010; Westerlind *et al.*, 2014). Therefore, the interactions between lifestyle and environmental factors with chromosomal sex, including the *X*-linked loci indicated in the genome-wide mapping study, should be further researched (Olsson *et al.*, 2017; IMSGC, 2019).

Environmental factors: Environmental exposure to various viruses, organic solvents, and living in a higher latitude has been associated with a higher risk of developing MS (Olsson *et al.*, 2017). Even passive exposure to smoking is related to an increased likelihood of developing MS (Hedström *et al.*, 2011*b*). This is potentially due to the increased role of immune-surveillance within the respiratory system, and additionally emphasized by organic solvent exposure that may potentially also act through lung irritation (Barragán-Martínez *et al.*, 2012). There is a long-standing observation of a latitude-dependent gradient of incidence and prevalence of MS, whereby a positive association has been observed with ascending latitude within Europe, that persists even when accounting for known genetic contributing factors (HLA-DRB1) (Simpson *et al.*, 2011). These meta-analysis findings are suggestive of ultraviolet radiation or active vitamin D levels playing an important role in the development of MS. Interestingly, studies of half-siblings, adoptees, and step-siblings observed no micro-environmental effect on the development of MS, suggesting that these environmental factors act more so at the macroscopic and population-level than individually (O'Gorman *et al.*, 2012). Viral exposure has also been linked to the development of MS, this theory is known as virus-induced autoimmunity in the brain (Mentis *et al.*, 2017).

1.1.3 Etiology and pathophysiology

The pathophysiology of MS has been theorized from the first observations of the disease. The predilection of early-onset lesion manifestation and expansion into the periventricular region of the brain led to the proposal of a causative disease agent or agents infiltrating the CNS via the CSF (Marburg, 1906; Dawson, 1916; Fog, 1965; Lumsden, 1970). An alternative mechanism, emphasizing perivenous lesion formation, was proposed after immune cell infiltrates in the parenchyma were identified to be of a subependymal perivenular origin (Adams *et al.*, 1987). More recent neuropathological findings, however, suggest that these two outside-in mechanisms may not be mutually exclusive, but instead represent two concurrent spatio-temporal immunological processes that work in concert with each other at differentially evolving relative rates throughout the disease course (Figure 3, Calabrese *et al.*, 2015; Lassmann, 2019).

MS pathology is most notably distinguished by lesions, representing focal demyelination that develop around a post-capillary central vein (NAIMS *et al.*, 2016). This process is related to blood-brain barrier disruption, whereby the upregulated integrins on the surface of lymphocytes recognize the adhesion molecules on the blood vessels' endothelial surface and interact to facilitate extravasation into the parenchyma (Rovira and Barkhof, 2018; Piehl, 2021). An additional site of lymphocytic penetration into the brain is the choroid plexus' fenestrated epithelium mediated blood-CSF barrier (Vercellino *et al.*, 2008). Much of our pathomechanistic understanding of MS is based on artificial biological models mimicking MS, most notably experimental autoimmune encephalitis (EAE), where an MS-like inflammatory response is induced by triggering immune-mediated demyelination in species, such as mice, rats, or even marmosets, to observe and catalog the pathological immune cascade (Lassmann and Bradl, 2017; Reich *et al.*, 2018). This type of analysis has most evidently implicated the role of T-cells in driving the inflammatory demyelination, specifically helper $CD4^+$ and cytotoxic $CD8^+$ T-cells (Reich *et al.*, 2018). However, it should be noted that comparable proportions of myelin reactive T-cells have also been observed in those without MS, suggesting dysfunction beyond myelin targeting or additional factors yet to be understood (Reich *et al.*, 2018). Importantly, B-cells have been observed to play a significant role in the pathophysiology of MS, but also in other autoimmune diseases such as systemic lupus erythematosus, rheumatoid arthritis and type-1 diabetes mellitus. However, MS stands out from these diseases, in that the dysregulation of autoreactive B-cells occurs only in the peripheral lymphoid organs instead of centrally in the bone marrow, possibly a consequence of regulatory T-cell dysfunction (Li and Bar-Or, 2019). The most substantial indicator of the importance of B-cells is the success of B-cell depleting therapies (Piehl, 2021), particularly the amount of therapies targeting memory B-cells (Ineichen *et al.*, 2020). Myeloid lineage cells, macrophages and microglia have been linked to the oxidative damage of both myelin and axons (Mahad *et al.*, 2015). The chronic oxidative stress environment in MS is highly destructive to the delicate balance of mitochondrial functioning, including, energy production, increased production of reactive oxygen species, and dysregulated calcium ion buffering, which all have been observed in demyelinated axons (Mahad *et al.*, 2015).

The plausible viral pathophysiology of MS, also referenced as viral-induced autoimmunity, has been indicated by linking exposure to numerous viruses. Some of the most notable of these viral candidates include species from the Herpesviridae family, where especially the Epstein-Barr virus (human herpesvirus-4, EBV) has been suggested to play a central role in triggering the disease (Ascherio *et al.*, 2001). However, also other herpes viruses, such as human herpesvirus-6 (HHV-6) (Challoner *et al.*, 1995), cytomegalovirus (human herpesvirus-5) and varicella-zoster virus (human herpesvirus-3, VZV), as well as non-herpes viruses e.g., human endogenous retroviruses (HERV), measles and influenza have been implicated (Mentis *et al.*, 2017). However, the specific mechanism by which a virus may potentially cause MS is less clear and requires further study. The more commonly known mechanism of viral-mediated autoimmunity is molecular mimicry, whereby the immune cells mistakenly identify self-cells' myelin proteins as those of endogenous viral proteins (Mentis *et al.*, 2017). While our understanding of viruses and the role they play in autoimmunity has substantially developed, the specific role viruses play in the pathophysiology of MS remains imprecise (Mentis *et al.*, 2017). Additionally, the recent findings of inflammatory neurologic manifestations of the current coronavirus disease 2019, COVID-19, pandemic necessitates the demand for further understanding of viral-induced autoimmunity (Klironomos *et al.*, 2020), particularly considering coronaviruses have been linked with autoimmune diseases (Almqvist *et al.*, 2020).

1.1.4 Diagnosis

The diagnosis of MS is difficult due to the variable clinical presentation. Thus, there have been numerous concerted efforts to identify the signs and characteristics unique to MS. One of the earlier more established efforts to coordinate MS diagnosis was by Schumacher from 1965-1983 (Schumacher *et al.*, 1965), followed by Poser that was applied from 1983-2001 (Poser *et al.*, 1983) and finally McDonald from 2001-present (McDonald *et al.*, 2001) with revisions in 2005 (Polman *et al.*, 2005), 2010 (Polman *et al.*, 2011), and 2017 (Thompson *et al.*, 2018). Through increased understanding of the disease, these various diagnostic criteria been refined and resulted in decreasing the average time to diagnosis, as demonstrated here, in Figure 2.

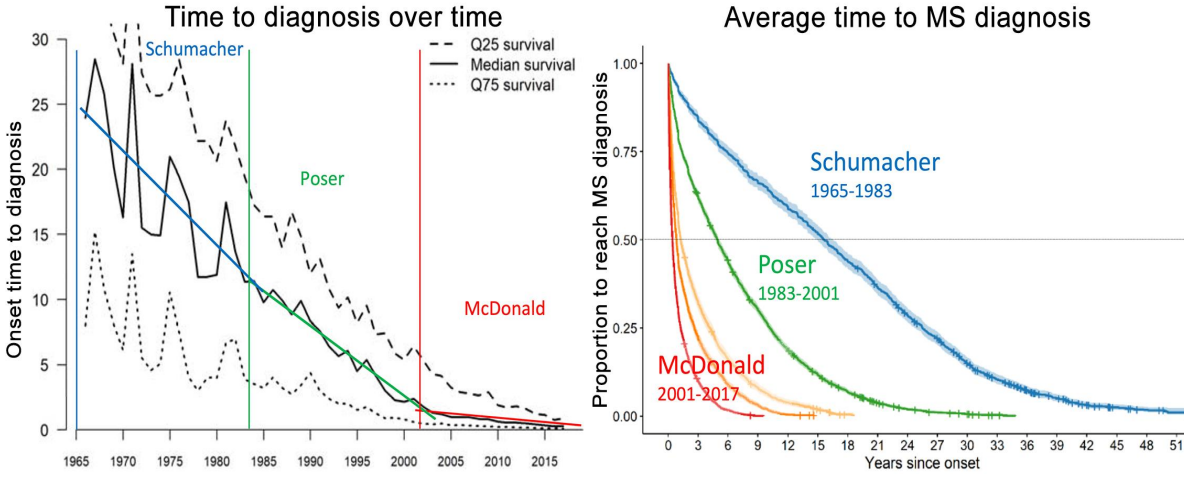

Figure 2. The decreasing time to MS diagnosis in Sweden. *Indicated by the three latest major MS diagnostic criteria (Schumacher, Poser, McDonald). Image courtesy of Leszek Stawiarz at the Swedish NEURO Registries and presented as the best Epidemiological Work at ECTRIMS 2019, Stockholm.*

However, the diagnosis of MS for the past two decades has been centered around the McDonald criteria and emphasized the role of MRI in the diagnosis of MS (McDonald *et al.*, 2001). The focus of the MS diagnosis is to demonstrate the dissemination of lesions in both time and space (DIT and DIS, respectively). The dissemination references that MS is a dynamic disorder that evolves not only over time but throughout the regions brain and spinal cord. The integration of MRI into the diagnostic criteria as a paraclinical tool alongside clinical observations has greatly increased the sensitivity and specificity of MS diagnosis and facilitated the differential diagnosis of mimicking disorders (Bakshi *et al.*, 2008; Thompson *et al.*, 2018). The diagnostic criteria for MS and the basis of DIT and DIS, as of the latest revision from 2017, are depicted here in Table 1 (Thompson *et al.*, 2018).

Clinical presentation	**Diagnosis and supportive paraclinical evidence**
2+ relapses, 2 different regions	**MS diagnosis** DIT and DIS demonstrated clinically. No additional paraclinical evidence is necessary but MRI should be performed as a baseline scan and to rule out potential mimics.
2+ relapses, 1 region	**DIS needed for MS diagnosis** Another clinical relapse implicating a different CNS region or MRI DIS*.
1 relapse, 2 regions	**Clinically Isolated Syndrome, DIT needed for MS diagnosis** Second clinical relapse **or** MRI DIT** or CSF oligoclonal bands
Only incidental MRI findings	**Radiologically Isolated Syndrome** DIS and DIT can be radiologically determined but a clinical relapse is still necessary for MS diagnosis

Table 1. *Simplified diagnostic criteria to highlight the role of paraclinical evidence to demonstrate Dissemination in Space (DIS) and Time (DIT), adapted from the 2017 McDonald criteria revisions (Thompson et al., 2018).*
**Lesions in 2+ regions (periventricular, cortical/juxtacortical, infratentorial, spinal).*
** Simultaneous contrast-enhancing and non-enhancing lesion(s) or new/enlarged lesion(s) on follow-up.

1.1.5 Clinical manifestations and subtype

MS clinical course: There are three traditionally recognized clinical phenotypes in MS, referred to as RRMS, SPMS, and PPMS (Thompson *et al.*, 2018). The RRMS stage represents the most common presentation of MS at diagnosis and is characterized by restricted episodes of worsening termed relapses. These may also be referred to as 'attacks', 'flare-ups' or 'exacerbations' ('skov' in Swedish) and are defined by sudden onset of new or worsening of existing neurologic deficits lasting >24 hours. In most cases symptoms of a relapse evolve over hours and days, followed by a variable degree of restoration of functioning. After some years or several decades, the RRMS stage is followed by a phase of relentless progression of symptoms, termed SPMS (Figure 3). The conversion of RRMS to SPMS is typically gradual and difficult to pinpoint exactly in time, emphasized here in Figure 3 that illustrates such a disease course. In a minority, roughly 10-15%, MS presents as a progressive disease from onset, PPMS, which typically begins later in life compared RRMS and at a comparable age to that of the RRMS to SPMS conversion phase (Reich *et al.*, 2018; Rovira and Barkhof, 2018).

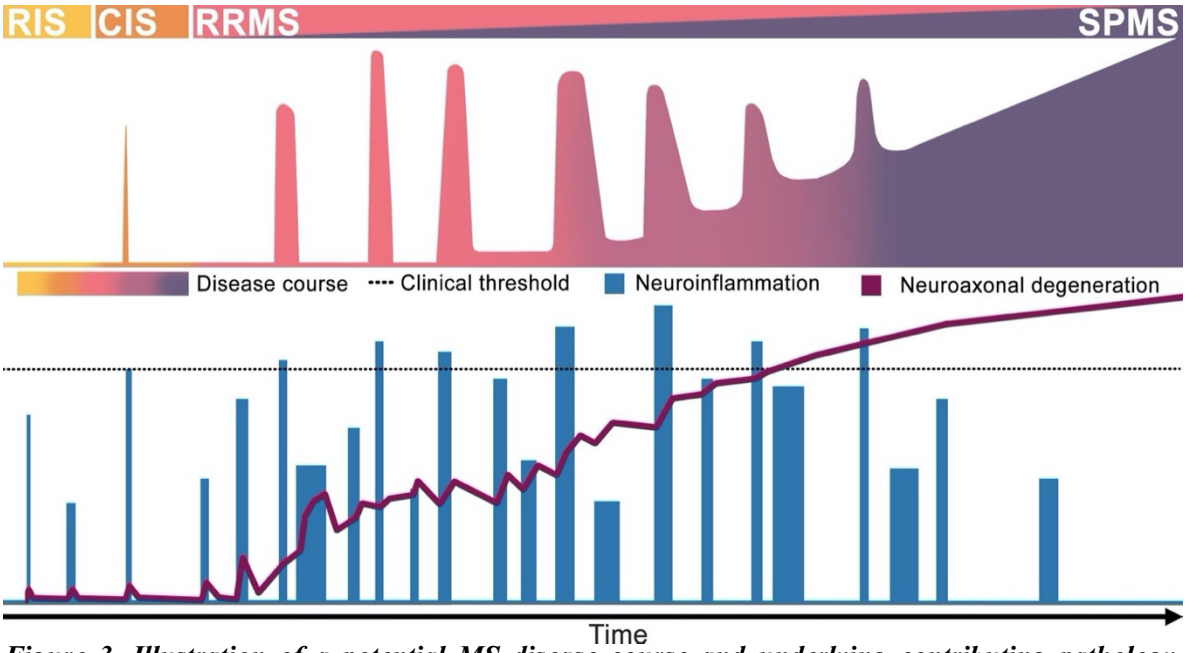

Figure 3. Illustration of a potential MS disease course and underlying contributing pathology. *As the disease progresses, potentially beginning with the stages of radiologically and clinically isolated syndromes preceding clinically definite MS, further developing into the RRMS phase with overt relapses and inflammatory activity, the neurodegenerative aspect becomes more evident in the SPMS. Note, patients may enter the disease course in the progressive phase (PPMS).*

More recently two disease stages preceding a formal diagnosis of MS have been described; clinically isolated syndrome (CIS) and radiologically isolated syndrome (RIS) (Lublin *et al.*, 2014). CIS is defined by a single bout or relapse, but without enough clinical or paraclinical evidence that is in support of the two cornerstones of MS diagnosis (see further below) (Thompson *et al.*, 2018). RIS refers to incidental MRI findings fulfilling radiological criteria for MS, however, in the absence of any corresponding clinical manifestation. This is, typically, a consequence of MRI being acquired for another indication or atypical/unspecific symptoms, most commonly headache (Granberg *et al.*, 2013).

The RRMS and SPMS stages of the disease are often considered to be distinct temporal phases with their own related characteristic pathologies and a slow transition of separation. However, there is increasing evidence that these processes are not as temporally distinct as previously thought, but rather that the disease mechanisms share considerable overlap and evolve at different relative rates (Lassmann, 2019). The RRMS subtype is most commonly associated with neuroinflammatory events in the CNS, particularly blood-brain permeability resulting in contrast enhancing lesions and active lesion development. Whereas SPMS has a prominent neurodegenerative component, including neuroaxonal degeneration resulting in atrophy of the brain and spinal cord regions. It has long been held that disability in the RRMS phase is driven mainly by the accumulation of lesions that, depending on location, will produce variable degrees of neurological dysfunction, leading to a stepwise worsening of clinical disability (Compston and Coles, 2008). In contrast, during the progressive stages of MS, worsening disability becomes more continuous as a result of chronic inflammation and neurodegeneration. However, there have been recent observations calling for a revision of this long-held perspective. One such example is a significant proportion of clinical disability worsening during the relapsing stage of MS left unexplained by relapses. Observed in a recent study of data from the phase III OPERA trials, approximately 80-90% of confirmed disability worsening occurred in the absence of recorded relapses (Kappos *et al.*, 2020). Additionally, neuroaxonal degeneration has been identified even in the earliest disease stages (Granberg *et al.*, 2017), including that of CIS (Deppe *et al.*, 2016). Together, these observations suggest that there is an evolution of MS pathology throughout the disease course that is vital to understand the possibility of therapeutically intervening with existing drugs, as well as to indicate future druggable targets.

1.1.6 Clinical disability measures

The earliest measures of tracking MS disease activity/progression and inferring the pathology within the CNS was by the attentive monitoring of disability, particularly considering the domains that are most prominently affected at the clinical presentation of MS. Sensory disturbances account for some of the more stereotypical features of RRMS. These episodic symptoms include temporary one-sided vision loss due to unilateral optic neuritis, double-vision, numbness/tingling in extremities, limb weakness or clumsiness, and bowel/bladder dysfunction (Rovira and Barkhof, 2018). Additionally, there are often cognitive symptoms that manifest in the form of fatigue, depression, anxiety, cognitive impairment and sensory loss. Thus, there are numerous clinical scores to capture such a variable disability profile. Here, only the tests directly related to this thesis will be described. Physical disability is one of the more classically identifiable aspects of MS. Particularly due to the more direct nature of the manifestations, such as gait dysfunction or limb weakness. Whereas cognitive dysfunction is more ambiguous and indirectly quantifiable. Therefore, the following metrics have been proposed and are typically applied in-clinical to track disability and disease progression.

The Expanded Disability Status Scale (EDSS) score ranges from 0, no indication of MS-related disability, to 10, representing an MS-related death. The EDSS is a composite of numerous sub-scores that is primarily weighted towards physical disability, despite having a cognitive sub-score. The EDSS score is determined by a neurologist and is the result of both physical examination and questions to the patient. However, a limitation with the EDSS is that ambulation will have a disproportionate impact compared to other functions, such as cognitive dysfunction. The timed 25-foot walking test measures ambulatory disability by walking 25 feet as swiftly as possible. The 9-hole peg test is a measure of fine motor ability, where the participant must place and then remove nine pegs from a bord. The MS Impact Scale (MSIS) is a self-report questionnaire based on the day-to-day activities of the individual over the two weeks prior (Hobart *et al.*, 2001). The MSIS provides two sub-scores, representing both physical and cognitive disabilities. The Symbol Digit Modalities Test (SDMT) details the functioning of information processing speed, which is a cognitive domain typically affected in MS. The SDMT is the most routinely acquired cognitive score for MS (Forn *et al.*, 2009). The SDMT is a substitution (deciphering) test where the participant has 90 seconds to translate symbols to the unique corresponding number as found in a reference key, thus, lower scores are more favorable and higher scores are more indicative of disability. The Rey–Osterrieth Complex Figure Test copy (ROCFT) reflects a variety of cognitive processes, including visuospatial capabilities, working memory, attention and executive functioning (Shin *et al.*, 2006). The test entails the recreation of a complex line drawing from memory. The F-A-S test is indicative of verbal fluency (Lezak *et al.*, 2012). The participant has 60 seconds to name as many words as possible beginning with the letter F, then the letter A and finally the letter S with intermittent breaks in-between. Importantly, this test is language-specific and considerations for native speaking must be considered. The Rey Auditory Verbal Learning Test (RAVLT) is a neuropsychological assessment focused on verbal memory with encoding and delayed recall. The test consists of a list of 15 words that are read to the participant who is then asked to recall as many words as possible five times over. This is followed by a second interference list that is similarly read to the reader and asked to recall; however, this list is only meant to overwrite the first list. Finally, the participant is asked to recall as many words from the first list as they can, this is the encoding portion. Lastly, in the retention portion, after about 20 minutes, the testee is again asked to recall as many words from the first list as they can.

1.1.7 Disease-modulatory therapies

Drugs that aim to benefit the long-term outcomes of clinical disability, annual relapse rate and MRI activity in MS are referred to as disease-modulatory therapies (DMTs) (Piehl, 2021). The importance of early treatment (in alignment with the ‘time is brain’-concept) is highlighted by the long-term outcome studies of the first DMTs. Early initiation of treatment with interferons has been found to be associated with a 47% reduction in all-cause mortality after 21 years, despite that, this treatment is considered moderately effective at best, by today’s standards (Goodin *et al.*, 2012). The addition of more efficacious treatment options (Brück *et al.*, 2013),

better treatment monitoring (Brownlee *et al.*, 2017) and earlier diagnosis for more swift therapeutic intervention can altogether be expected to improve the long-term prognosis of MS.

MS DMTs act on different aspects of, for the most part, the adaptive immune response. In contrast to several other autoimmune conditions, cytokine and interleukin inhibitors have not proven to be effective, but rather, as with blockers of tumor necrosis factor, to exert a negative effect on disease activity. Instead, interferon-beta became the first approved DMT in the 1990s, later joined by glatiramer acetate, a random mix of oligopeptides made of basic amino acids being common in myelin (Piehl, 2021). A subsequent breakthrough was made when natalizumab, which inhibits the flux of lymphocytes across the blood-brain barrier, was approved in the mid-2000s. This was later followed by fingolimod, which inhibits the recruitment of lymphocytes from lymph nodes and was approved around 2010. In the last decade more than a handful of new DMTs have been approved, including the oral compounds teriflunomide, dimethyl fumarate and cladribine, and the infusion drugs alemtuzumab, ocrelizumab and ofatumumab. The increased availability of multiple DMTs has led to an intense discussion about optimizing therapy to improve long term outcomes. The perspective of the escalation strategy suggests that a moderately effective DMT should be applied first and then changed to a highly effective DMT if the initial choice is not desirably effective. An alternative perspective that has gained significant momentum recently, is to first apply more highly effective DMTs from the beginning in order to limit potential CNS damage in the long run. However, the current format of most clinical trials is too short in duration to substantially inform on the long-term patient outcomes, thereby creating a need for real-world comparative benefit-risk studies across numerous DMTs. It is important to note that these studies will not hold the same weight as does clinical evidence, which likely contributes to the differences found in DMT choices around the world. The more recent evolution of ongoing DMTs prescribed in Sweden is exemplified here in Figure 4.

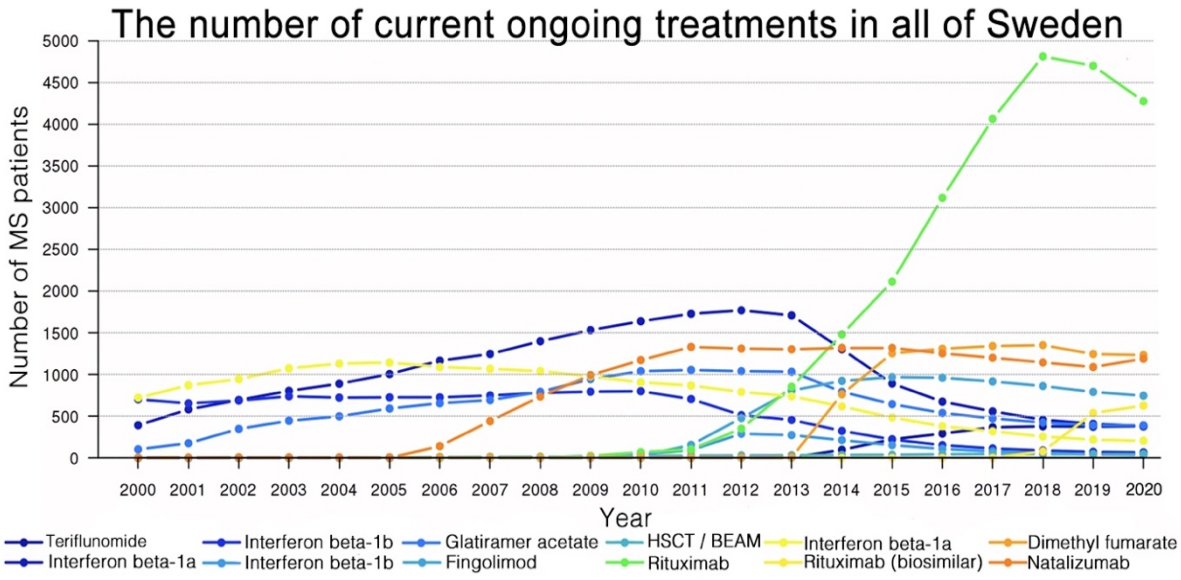

Figure 4. Distribution of Treatments over the last two decades in Sweden. *Image courtesy of Leszek Stawiarz at the Swedish NEURO Registries (Dec 30th, 2020). HSCT = human stem cell treatment*

A further complication is that there are a variety of different mechanisms of action for the various DMTs applied in MS. Interferon-beta and glatiramer acetate, both given by self-administered injections, have been considered a mainstay in MS treatment since their introduction. However, their modest efficacy and low tolerability have necessitated a search for more ideal therapeutic options. Both T- and B-cells have been strongly implicated in the pathogenic mechanism of MS and they are, therefore, logical intervention targets. Alemtuzumab is an anti-CD52 monoclonal antibody that targets both memory T- and B-cells (Katsavos and Coles, 2018; Piehl, 2021), translating into high effectiveness, but safety concerns such as secondary autoimmunity and cerebrovascular disease limit its use (Piehl, 2021). Similarly, the use of natalizumab, a highly effective VLA-4 blocker impeding the transmigration of lymphocytes into the brain, is limited by its risk of progressive multifocal leukoencephalopathy (PML), a severe opportunistic brain infection. More recently, targeting of B-cells with antiCD20 monoclonals such as ocrelizumab and ofatumumab has emerged as a treatment option combining high effectiveness with a tolerable safety profile (Ineichen *et al.*, 2020). For example, ocrelizumab exerts a striking effect on the appearance rate of new focal MRI lesions, which were reduced by 97-98% compared to interferon-1a in the second year of the study (Hauser *et al.*, 2017). Unique to Sweden, rituximab, an older antiCD20 approved for rheumatoid arthritis and lymphoma, has become the most common DMT prescribed to MS patients as shown in Figure 4.

The most characteristic feature of MS is demyelination, so naturally, there is a strong aim for the development of therapeutically facilitated myelin repair, termed remyelination, to support the recovery of those diagnosed with MS. The balance of remyelination and demyelination is a battle fought in each lesion. Remyelination is a process primarily mediated by the initial recruitment and subsequent differentiation of oligodendrocyte progenitor cells (Prineas *et al.*, 1993; Lassmann, 2018). Some oral small molecule compounds have been derived with some remyelination potential observed. For example, clemastine was observed to have the potential to stimulate oligodendrocyte mediated remyelination *in silica* on high throughput screening of compounds on artificial 3D axon-mimicking conical micro-pillar arrays (Mei *et al.*, 2014). A clinical effect of clemastine in improving nerve conduction in MS-associated chronic optic neuropathy was later shown (Green *et al.*, 2017), with additional compounds in clinical trials. These novel agents provide an opportunity to further improve the management of MS through the combination of existing DMTs aiming to halt demyelination with novel therapies that improve remyelination potential (Piehl, 2021). However, this also creates a demand to improve methods of gauging remyelination in living patients undergoing treatment by imaging or CSF-/blood-soluble biomarkers.

1.1.8 COVID-19 concerns in MS

The current COVID-19 pandemic has caused a bevy of global concerns and the field of MS has not been left exempt. Specifically, the virulence of SARS-CoV-2 has emphasized concerns for those with MS undergoing DMT to modulate immune-mediated processes that would leave them vulnerable to more severe development of COVID-19. A recent publication based on the

French MS registry data reported an increased risk of a more severe COVID-19 disease course among those with advanced age, disability level and comorbidity, with a more limited interacting effect of DMT (Louapre *et al.*, 2020). Among different DMTs, antiCD20s compared to other DMTs have been associated with increased risk of a severe disease course, but not mortality (Sormani *et al.*, 2020). Additionally, the role of genetic variance, population risk and environmental factors both for MS and COVID-19 seems to be moving the target for risk of developing COVID-19 in MS.

An additional concern, unspecific to MS, is the demonstrated neurotropism of SARS-CoV-2 and the neurologic manifestations of COVID-19 that have been well-demonstrated, specifically by MRI (Almqvist *et al.*, 2020; Klironomos *et al.*, 2020). The potential for future pathological development due to SARS-CoV-2 exposure and COVID-19 development that has been proposed between other human coronaviruses and MS by tissue extraction (Burks *et al.*, 1980), gene expression (Stewart *et al.*, 1992), RNA isolated in the CSF (Cristallo *et al.*, 1997) and antibodies isolated from sera of people with MS (Hovanec and Flanagan, 1983). Therefore, it is important that there be long-term follow-up of those developing severe COVID-19, not only for patient monitoring but also to learn more about the role of virus exposure and potential development of autoimmune disease development by the aforementioned mechanisms.

1.2 MAGNETIC RESONANCE IMAGING IN MULTIPLE SCLEROSIS

1.2.1 Background and physical principles of MRI

The principles of MRI are complex and span across the fields of quantum physics, nuclear chemistry, electromagnetism, mathematics, cryogenics, engineering and medicine (McRobbie *et al.*, 2006). These complexities are beyond the scope of this summary, thus only a simplified description is presented. Instead of relying on ionizing radiation as is done for X-ray, computed tomography or positron emission tomography (PET), MRI relies on the manipulation of atomic nuclei by magnetic fields. The strong primary static magnetic field is produced by a superconducting magnet, typically with a field strength of 1.5 or 3 Tesla (T), with 7 T recently becoming clinically approved. Clinical MRI is focused on hydrogen atoms, which are abundant in the human body and a nucleus that only consists of one positive component (a proton) surrounded by a single negative component (an electron), which, in a simplified view, can be imagined to function as does a bar magnet. When protons are introduced to a strong magnetic field, they will align with (parallel) or opposed to (antiparallel) the magnetic field, resulting in a small net excess in the parallel direction. A stronger magnetic field will produce more protons in parallel alignment that can then be manipulated for the purposes of imaging (McRobbie *et al.*, 2006). Thus, a stronger magnetic field results in higher measurable signal. Importantly, the protons also spin at a rate that is directly proportional to the magnetic field strength (42.58 MHz/T), known as the Larmor frequency.

The imaging is performed by applying spatial and temporal variations to the magnetic field using gradient coils and stimulating the protons using radiofrequency pulses that resonate with the Larmor frequency. These variations and stimuli are referred to as pulse sequences and it is

by highly specific timing and duration that these pulses manipulate the hydrogen protons. It is also these pulse sequence variations that produce the characteristic loud banging, knocking and high-pitched beeping noises that are associated with the MRI scanning. The gradient coils are hardware on the inside of the MRI scanner tunnel (bore) that generate magnetic fields (gradients) that in turn affects the protons' spin to slightly change in frequency or phase, making spatial encoding possible. Each gradient directionality has its own respective coil for slice selective localization within the sagittal (*x*), coronal (*y*) and axial (*z*) planes. Further, the transmit radiofrequency coils, also within the MRI scanner, emit energy in the form of radiofrequency waves that resonate with the hydrogen protons causing them to spin in phase and raising them to the higher energy state. After the transmit pulse is turned off, the protons will start to spin increasingly out of phase (the timing of which is referred to as T_2/T_2* relaxation) and they will return to their original low-energy state of being aligned with the main magnetic field (the timing of which is referred to as T_1 relaxation). The echoes of these processes are captured by receive coils, which are loops of copper wiring where the spinning protons, when in phase, induce measurable currents. The receiving coil for the head typically looks similar to a helmet and needs to fit snugly to capture the weak signal emitted from the spinning protons. The key attribute that allows for the differentiation of atoms and the generation of the final image by the receive radiofrequency coils is the unique local micro-environment surrounding the individual hydrogen protons, which will affect the manner and time in which these protons return or relax back from their high energy state to their equilibrium state.

1.2.2 Paraclinical role of MRI in MS diagnosis

Magnetic Resonance Imaging (MRI) is the most valuable paraclinical tool in MS, since it facilitates diagnosis, monitors disease status and response to treatment (MAGNIMS, 2015, MAGNIMS *et al.*, 2015*b*; Filippi *et al.*, 2016). The most apparent MRI finding in MS is lesions, that, depending on the type of MRI sequence used, will appear brighter or darker relative to the surrounding normal-appearing tissue. Diagnostically, typical MS lesions will occur in periventricular, cortical/juxtacortical and infratentorial brain regions and the spinal cord (Bakshi *et al.*, 2008; Thompson *et al.*, 2018). Examples of characteristic MS lesions are shown on the following page in Figure 5. The optic nerves are another predilection site, but it has yet to become part of the radiological diagnostic criteria. MRI is becoming increasingly sensitive to MS pathology and as we learn more of the biomarkers we currently have and identify new markers of disease, the role of MRI expands. Additionally, MS specificity has been heightened by the clinical implementation of ultra-high field 7 T MRI in observing more lesions, specifically cortical lesions (Mainero *et al.*, 2009), the central vein sign (NAIMS *et al.*, 2016), a paramagnetic rim on T_2*-weighted or susceptibility-weighted images (Absinta *et al.*, 2013; Kilsdonk *et al.*, 2014; Thompson *et al.*, 2018).

There have been organized efforts to coordinate MRI acquisitions in MS by expert panels. The Magnetic Resonance Imaging in MS (MAGNIMS), Consortium of Multiple Sclerosis Centers and the Swedish MS Society, have recommended standardized MRI protocols for MS (Simon

et al., 2006, MAGNIMS *et al.*, 2015*b*; Vågberg *et al.*, 2017). One of the most often referenced conventional MRI volumetrics that correlates with clinical disability is the lesion volume/fraction, typically acquired from T_2-weighted Fluid-Attenuated Inversion Recovery (T_2-FLAIR) and contrast-enhancing lesions on T_1-weighted imaging. Longitudinal studies have identified T_2 lesion volume as a key and important component in the progression of MS (Fisniku *et al.*, 2008; Dwyer *et al.*, 2018; Ouellette *et al.*, 2018). Neurodegeneration is acquired often in a research setting and increasingly in a clinical setting and is assessed using volumetric analysis of T_1-weighted images to segment the various brain structures that have been found to correlate with disease disability and progression, including the thalamus (Cifelli *et al.*, 2002), cortex (Sailer *et al.*, 2003, Ouellette *et al.*, 2020*b*), corpus callosum (Granberg *et al.*, 2015) hippocampus and spinal cord (Ouellette *et al.*, 2020*b*). Despite the advances in MRI, the associated findings have not fully accounted for the variability seen in MS patients' clinical disability, termed as the 'clinico-radiological paradox' (Barkhof, 2002). It is therefore important to continue to probe the underlying subtle changes that characterize MS pathology.

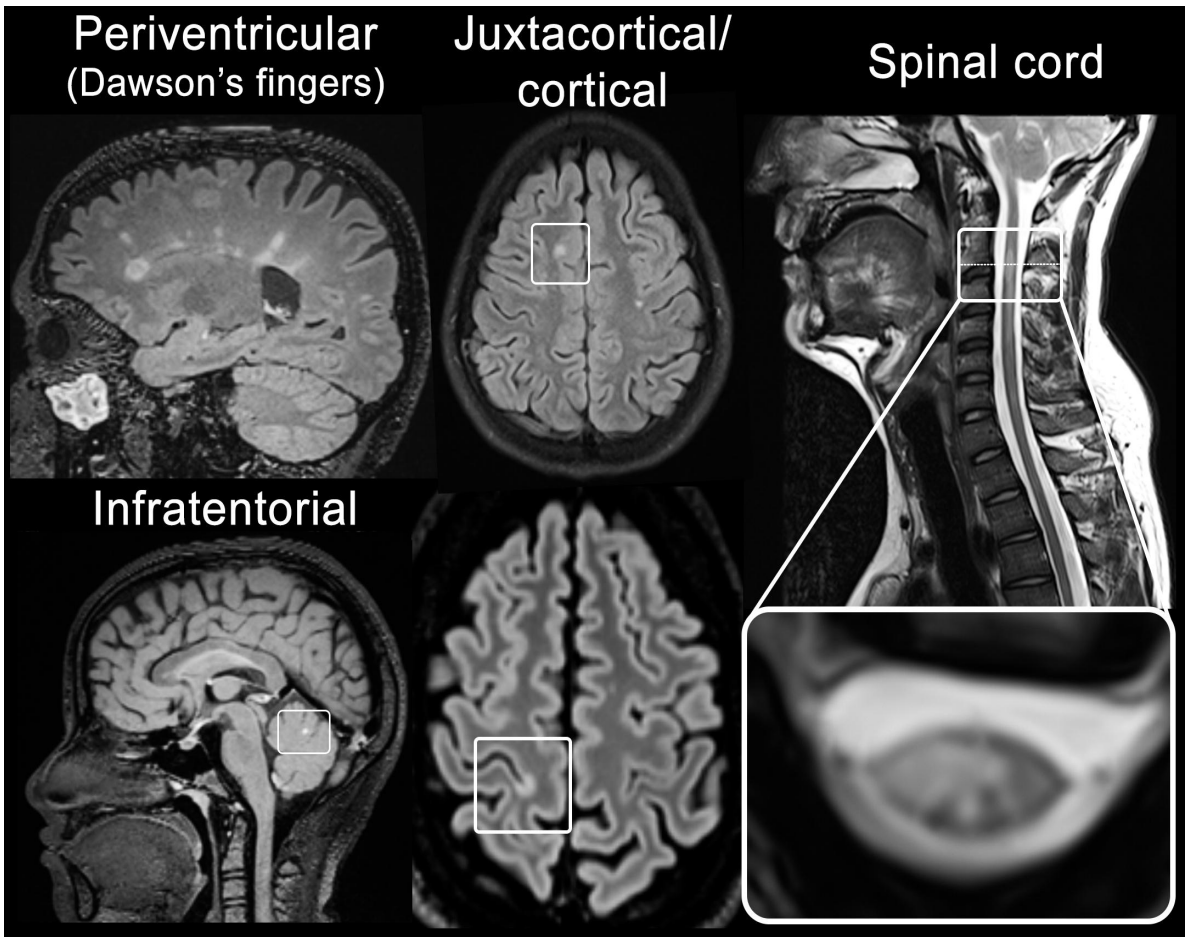

Figure 5. Characteristic MS lesions. *MRI examples of characteristic lesions at 3 T that contribute to fulfilling the MS diagnostic criteria in key areas of interest.*

1.2.3 Conventional MRI techniques in MS

T_1-weighted imaging: T_1-weighted images are produced by the local environmental differences around protons that affect the longitudinal relaxation rate at which protons in the high energy state return to the low energy state of net magnetization equilibrium. Most of the

signal or brightness in T_1-weighted imaging, particularly in the brain, is representative of fat that has a very fast longitudinal relaxation time. Whereas fluids, such as CSF, have longer longitudinal relaxation times, less signal and appear darker. The more typical parameters for T_1-weighted sequences entail short echo and medium repetition times. Modern T_1-weighted images commonly convey reasonably accurate 3D structural information, which can be applied to monitor volumetrics of tissues and/or anatomical structures by manual delineation or automatic/semi-automatic segmentation tools. When imaging the brain, much of the T_1-weighted signal and contrast is derived from hydrogen protons interacting with the fatty acids comprising myelin, the lipid-rich insulation wrapping the length of the nerve fibers (axons). In MS, the focal loss of signal on T_1-weighted images relative to the surrounding normal-appearing tissue is interpreted as a loss/damage of myelin and possibly axonal loss. These T_1-weighted hypointense lesions were formerly often referred to as '*black holes*' on spin-echo T_1-weighted images and were the first biomarker applied to monitor MS pathology *in vivo* (Rocca *et al.*, 2017). This terminology has in recent days become somewhat obsolete since gradient-echo based T_1-weighted images are often applied in MS today, where most (or at high field strengths all) lesions are hypointense to a varying degree, making it hard to define an arbitrary cut off for what would be considered a 'black hole'. It has been shown that the traditional black holes are to a larger extent characterized by more severe demyelination, axonal degeneration and permanent disability than those lesions not visible on spin-echo T1-weighted imaging. Our current understanding of T_1-weighted hypointense lesions has evolved and is summarized by a systematic review of 59 key studies, to be related to longitudinal physical disability by EDSS (Rocca *et al.*, 2017). The primary limitation of T_1-weighted hypointense lesions as a quantifiable biomarker is that they are not fully indicative of MS pathology, as they do not reflect the full extent of lesions present, but rather those that are the most pathologically advanced. However, when combined with more contemporary lesion identification sequence methods there is a stronger relation to EDSS physical disability (Akaishi *et al.*, 2020).

T_2-weighted imaging: T_2-weighted images are similarly produced by the local environmental differences around the individual atoms that affect the transverse relaxation rate at which the precession of in-phase protons becomes de-phased over time. T_2-weighted sequences typically have longer echo and repetition times. T_2 relaxation times are always shorter than that of the corresponding T_1 relaxation times. The longer the T_2 relaxation time, the brighter the signal intensity on T_2-weighted imaging, this is primarily found in fluids, such as CSF. This sensitivity to water is one of the main advantages in MS. Where lesions are localized pockets of focal inflammation and edema, the swelling is revealed as a hyperintense signal relative to the surrounding tissue. However, this sensitivity to water content can be problematic. This is emphasized in the periventricular region, where an increased number of MS-specific lesions occur, and the intense signal from the ventricular system drowns out the contrast within the surrounding tissues.

T_2*-weighted imaging: Importantly, note that the MRI hardware makes the magnetic field as homogeneous, or as stable and constant, as possible. However, once a person is placed in the middle of the MRI the magnetic field is drastically perturbed and becomes '*imperfect*' based

on the inherent magnetic susceptibility differences of tissues in the body. It is these field imperfections that are the premise of T_2*-weighted imaging. The T_2* '*apparent*' relaxation time is the combination of the T_2 spin-spin relaxation further quickened by the local magnetic field inhomogeneities produced within tissues. Various tissues throughout our body have varying magnetic properties and these differences between tissues are significant enough to create local magnetic field gradients between the tissue that can be imaged (McRobbie *et al.*, 2006). This type of imaging is often applied at 7 Tesla because the T_2* effects increase exponentially with the field strength, thus improving the contrast-to-noise ratio in the T_2*-weighted images that also provides means of ultra-high resolution.

Proton density (PD) weighted imaging: Proton density (PD), rather intuitively, is reflective of the proton concentration within a given tissue, which produces a proportionate amount of signal (brightness) to that of the respective proton concentration. PD-weighted imaging is essentially the maximum signal without traditional T_1- or T_2-weighted, with a long repetition time for complete T_1 relaxation and a short echo time to avoid a loss of contrast by T_2/T_2* effects (McRobbie *et al.*, 2006).

Inversion recovery (IR) imaging: IR sequences are a common type of clinically applied MRI sequence, primarily due to their improved lesion-to-normal tissue contrast. They fundamentally entail one inversion pulse that selectively suppresses the signal of a specific tissue type, which allows better interpretation of the remaining signal. **Fluid-attenuated IR (FLAIR)**, as the name indicates, selectively suppresses the signal associated with fluids. In the brain, the signal that is most predominantly suppressed is that of the CSF. This sequence has particular importance in the clinical imaging of MS since lesions often occur close to the ventricles. Moreover, neurodegeneration over time produces ventricular expansion and widening of the sulci, both of which contain CSF. A notable aspect of T_2-FLAIR imaging is that only the typical CSF signal is suppressed, whereas edema produced by localized inflammation, remains bright as with traditional T_2-weighted imaging. It should be noted that artifacts can more easily manifest on FLAIR imaging due to flow, i.e., trying to suppress the signal of a moving target. Therefore, 3D imaging has been key in overcoming the production and interference of artifacts on T_2-weighted FLAIR, nevertheless, lesions sometimes need to be verified on some of the aforementioned imaging techniques, namely PD-, T_1- or T_2-weighted images (Naganawa *et al.*, 2004). Examples of T_2-FLAIR images alongside the corresponding lesion mask volumes are shown on the following page to the right in Figure 6. **Short Tau IR (STIR)** is often referred to as short T_I IR because it is a T_1 based imaging technique that suppresses the signal from fatty tissues. STIR imaging is typically applied in MS diagnostics to capture optic neuritis. **Double IR** has two inversion pulses that, as a combination of FLAIR and STIR, suppress the signal from both CSF and fat, which is particularly useful in isolating cortical lesions. **Phase-Sensitive IR** is another T_1-based sequence that has demonstrated sensitivity to identifying cortical lesions.

1.2.4 Conventional MRI biomarkers in MS

The radiological report is conducted by (neuro)radiologist(s) based on the images provided in the current and any previous MRI exams. The intent of the report is to concisely convey the information contained therein with a clinical focus supporting patient management and describing the presence of MRI disease activity and progression (Rovira and Barkhof, 2018). Some of the specific relevant findings in a radiological report could include the: total T_2 lesion number, number of new/enlarging lesions, qualitative (categorical) description of T_2- and T_1-weighted lesion load (mild, moderate and severe), and qualitative (categorical) description of brain atrophy (normal, mild, moderate and severe) (Rovira and Barkhof, 2018). Within the context of this work, 'conventional' references the biomarkers of MS-related pathology that have been traditionally applied within a research context. This is because the methodology applied in-clinic, counting total or new lesions, either continuously or on an ordinal scale, is a method that, alone, would not be an acceptable approach at a research peer-reviewed level.

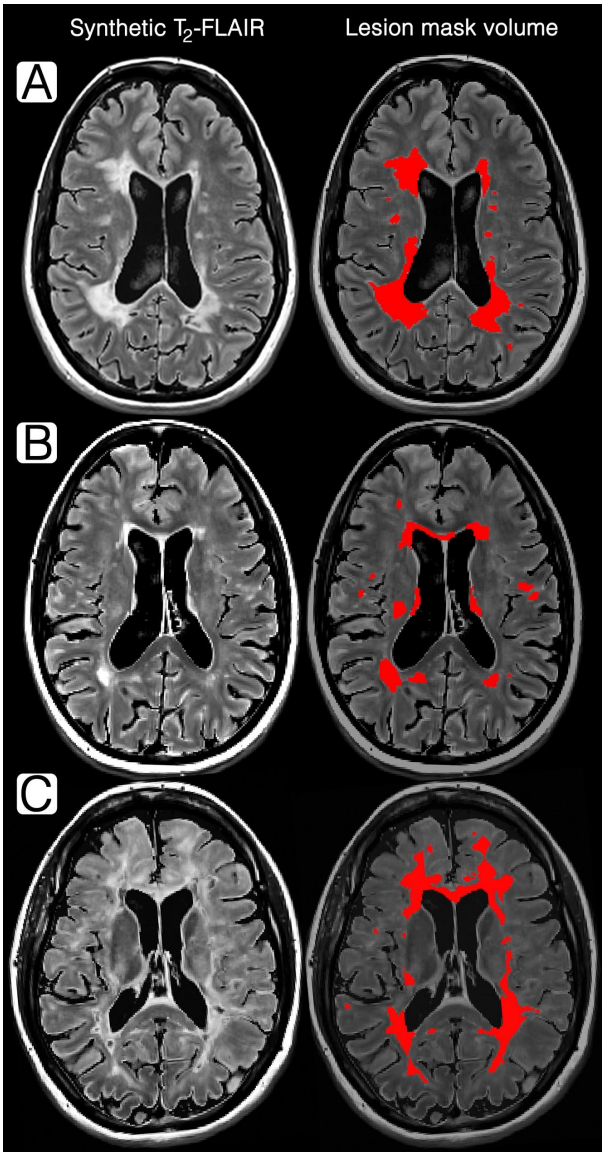

Figure 6. T_2-FLAIR lesion segmentation. *Synthetic T_2-FLAIR images alongside the corresponding semi-automatic lesion masks in a;* ***A.*** *40-year-old female with RRMS, 14-year disease duration, EDSS 1.0, SDMT z-score -1.0* ***B.*** *33-year-old female with RRMS, 1.3-year disease duration. EDSS 2.0, SDMT z-score -3.0.* ***C.*** *50-year-old female with SPMS, 17-year disease duration, EDSS 3.5, SDMT z-score -2.5*

Lesions: The conventional approach used to describe lesions in MS research began by counting lesions, comparable to what is currently done in the clinical setting. Enumerating total lesions and new lesions, at follow-up, either continuously or categorically by mild, moderate and severe. It is important to note that as the disease progresses, lesions can slowly expand, simultaneously the brain atrophies under the environment of chronic inflammation. The effect of these two processes is that lesions may become confluent, thereby distorting the value of the lesion count. Furthermore, a small lesion in an eloquent location may have a stronger clinical manifestation than that of a large lesion in a non-critical topography. A more current research method of presenting the lesion pathology in MS is by segmenting lesions volumetrically, but the lesion volume should then be normalized by the size of the intracranial

volume to produce the lesion fraction. However, each individual lesion is highly unique, with a variable profile of concurrent de- vs. remyelination, which makes it very difficult to succinctly convey the overall picture of lesion pathology with one number. Examples of lesions alongside the corresponding T_2-FLAIR volume from which they were based are presented in Figure 6.

Atrophy: In clinical practice, atrophy is often qualitatively and categorically described as normal, mild, moderate, or severe. However, the coarseness of these metrics and subjective interpretation removes much of the sensitivity for monitoring patients. Therefore, more current methodologies include automatic segmentation pipelines based on standardized anatomical atlases. These techniques segment and subsegment most all of the distinct anatomical regions of the CNS, such as those highlighted here in Figure 7.

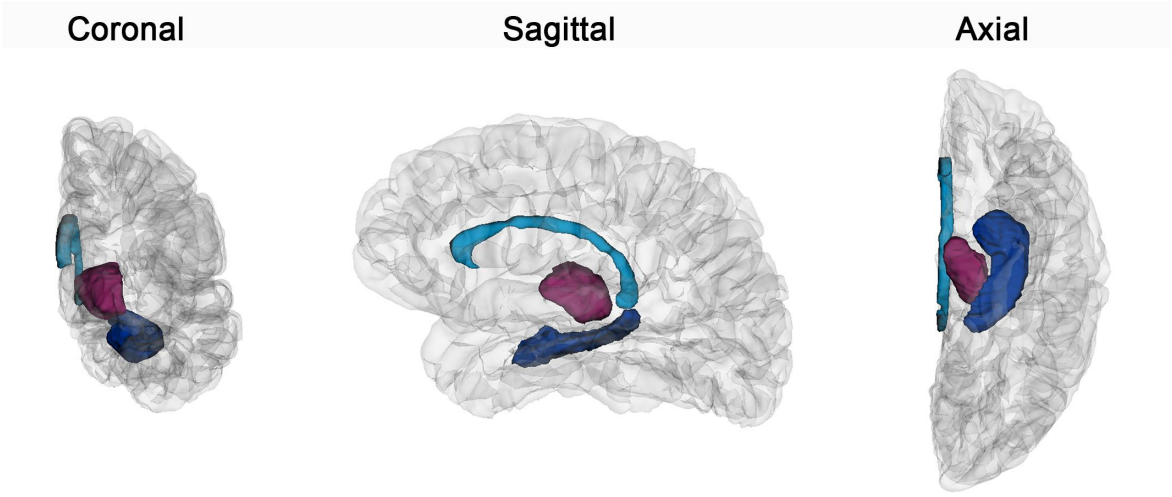

Figure 7. Neuroanatomical volumes.
Volumetric rendering of neuroanatomic regions of interest that have been found to be affected by MS pathology and contribute to MS-related neurologic disability: the corpus callosum (cyan), the thalamus (plum), and the hippocampus (navy) in the left hemisphere of a 55-year-old female patient with SPMS.

1.2.5 Non-conventional MRI and advanced imaging biomarkers

MRI has been a revolutionary tool in the medical field, allowing clinicians to detect and monitor pathologies *in vivo* (Laule and Moore, 2018). Conventional MRI weightings are arbitrarily scaled, which means that they cannot easily be compared between patients between scanners over time or between sites and remain unspecific to MS pathology (MAGNIMS *et al.*, 2015*a*; Laule and Moore, 2018; Filippi *et al.*, 2019). The slow implementation of more advanced and quantitative MRI in clinics is primarily attributed to their inherent technical complexity and difficulty in processing, analysis and interpretation of the images (MAGNIMS *et al.*, 2015*a*). Rather, non-conventional imaging techniques are most often applied in a research basis and, less often, in treatment trials (MAGNIMS *et al.*, 2015*a*; Filippi *et al.*, 2019). With next-generation treatments aiming to promote repair, protection or stimulate remyelination (Brück *et al.*, 2013, MAGNIMS *et al.*, 2015*a*; Green *et al.*, 2017), MS-specific microstructural imaging techniques that monitor lesion activity, myelin dynamics and axonal

density will prove valuable to determine treatment efficacy (MAGNIMS *et al.*, 2015*a*; Laule and Moore, 2018; Filippi *et al.*, 2019).

Before new imaging methods can be applied for patient care in clinics, there are important considerations that must be made beforehand. First, the biological meaning of what is being imaged must be described, i.e., a validation of the tissue-specificity, typically done by histopathological correlation. Second, the assessment of precision, repeatability and reproducibility should be made to determine the measurement variability/error of the technique to then consider if the method is reliable over time. Standardization of the MRI acquisition strategy and harmonizing the data processing pipeline are very important factors to mitigate variability and ensure comparability of data between sites (Vågberg *et al.*, 2017). Importantly, there must also be an evaluation of the clinical significance of the metrics produced by the technique, ideally compared to other imaging biomarkers, elsewise there is no rationale for the particular technique. Another very important consideration is how interpretable the results are clinically. Particularly for radiologists, who already have a bevy of numbers and indices to consider and report on, to facilitate their conclusions and support neurologists' decision making.

While lesions and atrophy are well-established biomarkers for the prognosis of MS, there is still much to be considered in the non-lesioned 'normal-appearing' white and grey matter, which have been histopathologically shown to have diffuse/subtle MS pathology (Filippi *et al.*, 2019). Recent advances in MRI acquisition and analysis, especially new quantitative MRI methods, have led to promising non-conventional imaging techniques to probe the MS tissue microstructure (MAGNIMS *et al.*, 2015*a*). Many of these techniques aim to capture the pathological processes that precede lesion formation and subsequent axonal degeneration. Each technique holds promise, though they all present their own unique strengths and limitations to being applied clinically. A review of some of the most popular techniques in MS is provided below.

T_2*-weighted imaging: The field imperfections that produce variable disturbances in the magnetic field, best captured in T_2*-weighted imaging (but also T_1- and T_2-weighted), have been demonstrated to be related to the tissue-microenvironmental architecture (Langkammer *et al.*, 2010; Cohen-Adad *et al.*, 2012). Specifically, these magnetic field inhomogeneities are derived from the presence of iron, an element with well-understood magnetic properties. The physiological role of iron in the CNS remains undetermined, but it has been identified in the form of ferritin, transferrin and iron, in varying degrees, in the oligodendrocytes that produce the myelin lamellae around the axons (Connor and Menzies, 1996). Quantitative T_2* relaxometry measures have been applied to capture the tissue microstructure (Mackay *et al.*, 1994) through the introduction of multiple echoes in T_2*-weighted imaging and quantitative fitting of the relaxation curve allows for the characterization and distribution of iron and the myeloarchitecture (Langkammer *et al.*, 2010; Cohen-Adad *et al.*, 2012; Mainero *et al.*, 2015; Louapre *et al.*, 2018).

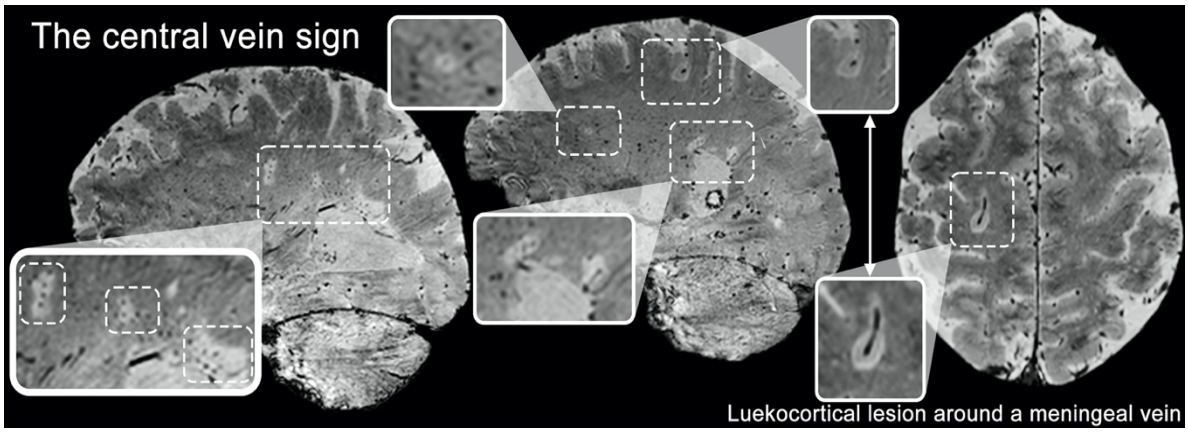

Figure 8. The MS central vein sign.

Examples of the MS characteristic central vein sign in white matter and grey matter lesions on susceptibility-weighted imaging (SWI) at 650-micrometer 3D resolution in two participants diagnosed with RRMS at 3 T.

Susceptibility-weighted imaging (SWI) is another promising method to assess MS pathophysiology, which is based on more advanced T_2* imaging (MAGNIMS *et al.*, 2015*a*). In clinical MRI, the image viewed by the radiologist is usually the magnitude image. The SWI technique applies post-processing that integrates information from the phase image with the magnitude image. Clinically, the T_2* shortening caused by the paramagnetic deoxygenated blood on SWI can help identify the central venule, exemplified above in Figure 8, within focal white and grey matter lesions (i.e., the central vein sign), which are specifically indicative of MS (NAIMS *et al.*, 2016; Filippi *et al.*, 2019). Susceptibility imaging is also able to identify a hypointense rim around white matter lesions (Hagemeier *et al.*, 2014), which may indicate the surrounding macrophages clearing the myelin debris in an active lesion leading to iron deposition and generation of free radicals (Absinta *et al.*, 2013). The phase image can be further analyzed using quantitative susceptibility mapping (QSM) (Li *et al.*, 2011; Wang and Liu, 2015) to assess underlying tissue magnetic susceptibility differences in a quantitative manner (Haacke *et al.*, 2015). QSM has demonstrated sensitivity to iron deposition, blood and its oxygenation level, myelin density and the venous capillary network (MAGNIMS *et al.*, 2015*a*; Wang and Liu, 2015).

Diffusion-weighted imaging: Advanced diffusion-weighted imaging is an MRI technique that can provide a description of the molecular diffusion of water within a certain defined area. Diffusion Tensor Imaging (DTI) is a mathematical approach to describe diffusivity. DTI is used to evaluate the microstructure of the axon bundles in the CNS and can be used to follow and visualize tracts, a process known as tractography (Filippi *et al.*, 2012). DTI and tractography function on the simplified principle that axons are structurally analogous to straws bundled together in fibers, where water can readily diffuse along the length of the axon but is restricted in the perpendicular direction due to the mechanical barrier of the axonal membrane and myelin lipid bilayers.

In participants with MS, mean diffusivity, radial diffusivity and fractional anisotropy (a composite measure of the axial and radial diffusivity) were found to significantly differ in MS participants with high disability as compared to those with low disability (Oh *et al.*, 2013). Radial diffusivity has been linked to myelin sheath integrity (Kronlage *et al.*, 2017) and electrophysiological markers of demyelination, while axial diffusivity and fractional anisotropy are more closely related to axonal integrity (Tu *et al.*, 2016). The dynamic pathophysiology of MS entails inflammation, de-/re-myelination and potential axonal loss, which is a problematic scenario for axial and radial diffusivity to disentangle (Winklewski *et al.*, 2018). More advanced diffusion methods have been proposed that incorporate multiple diffusion weightings applied in many directions into the model, such as Neurite Orientation Dispersion and Density Imaging (NODDI), featured here in Figure 9 (Zhang *et al.*, 2012) or Composite Hindered and Restricted Model of Diffusion (CHARMED) (Assaf and Basser, 2005; De Santis *et al.*, 2019; Toschi *et al.*, 2019). Pathology in the normal-appearing non-lesioned tissue was identified in participants diagnosed with early MS using both NODDI (Granberg *et al.*, 2017) and CHARMED

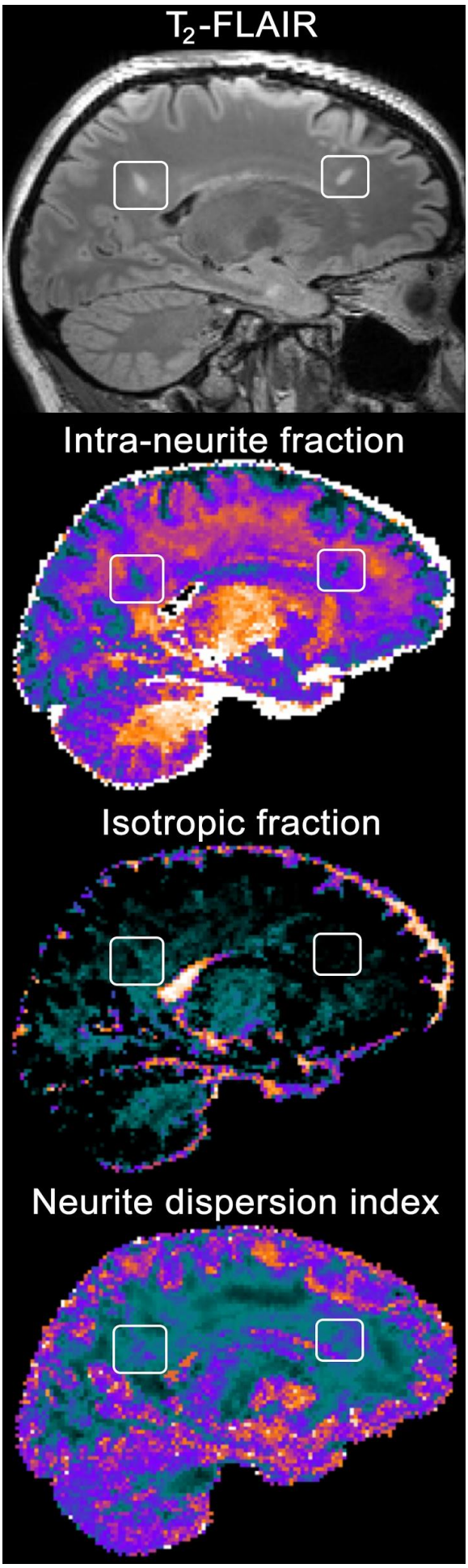

Figure 9. Advanced diffusion modeling.
T_2-FLAIR images of two apparently similar MS lesions in a young female with RRMS. NODDI reveals that the posterior lesion (left-most in the image) is differentiated by less pronounced axonal loss, more edema and heterogenous microstructural alignment as compared to the frontal lesion (right-most in the image). The Intra-neurite fraction is representative of axonal density. The isotropic fraction infers CSF or edema. The neurite dispersion index is suggestive of axonal fanning. NODDI measures are a quantitative unitless scale of 0-1.

(De Santis *et al.*, 2019). The potential maximum capability of diffusion MRI has been recently demonstrated at *in vivo* 760-micrometer resolution, however, acquired across 9 different MRI sessions (Wang *et al.*, 2020).

Myelin imaging: Conventional MRI is sensitive to MS pathology but does not specifically reflect the histopathological hallmark of the disease, demyelination, nor the diffuse pathology in normal-appearing tissues (MAGNIMS *et al.*, 2015*a*; Laule and Moore, 2018). Therefore, different myelin-imaging techniques have been developed as more sensitive and tissue-specific approaches to quantify myelin, including one such method shown here in Figure 10. The reference technique of myelin imaging is known as myelin water imaging or myelin water fraction, which uses a multi-echo spin-echo approach to construct a multi-exponential T_2 decay curve (Mackay *et al.*, 1994). The T_2 decay curve is used to isolate the signal from fast relaxing water that is confined between the myelin lipid bilayer wrappings about the axon. Some other methodologies have also been developed to isolate the fast-relaxing myelin water signal. One of the first being gradient spin-echo imaging (Oshio and Feinberg, 1991; Prasloski *et al.*, 2012). A more recent method is steady-state imaging or multicomponent driven equilibrium single pulse observation of T_1 and T_2 (Deoni *et al.*, 2008), which applies multiple

Figure 10. REMyDI myelin imaging.

T_2-weighted FLAIR image and the corresponding myelin map in four representative study participants. ***Healthy control:*** *a 56-year-old female healthy control.* ***PPMS:*** *a 53-year-old female participant (9-year disease duration, EDSS score 3.5, SDMT z-score -0.4).* ***RRMS:*** *a 40-year-old female participant (14-year disease duration, EDSS score 1.0, SDMT z-score -1.0.* ***SPMS:*** *a 44-year-old female participant (19-year disease duration, EDSS score 7.5, SDMT z-score -3.7).*

flip angles to observe the signal differences of two short gradient echoes and resolve the intracellular vs. extracellular water compartments (Laule and Moore, 2018). In MS participants, multicomponent driven equilibrium single pulse observation of T_1 and T_2 has found a relationship between the myelin water fraction and worsening EDSS. scores (Kolind *et al.*, 2012). The same method also identified lower myelin content in normal-appearing white matter in PPMS as compared to controls (Kolind *et al.*, 2015.

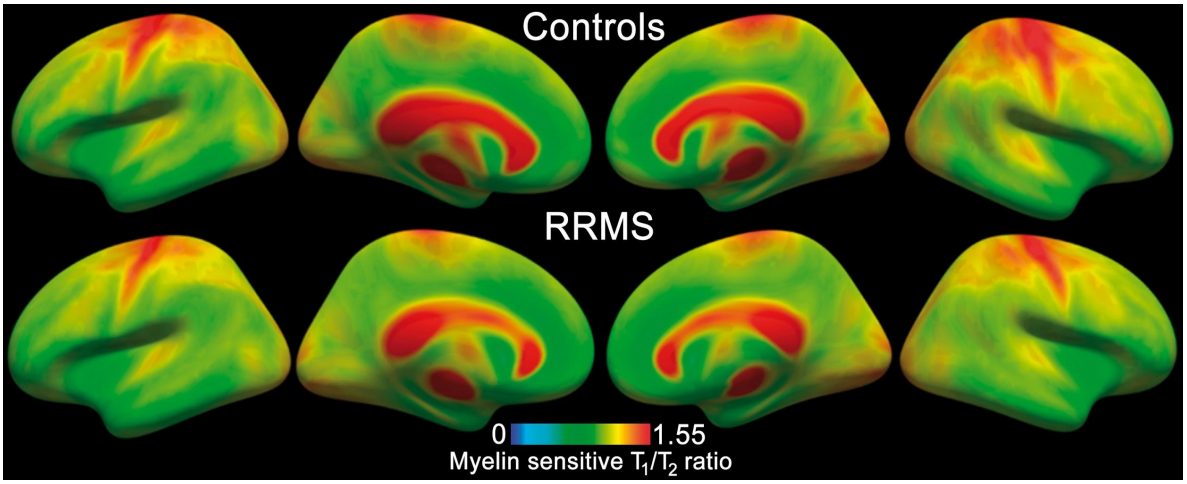

Figure 11. Topographical distribution of myelin.
Sampled at the mid-cortical depth on a group level of 26 participants with RRMS (all below 5-years disease duration) and 24 controls. A trend of lower myelin relative content in the superior frontoparietal regions was visually identified in RRMS participants.

In Magnetization Transfer imaging, protons are simplified to exist in two states, those that are freely diffusing and those that are bound or closely related to molecular interactions of the much larger macromolecules (MAGNIMS *et al.*, 2015*a*). The bound protons can be saturated using off-resonance radio frequency pulses, after which the magnetization is transferred to the free protons and can be imaged by MRI. The magnetization transfer results in a corresponding signal decrease, compared to the same imaging without the off-resonance pulse, and is expressed as the ratio between the two states, Magnetization Transfer Ratio (MTR) (MAGNIMS *et al.*, 2015*a*). The relative concentration of myelin-bound protons is considered to biologically reflect the degree of myelination in the CNS (MAGNIMS *et al.*, 2015*a*). In SPMS participants, MTR in the normal-appearing white and grey matter correlates with MS functional composite scores. However, it has been reported that MTR myelin estimates are confounded by inflammation and edema, which raises specificity concerns in the inflammatory environment of MS (Vavasour *et al.*, 2011). Inhomogeneous magnetization transfer ratio (Girard *et al.*, 2015) aims to address this issue, correlating more strongly with physical disability in various white matter structures than conventional MTR (Van Obberghen *et al.*, 2018). Quantitative MT has been shown to have increased sensitivity to capture remyelination, compared to myelin water fraction, likely attributed to the lower measurement variability in quantitative MT compared to myelin water imaging (Levesque *et al.*, 2010). Another recent method is the macromolecular proton fraction (Yarnykh, 2012), which has been histologically validated in rats (Khodanovich *et al.*, 2017) and shown cross-sectional correlations with

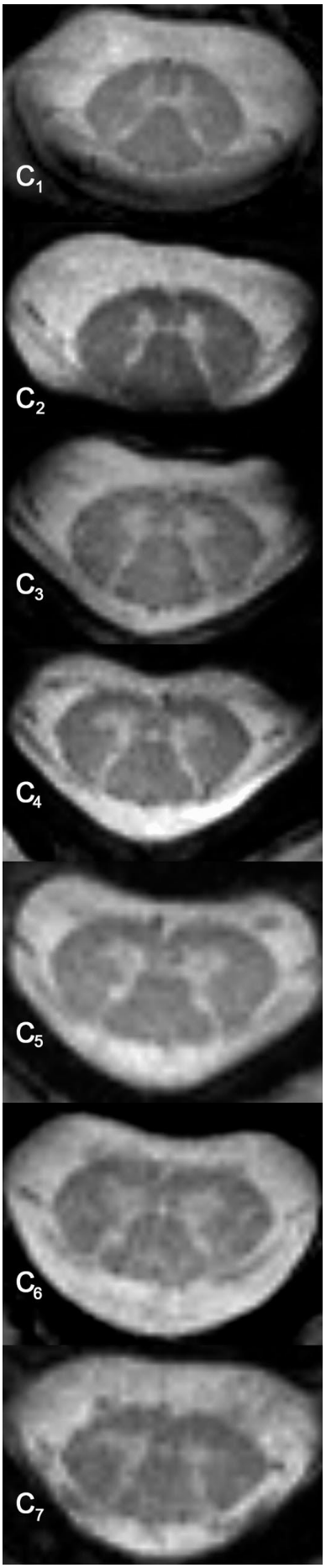

physical and cognitive disability in grey and white matter in MS (Yarnykh *et al.*, 2015). Currently, Inhomogeneous magnetization transfer ratio and QSM have demonstrated the highest myelin specificity, as determined by the coefficient of determination (R^2), however, most techniques have never been directly compared (van der Weijden *et al.*, 2020).

Some emerging *in vivo* myelin imaging methods have been developed more recently. These, however, warrant further investigation and validation to determine how they can be applied to monitor MS disease progression and treatment response. The T_1/T_2-weighted ratio demonstrated sensitivity to myelination, by taking advantage of the differing MRI signal intensities across the cortex, driven primarily by the differences in myelination (Sigalovsky *et al.*, 2006; Glasser and Van Essen, 2011). The method proposes that the degree of myelination directly/indirectly affects the T_1-weighted and T_2-weighted signal in opposite directions and that the ratio thus results in an increase in the contrast-to-noise ratio between low and high myelinated regions while simultaneously canceling out intensity field bias from the images (Glasser and Van Essen, 2011). The T_1/T_2-weighted ratio could discriminate between myelinated and demyelinated cortex *ex vivo* (Nakamura *et al.*, 2017) and, shown on the page prior in Figure 11, was able to detect differences in both the cortex and the white matter of early-stage MS patients compared to controls (Granberg *et al.*, 2017). However, the T_1/T_2-weighted ratio is only a reliable myelin marker in the cortex since its specificity to myelin in white matter is limited (Klaver *et al.*, 2015; Arshad *et al.*, 2017; Righart *et al.*, 2017), therefore further validation is necessary. Rapid Estimation of Myelin for Diagnostic Imaging (REMyDI) (Warntjes *et al.*, 2016) is based on synthetic MRI, a multi-echo saturation-recovery quantitative MRI sequence is used to perform simultaneous PD-, T_1- and T_2-mapping (Warntjes *et al.*, 2008). REMyDI (Figure 10) is estimated by assuming a magnetization exchange between the intracellular and extracellular water compartments, where myelin reduces the observable R_1, R_2, and PD values (Warntjes *et al.*, 2016). REMyDI has been clinically approved, validated in *ex vivo* MRI (Warntjes *et al.*, 2017, Ouellette *et al.*, 2020*a*), found to be more sensitive to

Figure 12. 7 T MRI of the full cervical spinal cord (C1–C7). *In a 40-year-old female RRMS participant (3-year disease duration, EDSS score 2) without any spinal cord lesions.*

MS lesions than the corresponding individual relaxometry measures (Hagiwara *et al.*, 2017*a*, *b*) and related to clinical measures of MS neurologic disability (Ouellette *et al.*, 2020*a*).

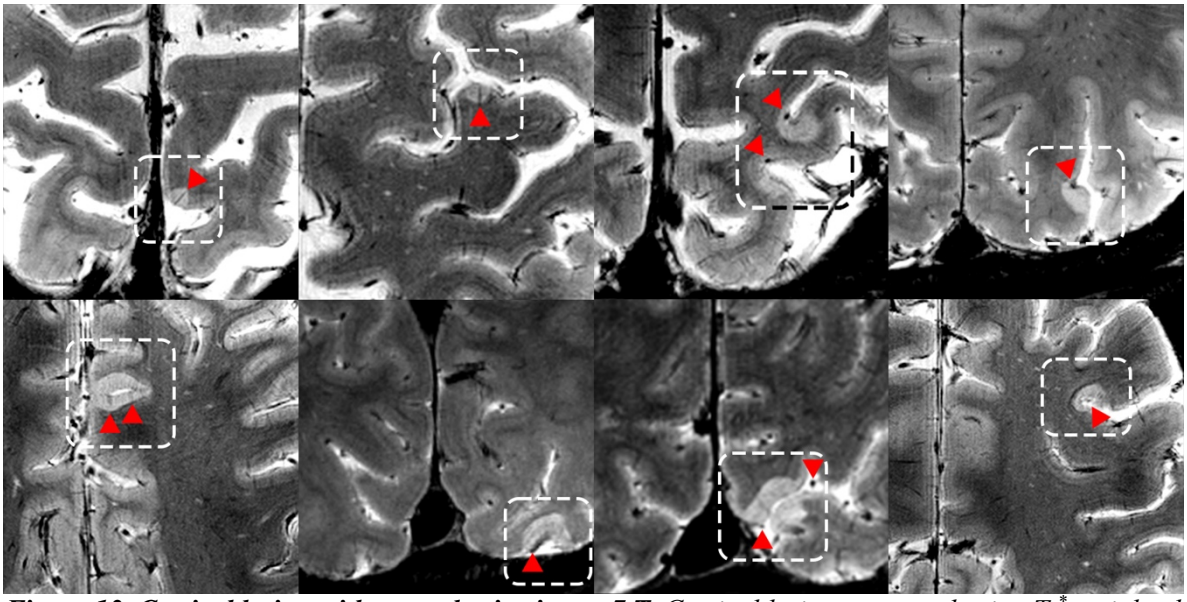

Figure 13. Cortical lesion with central vein sign at 7 T. *Cortical lesions captured using T_2^*-weighted imaging at ultra-high field 7 T MRI with the corresponding central vein(s) (red arrow) in a 45-year-old male diagnosed with RRMS (4-year disease duration, EDSS score 2). Due to the convoluted nature of the cortex some of the central vein(s) may seem peripherally located in the 2D slice.*

Ultra-high field 7 T MRI: The increased signal and contrast at 7 T compared to conventional 1.5/3 T imaging allows for higher spatial resolution imaging, so that smaller more eloquent structures may be more clearly visualized, as shown in Figures 12-14 (Ouellette *et al.*, 2020*b*). MS has historically been characterized primarily as a white matter disease. Despite histopathological studies demonstrating lesions and demyelination occur in grey matter structures (Lucchinetti *et al.*, 2011), *in vivo* MRI had great difficulty to visualize these findings (Barkhof, 2002) since lesions are often located at CSF interfaces, which causes problematic partial volume effects. Ultra-high field MRI can identify MS cortical lesions and subtype them (Mainero *et al.*, 2009). Cortical lesions, shown in Figure 13, and are found in roughly 90% of MS participants at 7 T even in the early stages of the disease (Granberg *et al.*, 2017). Longitudinally, cortical lesions were found to progress in roughly 80% of MS participants over a time span of 1.5 years and to have an even greater accumulation rate than the white matter lesions (Treaba *et al.*, 2019), these findings, therefore, overturn the previous reigning dogma of MS as a white matter disease. Quantitative T_2^* imaging at 7 T was able to identify a gradient in cortical pathology extending inward from the subpial CSF surface and thalamic pathology extending inwards from the periventricular CSF surface (Mainero *et al.*, 2015; Louapre *et al.*, 2018). The increased resolution at 7 T also supports the utility of the 'central vein sign', a novel biomarker for MS diagnosis (NAIMS *et al.*, 2016), portrayed in Figure 13. SWI at 7 T demonstrated a heightened sensitivity to iron deposition and could identify lesions with a 'smoldering rim' representing microglia/macrophages that have taken up the iron-associated myelin debris (Dal-Bianco *et al.*, 2017). The increased signal of 7 T MRI also aids in imaging the spinal cord, meanwhile the increased contrast also aids in imaging the small grey-white matter border (Barry et al., 2018, Ouellette et al., 2020b), as shown in Figures 12 and 14.

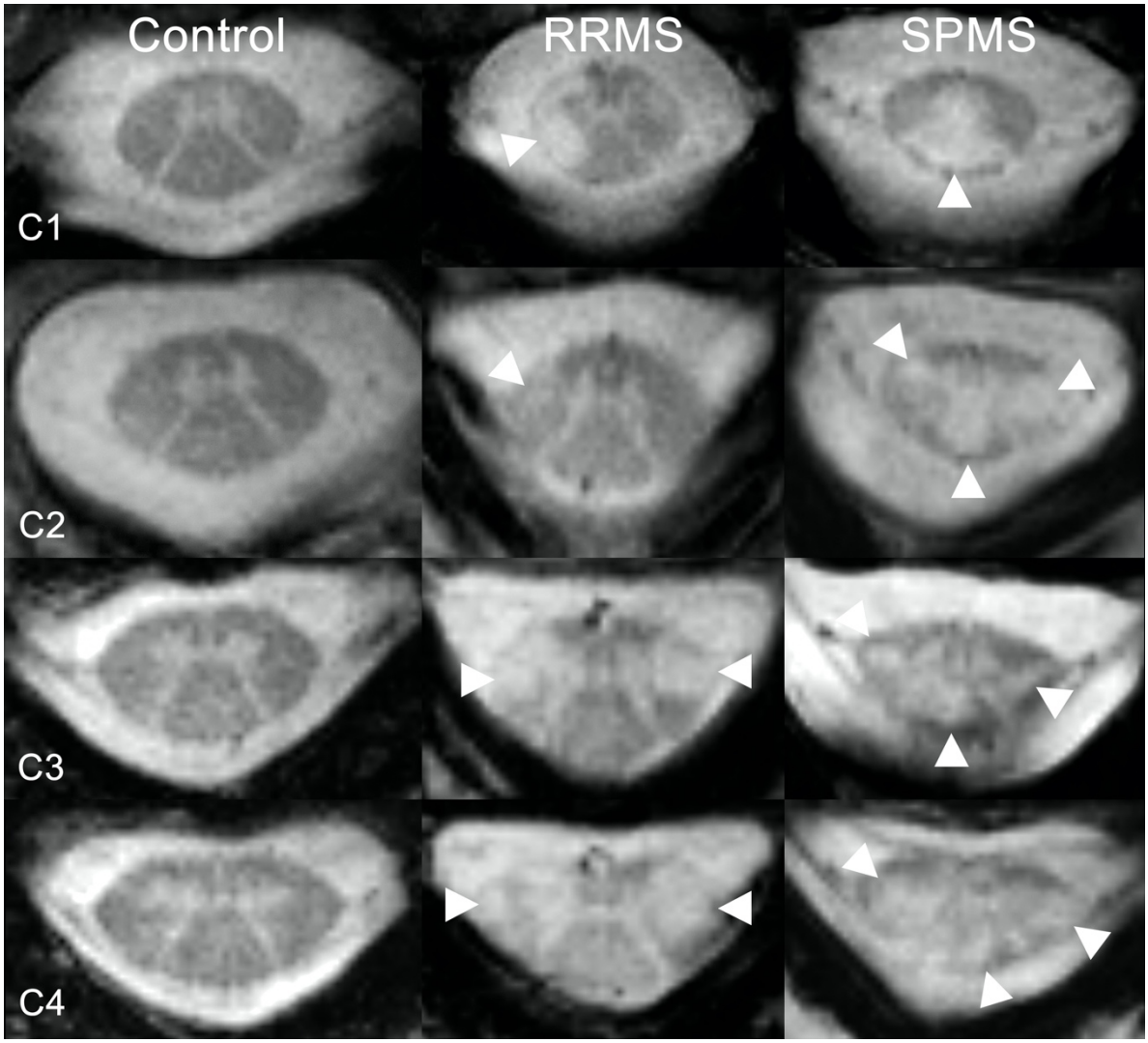

Figure 14. 7 T imaging of cervical levels (1–4).
A 42-year-old female healthy volunteer, 45-year-old male RRMS participant (4-year disease duration, EDSS score 2) and 36-year-old male SPMS participant (20-year disease duration, EDSS score 6.5).

Molecular imaging: Positron Emission Tomography (PET) is distinct from each of the aforementioned MRI techniques since it relies on the injection of a radioactive isotope in the body and directly images a specific molecular target. However, PET can be applied in conjunction with MRI and warrants further discussion. For example, the MRI-based myelin imaging techniques may be capable of indirectly imaging myelin through the associated fast relaxing signal (Laule and Moore, 2018), whereas PET imaging can use off-target [^{11}C]Pittsburgh compound B (PiB) binding to image myelin (Stankoff *et al.*, 2011), despite being developed as an amyloid imaging tracer for Alzheimer's disease, but has shown sensitivity to demyelination and remyelination in a rodent model (de Paula Faria *et al.*, 2014) and found to capture myelin dynamics in the lesions of MS patients (Bodini *et al.*, 2016). [^{11}C]-PBR28 is a molecular marker that aims to quantify the expression of the translocator protein, a marker of activated microglia/macrophages (Herranz *et al.*, 2016). A multimodal PET and 7 T MRI study found that activated microglia/macrophages are present within the cortex, cortical lesions, deep grey matter, and normal-appearing white matter. Moreover, this activation is related to poor clinical outcome, and partly to neurodegeneration (Herranz *et al.*, 2016).

2. AIMS OF THIS THESIS

The overall purpose of this thesis was to quantify MS pathology using volumetric brain MRI, ultra-high field brain and cervical cord 7 T MRI, as well as a newly developed rapid myelin imaging technique, in relation to cognitive and physical MS disability.

The specific objectives of each study were to:

Study I (i) Investigate the long-term progression of cognitive and physical disabilities in MS and their neuroanatomical correlates based on volumetric brain MRI; (ii) Explore the predictive value of the volumetric imaging markers.

Study II (i) Characterize the extent of grey and white matter lesions and atrophy in the cervical spinal cord in MS; (ii) Evaluate whether spinal cord lesions preferentially occur in close proximity to CSF surfaces, possibly implying an association with CSF-mediated inflammatory factors; and (iii) Investigate the relationship between brain and spinal cord pathology and their relative contributions to neurological disability.

Study III Validate REMyDI *ex vivo* and apply it *in vivo* in MS; (i) First by histopathological analysis in postmortem MS tissue to study its tissue specificity; (ii) Assess scan–rescan repeatability measures in both healthy controls and MS participants; (iii) Apply the technique in a prospective cohort of healthy controls and MS participants with longitudinal clinical follow-up.

Study IV (i) Characterize the distribution of pathological demyelination using both *in vivo* and *ex vivo* techniques in MS; (ii) Determine the correlation between the distribution of demyelination and MS-related physical and cognitive disability.

3. MATERIALS AND METHODS

3.1 ETHICAL CONSIDERATIONS

These studies were conducted in accordance with the Declaration of Helsinki and were approved by the respective local Institutional Review Boards at both research sites. Written informed consent was obtained from all the *in vivo* participants preceding study enrolment. The *ex vivo* brain tissue samples were donated to the Rocky Mountain Tissue bank with informed consent. The specific study ethical permits for the respective institutions are as follows:

Study I

EPN 21/95: Baseline data acquisition for the cohort.

EPN 04-906/4: First follow-up (9-year) data acquisition for the cohort.

EPN 2012/858-31/2: Second follow-up (17-year) data acquisition for the cohort.

Study II

IRB MGH 2007P001274: MRI and clinical data acquisition for the cohort.

Studies III and IV

EPN 2013/1635-31/2: Acquire the SyMRI sequence *in vivo*.

EPN 2016/2024: Process the SyMRI sequence to extract the REMyDI myelin content.

IRB MGH 2007P001274: Acquire and analyze the *ex vivo* brain tissue samples.

3.2 PROCEDURES AND PARTICIPANTS

Study I. A prospective longitudinal cohort consisting of 37 participants with MS according to the, at the time of study initiation, concurrent diagnostic criteria (Poser *et al.*, 1983) (26 females; 42±10 years old; 11±8.5 years disease duration; median EDSS 4.5, range 0.0–8.0), were consecutively recruited from the Department of Neurology, Karolinska University Hospital in Huddinge. At baseline, 23 participants were diagnosed with RRMS, 11 with SPMS and 3 with PPMS. Baseline study involvement consisted of standardized neurological and neuropsychological testing but only a standard 2D brain MRI. Clinical and volumetric 3D brain MRI were completed after 9 years and 17.5 years (mean 17.5±0.4 years). All of the participants enrolled participated in the initial 9-year follow-up, while 23 participants remained at the last time point (18 females; 57±8.0 years old, 27±6.9 years disease duration; median EDSS of 6.0 (range 1.5–8.0); 3 RRMS, 20 SPMS, 0 primary progressive MS). Losses to follow-up at the final time point were due to: death (N=5), acquired MRI contraindications (N=3), declined further participation (N=3), unreachable (N=3).

Study II. We prospectively enrolled 35 study participants diagnosed with MS (20 RRMS, 15 SPMS) according to the concurrent 2010 McDonald criteria (Polman *et al.*, 2011). The specific inclusion criteria were as follows: between 18 to 65 years of age; on stable DMT or off DMT for at least three months; absence of relapse(s) within the preceding three months and no corticosteroid use within a month prior to study enrolment. All of the RRMS participants were within five years of disease onset and considered in the early stage of the disease. We also recruited 11 age-/gender-matched healthy volunteers (five females, age 43.5±9.1 years) as controls. The general exclusion criteria included MRI contraindications, significant medical history or comorbidities, and/or any neurological disease (other than MS).

Studies III and IV. Studies III and IV consisted of *ex vivo* and *in vivo* sub-studies. The prospective *ex vivo* sub-study consisted of three coronal hemispheric brain tissue samples from different donors with MS that were acquired from the Rocky Mountain Tissue Bank. All donors were diagnosed with SPMS, including a 46-year-old female, a 71-year-old female and a 56-year-old male. The prospective *in vivo* sub-study included 92 consecutively enrolled participants, including 71 participants diagnosed with MS in accordance to the concurrent 2010 McDonald criteria (Polman *et al.*, 2011) accounting for all MS subtypes and an additional 21 age-/gender-matched controls. The pre-defined exclusion enrolment criteria were MRI contraindications, neurological comorbidities or a history of head trauma; none of which applied to the cohort. Study participants were grouped into healthy controls (*N=21*), RRMS (*N=53*), SPMS (*N=15*) and PPMS (*N=3*). Study III additionally included a repeatability cohort (13 MS, 19 controls) that were scanned once and again after repositioning to assess the robustness of the myelin model. In Study IV, the progressive MS (PMS) participant group consisted of the SPMS (*N=15*) and PPMS (*N=3*) participants.

3.3 CLINICAL EVALUATIONS

Study I. Physical disability in participants with MS was assessed with the Expanded Disability Status Scale (EDSS) by the same neurologist (S.F.) at all time points (Kurtzke, 1983). The standardized neuropsychological evaluation of all participants at all of the time points was administered by the same neuropsychologist (Å.B.). The testing battery consisted of four tests, representing different cognitive functions. The specific tests were the; Symbol Digit Modalities Test (SDMT), Rey–Osterrieth Complex Figure Test copy (ROCFT), F-A-S Verbal Fluency Test (FAS) and Rey Auditory Verbal Learning Test (RAVLT) with encoding and 30-min retention. However, due to a different native spoken language other than the testing language (Swedish), FAS was not performed in one patient and one control. Additionally, one patient was unable to participate in the SDMT and ROCFT at follow-up due to impaired vision following optic neuritis. The raw test scores were normalized into *z*-scores based on normative reference data concerning age, gender and educational level (Hawellek *et al.*, 2011; Lezak *et al.*, 2012). Abnormally low values were defined as being less than two standard deviations of the normative score. Cognitive impairment was defined as having an abnormally low score in any one of the four tests representing unique cognitive domains. To reduce the dimensionality of the results, we transformed the cognitive measures into a singular weighted metric, a

cognitive index reflecting the overall global neuropsychological functioning by extracting the principal component analysis of the transformed *z*-scores of all tests in RStudio 0.99.489 (Hawellek *et al.*, 2011).

Study II. Neurologic disability was assessed using the EDSS (*N*=35) within a week from the imaging procedures as part of the MS participants standard clinical work-up with the referring physician. Ambulatory disability was determined by the timed 25-foot walking test. Disability in fine motor skill was determined by 9-hole peg test. The SDMT, while routinely applied and reflective of cognitive disability was not chosen to be included since this study primarily relates the spinal cord and physical disability, but also to limit the number of variables in the study.

Studies III and IV. Physical disability (EDSS) in participants with MS was assessed by an experienced neurologist in MS (S.F.) (Kurtzke, 1983), except for one patient (*N*=70). Cognitive disability was measured using the SDMT (Langdon *et al.*, 2012) (*N*=48). Baseline clinical assessments were made within six months of the MRI acquisition. Longitudinal cognitive and physical disability assessment was repeated for both EDSS (*N*=70) and SDMT (*N*=32), with a mean respective follow-up time of 2.0±0.8 years and 1.5±0.4 years. The raw SDMT scores were then normalized into *z*-scores, similarly to Study I. Additionally, in Study IV, we also included the MSIS physical (*N*=40) and psychological (*N*=39) (Hobart *et al.*, 2001), and EuroQol-5D (EQ-5D, *N*=38) as a quality-of-life indicator (Balestroni and Bertolotti, 2012).

3.4 MRI ACQUISITION

Study I. Volumetric brain MRI was performed at the latter two time points (9- and 17.5-year follow-up) using clinical 1.5 T MRI scanners: Siemens Magnetom Symphony and Avanto (Siemens Healthcare, Erlangen, Germany). The mean time between the follow-ups was 8.3±0.4 years. T_2-FLAIR images were acquired for lesion segmentation (resolution 1.0×1.0×3.0 or 1.0×1.0×1.5 mm^3; inversion pulse flip angle 180°/variable 120°; repetition, echo and inversion times 9000/5000, 7.0/3.1, 3000/1100 ms). T_1-weighted 3D images were obtained for volumetric analysis (resolution 1.0×1.0×1.5 mm^3; flip angle 15°; repetition, echo and inversion times 1350/1910, 110/411, 2500/1800 ms).

Study II. All of the study participants had brain and spinal cord imaging on a research-grade 7 T MRI scanner (Siemens Healthcare, Erlangen, Germany). Spinal imaging was acquired with an in-house developed 19-channel receive array and a 4-channel transmit array coil (Zhao *et al.*, 2014). The imaging protocol consisted of both axial and sagittal 2D multi-echo fast low-angle shot (FLASH) T_2^*-weighted spoiled gradient-echo sequences (axial and sagittal: repetition, echo time = 500, 7.8/13.73/18.42 ms, flip angle = 55°, resolution = 0.4×0.4×3.0 mm^3). Axial acquisitions were aligned perpendicularly to the spinal cord. The entire cervical spinal cord (C1 to C7) was imaged axially using two or three slabs at perpendicular alignment depending on the natural degree of spinal cord curvature, as demonstrated in Figure 15 on the following page. To enhance image quality by mitigating bulk movement all study participants were coached preceding the scanning acquisition to lessen physiological noise such as swallowing, respiration and lingual movement (Kearney *et al.*, 2015).

Brain 7 T imaging was performed in 29 of 35 MS participants and all the controls with a custom-built 32-channel phased-array head coil to acquire a 2D single-echo FLASH T_2^*-weighted spoiled gradient-echo pulse sequence (repetition time, echo time = 1700, 21.8 ms, resolution = 0.33×0.33×1.0 mm^3) for cortical lesion segmentation. Study participants were additionally scanned on the 3 T Skyra CONNECTOM scanner (Siemens Healthcare, Erlangen, Germany) using a custom-made 64-channel head coil to acquire a 3D T_1-weighted multi-echo magnetization-prepared rapid gradient-echo sequence (MEMPRAGE, repetition/inversion/echo times: 2530, 1100, 1.15/3.03/4.89/6.75 ms, flip angle 7°, resolution 1.0×1.0×1.0 mm^3) for cortical surface reconstruction and to measure cortical thickness. Additionally, a 3D T_2-FLAIR (repetition, inversion, echo time = 5000, 1800, 393 ms, resolution 1.0×1.0×1.0 mm^3) was acquired at 3 T for manual lesion segmentation.

Studies III and IV. The *ex vivo* sub-study MS brain tissue specimens were scanned at room temperature to ensure even temperature throughout the tissue. The quantitative multi-parametric sequence (Warntjes *et al.*, 2008) was acquired using a Siemens Trio 3 T MRI scanner and a 32-channel head coil to obtain a high signal-to-noise ratio. High-spatial resolution was of primary importance to reduce partial volume effects and allow for better registration with histology, (coronal: resolution: 0.39×0.39×2.0 mm^3, with a 0.75 distance factor, repetition, echo time: 2400 ms, 25/101 ms, flip angle 120°, 6 averages, total acquisition time 32:47

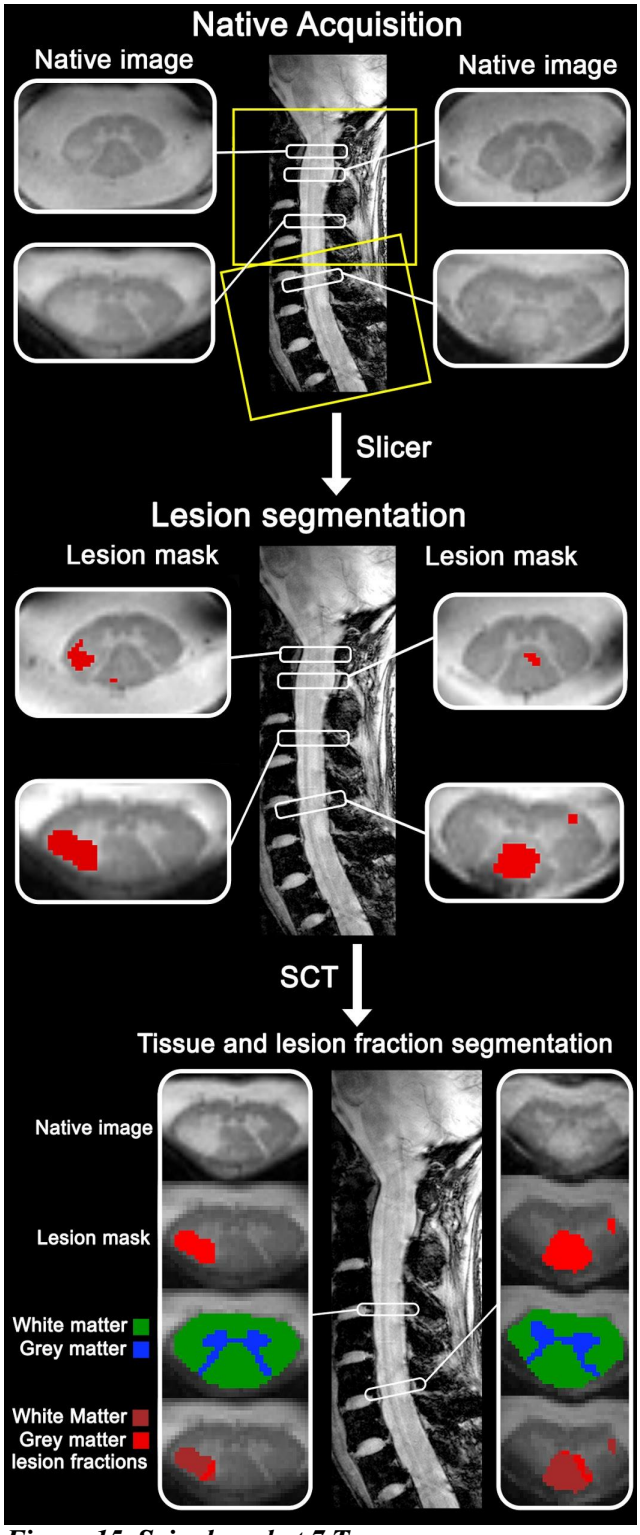

Figure 15. Spinal cord at 7 T.

A 32-year-old female participant with RRMS (4.8-year disease duration, EDSS score 2.5). Acquisition with full cervical coverage aligned orthogonally to the spinal cord to reduce partial volume effects. Spinal cord lesions were manually segmented in Slicer and then combined with the white matter and grey matter tissue segmentations from SCT to isolate the grey matter and white matter lesion fractions.

minutes). SyMRI (version 11.0 beta 4 for Mac; Synthetic MR, Linköping, Sweden) was used to extract the R_1, R_2 and PD maps. To compensate for the fixation and temperature effects, the R_1 and R_2 rates were rescaled by a factor of 3.3 and 1.9 respectively, based on correction factors available in the literature (Birkl *et al.*, 2016). SyMRI was also used to generate PD-weighted images (repetition and echo time = 8000, 10 ms) for manual tissue segmentation. The *in vivo* sub-study applied the same scanner, model, software and sequence that were used *ex vivo,* however the synthetic MRI sequence was acquired in a more clinically feasible time frame (axial, voxel size: 0.9×0.9×3.0 mm^3 with a 0.5 distance factor, repetition, echo, effective inversion times: 4260, 22/100, 150/580/2000/4130 ms, flip angle 120°). The duration of the acquisition varied from 6:50-7:47 minutes, due to the number of slices to cover the full intracranial volume. A 12-channel head coil was used *in vivo* since it was routinely applied in the clinical MS protocol and allowed for large head sizes and headphones for patient comfort. The SyMRI processing suite was then used to produce the quantitative maps, tissue maps, REMyDI, T_1-weighted images (repetition, echo times: 500, 10 ms) and T_2-FLAIR images (repetition, echo, inversion times: 15000, 100, 3000 ms).

3.5 IMAGE PROCESSING

Lesion segmentation. Across Studies I, III and IV the respective T_2-FLAIR images were used to perform probabilistic segmentation of MS lesions in Lesion Segmentation Toolbox (versions 2.0.12 and 2.0.15 in Studies I and III/IV respectively, Technische Universität München, Munich, Germany). Initial probabilistic maps were thresholded by a value of 0.5 to binary lesion masks in FMRIB Software Library (FSL, version 5.0, Oxford University, Oxford, UK) (Jenkinson *et al.*, 2012). The binarized lesion masks were then manually corrected and then cross-reviewed by trained raters (R.O. and M.P.) to be finally verified by an experienced rater (T.G., radiologist) in ITK-SNAP (version 3.6.0, University of Pennsylvania, Philadelphia, USA) (Yushkevich *et al.*, 2006). Examples of lesion masks from LST are shown in Figure 6.

The lesion masks in Study II, for the brain and spinal cord, were fully manually segmented on the T_2^*-weighted gradient-echo image in Slicer (Figure 15, page prior) (v. 4.2.0) (Fedorov *et al.*, 2012), based on the consensus by two experienced raters (C.A.T and C.M.). Cervical spinal cord lesions were axially segmented and then confirmed on the corresponding sagittal acquisition. Spinal cord lesion fractions were quantified as the proportion of lesioned tissue in grey and white matter respectively, by combining the lesion mask with the grey and white matter segmentations. Representative examples of spinal cord lesion segmentations are shown in Figure 15. Before manual segmentation of brain lesions, the two axial T_2^*-weighted imaging slabs were boundary-based registered together into the same space as the 3 T anatomical FreeSurfer reconstructions as previously detailed (Greve and Fischl, 2009; Mainero *et al.*, 2015; Louapre *et al.*, 2018). Brain 7 T scans had to be discarded in 6 of the 46 study participants because of severe motion artifacts. For those with motion the brain lesion segmentation was instead manually done using the 3 T 3D T_2-weighted FLAIR volumes. Brain lesion volumes were extracted using FSLstats.

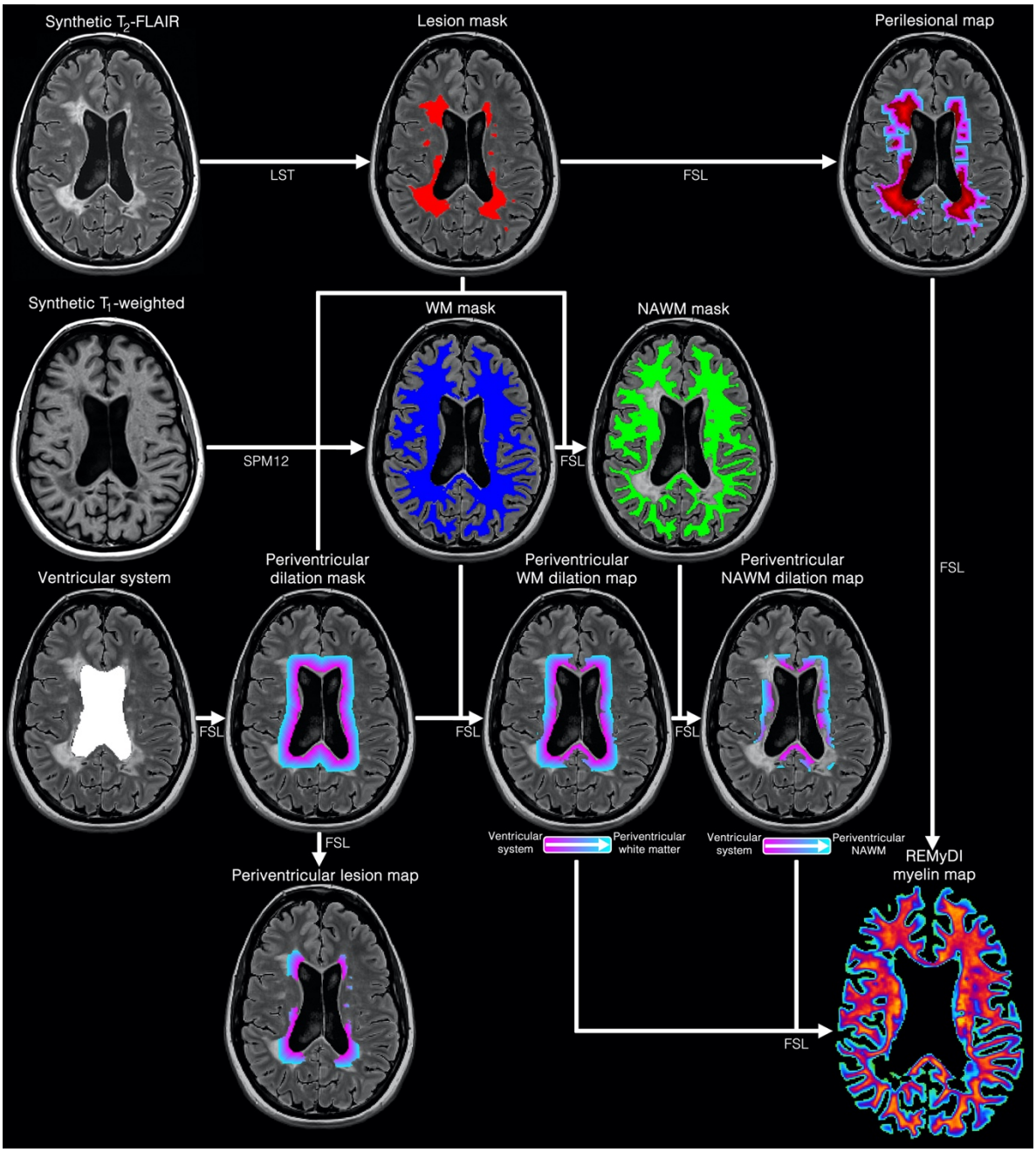

Figure 16. Periventricular myelin and lesion mapping schema.

The synthetic T_2-FLAIR is used as input for semi-automatic lesion segmentation by LST. Synthetic T_1-weighted image used as input for SPM to segment the white matter (WM), to then subtract the lesion mask to create the (normal-appearing white matter) NAWM mask. The CSF mask is automatically produced in SyMRI and was manually edited to contain only the ventricular system and choroid plexa. Ten voxel-wise concentric dilations were seeded from the ventricular system mask using FSL tools to generate the periventricular dilation mask. Periventricular voxel-wise dilations were masked to represent the white matter, NAWM and lesioned masks. The mean REMyDI myelin value within the respective layers was extracted using FSL tools.

Volumetric segmentations. For Study I the intracranial volume, grey matter fraction, white matter fraction, thalamic fraction and hippocampal fraction (Figure 7) were segmented using VolBrain 1.0 (Universitat Politècnica de València, Valencia, Spain). The corpus callosal fraction (Reuter *et al.*, 2012) was extracted from brain reconstructions processed using the longitudinal stream of FreeSurfer (v5.3.0, Harvard University, Boston, USA). To reduce individual scaling effects, all measurements were normalized to the intracranial volume, yielding the grey matter fraction, white matter fraction, lesion fraction, corpus callosal fraction, hippocampal fraction and thalamic fraction.

For Study II, the segmentation of the cervical spinal cord and cross-sectional areas measurements were obtained with the Spinal Cord Toolbox (SCT, v3.0.1) (De Leener *et al.*, 2017), a publicly available free tool (Figure 15). SCT begins with "PropSeg" algorithm that applies a support vector machine that identifies the spinal cord center (Gros *et al.*, 2018), then SCT applies a deformable model to propagate the tubular surface around the spinal cord edge and along the length of the cord (De Leener *et al.*, 2014). The grey and white matter were then obtained by first registering each individual to the PAM50 template (De Leener *et al.*, 2018) by a combined multi-atlas template-based approach (Dupont *et al.*, 2017), chosen because of the inherent T_2^*-weighted image contrast. The grey and white matter tissue segmentation was done on the axial spinal images. Cervical spinal cord cross-sectional areas (mm^2, at C2-C3) for both grey and white matter were automatically calculated in SCT. The cortical surface reconstruction was generated using FreeSurfer (v. 5.3.0) (Fischl, 2012) with the 3D 3 T T_1-weighted (MEMPRAGE) images as input. White matter hypointensities and defects in the topological cortical surface due to white matter and leukocortical lesions were semi-automatically corrected by lesion in-painting in FreeSurfer. The mean cortical thickness and total intracranial volume were calculated from the finalized reconstructions. The ventricular system including the choroid plexa and white matter segmentations were also from FreeSurfer.

For Studies III and IV, the quantitative maps in SyMRI were used to calculate the intracranial volume (Ambarki *et al.*, 2012; Granberg *et al.*, 2016). To extract the myelin content specifically in normal-appearing grey and white matter, semi-manual segmentations were performed. The T_1-weighted images were segmented using Statistical Parametric Mapping 12 (SPM, University College London, London, UK) (Ashburner and Friston, 2005), to obtain probabilistic maps of the grey matter and white matter. The T_2- FLAIR-based lesion mask was subtracted from the WM mask to produce the normal-appearing white matter (NAWM) mask using FSL. The ventricular mask from Study II was derived by combining the different ventricles and choroid plexus segmentations in FreeSurfer. However, the ventricular mask in Study IV was extracted from the quantitatively derived CSF mask in SyMRI due to the inherent registration of the CSF mask. Moreover, FreeSurfer has been optimized on a 3D T_1-weighted image acquired at 3 T, and the SyMRI volume is a 2D acquisition with rather thick slices. The SyMRI CSF mask was manually edited to include only the ventricular system (including choroid plexa) by a trained rater (R.O.) to be reviewed by a radiologist (T.G.) and finalized by expanding the volume by one voxel, using FSL tools, to account for CSF partial voluming effects. The processing pipeline for Study IV, is shown fully in Figure 16 on the page prior.

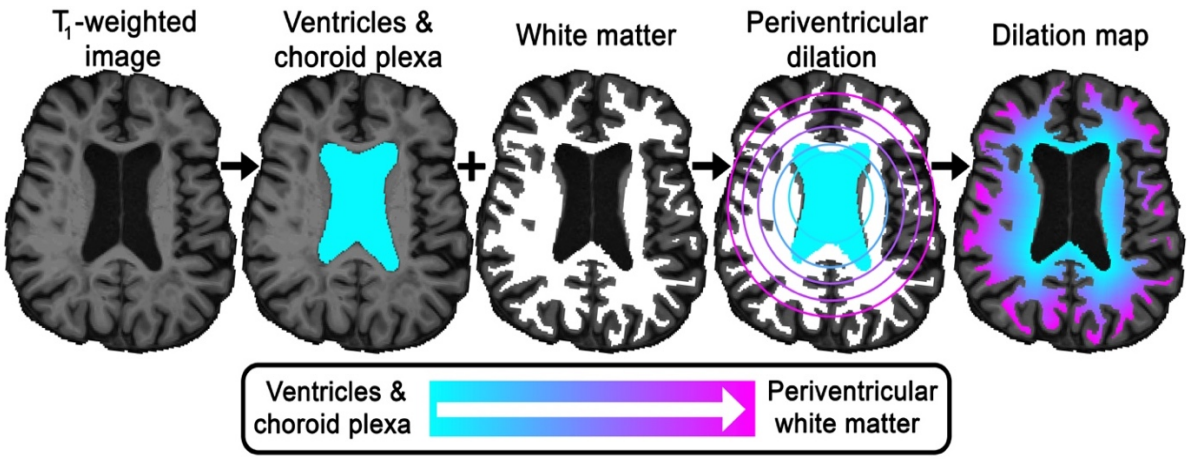

Figure 17. Periventricular dilation mapping schema. *A representative example of the CSF-proximity mapping in the periventricular region for Study II in an SPMS participant (female, 63-years-old, 33-year disease duration, EDSS score 2). The ventricle and choroid plexus segmentations (FreeSurfer) were combined, from which concentric 3D voxel-wise dilations expanded radially using scikit-image. The concentric dilation map was then masked to isolate the lesion dilation map, which can then measure lesion fraction as a function of distance from the ventricular system CSF.*

Distance-based sub-segmentations. The concept of distance-based voxel-wise lesion segmentations was first conceptually applied in Study II (Figure 17) for the spinal cord and then the brain using scikit-image (version 0.14.1) NumPy and SciPy to create a concentric layer map on the basis of distance from the CSF. In the brain, concentric dilations were seeded in the ventricular system, which is continuous with the central canal. In the spinal cord, dilations began at the inner central canal CSF-surface, to project through the central spinal cord tissue outwardly ending at the outer subpial CSF-surface (van der Walt *et al.*, 2014; Louapre *et al.*, 2018). In the brain, dilations began at the ventricle and white matter CSF surface and extended into the surrounding white matter (Figure 17). Concentric voxel-wise dilations expanded with 10 iterations, in widths of 2 and 4 voxels, in the cervical spinal cord and brain respectively (Louapre *et al.*, 2018). The layer directly bordering the ventricular CSF-surface was removed in Study II, based on the recommendation of a previous spinal cord study, because of CSF signal producing partial volume effects (Kearney *et al.*, 2014; Liu *et al.*, 2015). Lesions were mapped as a function of CSF-proximity from the central canal and ventricular surfaces by isolating the lesion volumes from the MS participants' spinal cord and brain lesion segmentation in FSL tools. The participant's individual dilation level lesion volume was then normalized to the total lesion volume of each MS patient and the volume of each respective concentric dilation level both in the spinal cord and brain. This process was for all lesion mapping techniques. A subgroup analysis was also done where the rank difference between MS subtypes was calculated in the cervical spinal cord and brain.

The periventricular concentric dilation scheme for Study IV was again seeded in the ventricular system, first dilated by one voxel accounting for CSF signal contamination, and then expanded outwards into the parenchyma in 10 voxel-wise iterations. The periventricular dilation mask was then selectively masked using three tissue-specific masks, the NAWM, WM and lesions, using FSL tools, highlighted in Figure 16. Mapping of the periventricular lesion fraction was

done by normalizing the individual lesion volume captured in that individual dilation layer by the total lesion volume in the brain and the volume of the individual dilation layer (as administered in Study III). Lastly, the lesion mask was separately iteratively eroded and concentrically expanded from the lesion border, masked by the WM mask, and combined to create the perilesional volume, using FSL tools. Lastly, the mean myelin content of the individual concentric rings within the periventricular WM/NAWM dilation maps and median perilesional maps were extracted from the REMyDI myelin map using FSL tools, as shown here in Figure 18.

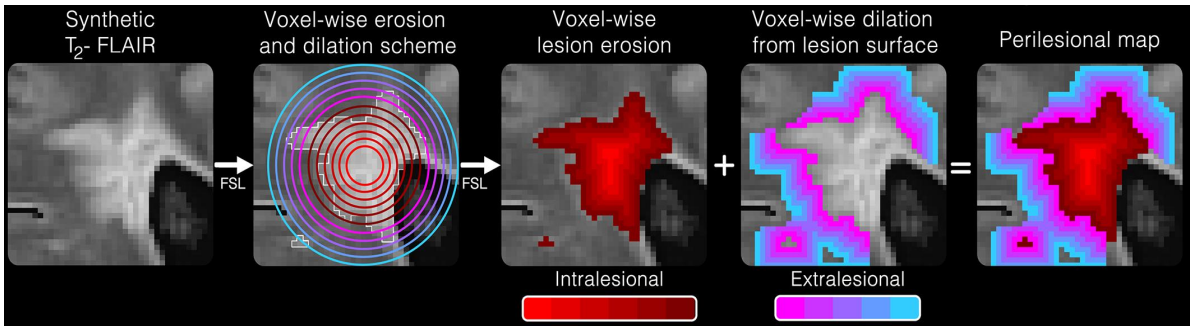

Figure 18. Perilesional myelin mapping schema. *A 40-year-old female participant with RRMS (14-year disease duration, EDSS score 1.0, SDMT z-score -1.0). The lesion mask is separately and sequentially eroded and expanded. The mean REMyDI myelin value within the respective layers is then extracted.*

3.6 HISTOLOGICAL EVALUATION

The histological slicing and the three staining methods were conceptualized and executed by a trained histological technician (I.P.) and first optimized on sections from a bovine brain tissue sample of comparable size with the intent to ensure an even staining uptake across the sample's entirety. All of the histological analyses were conducted by the same trained histological technician. The slicing procedure was guided by the *in vivo* MRI images such that we could attain the most optimal level for comparison of *in vivo* MR images to the 10-micrometer thick cryomacrotome *ex vivo* slices. The PLP-immunostaining was based on PLP1 primary monoclonal antibody: plpc1 Mouse/IgG2a (Cat# MA1-80034) kit was used for the staining procedure. Luxol Fast Blue-cresyl echt violet staining was administered through an *American Master Tech Scientific* kit (Cat# KTLFB). The Bielschowsky silver staining was applied by the standardized method. The PD-weighted image was used to guide the registration of the MRI and histological images using a ANTsRegistration (v2.1.0, Tustison *et al.,* 2014) and are shown in Figure 19.

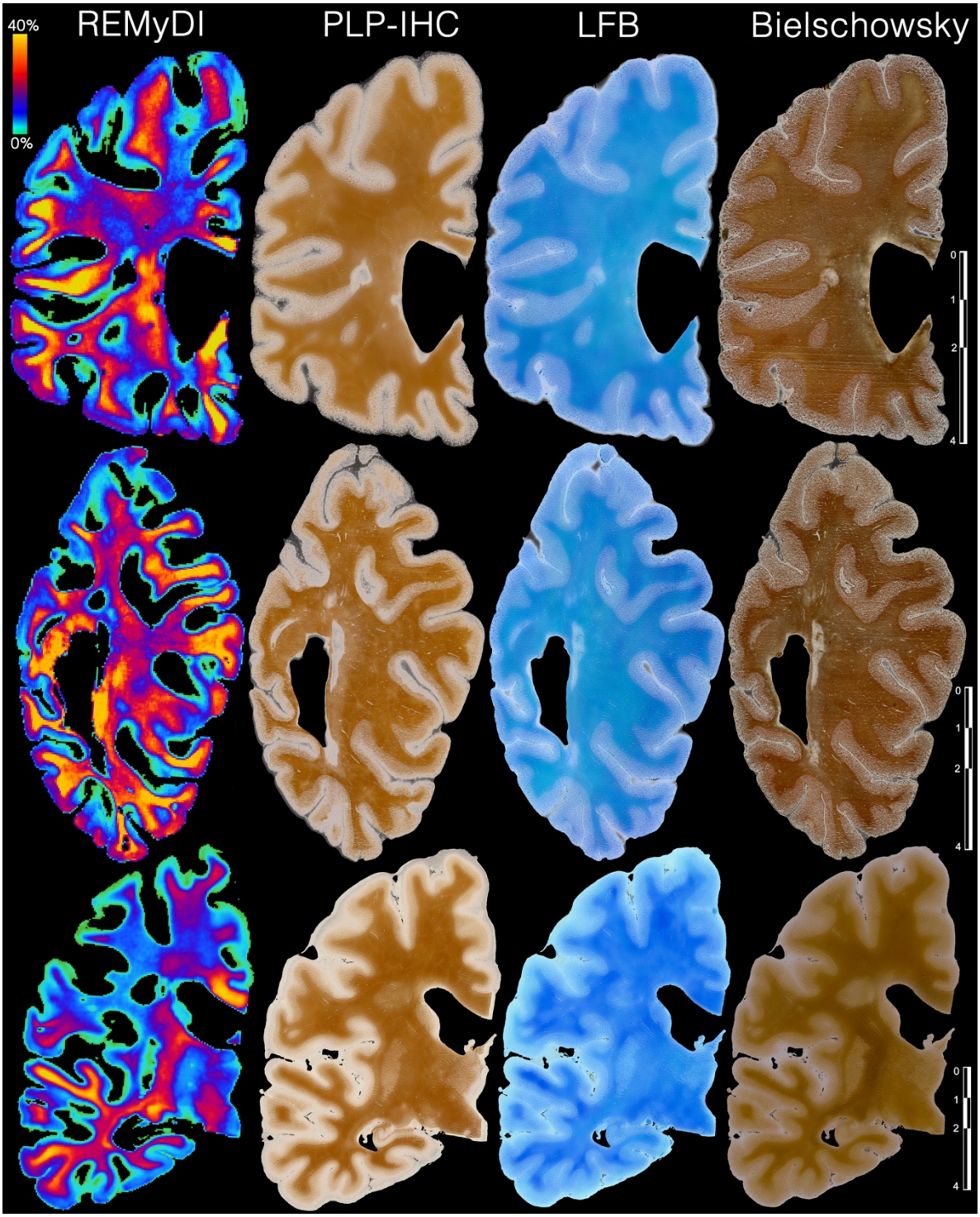

Figure 19. Myelin imaging. *Coronal whole-hemispheric10 µm-thick brain tissue samples from three SPMS donors.* ***Top row:*** *Frontal coronal brain tissue sample from a 46-year-old donor.* ***Middle row:*** *Parietal coronal brain tissue sample from a 71-year-old donor.* ***Bottom row:*** *Frontotemporal coronal brain tissue sample from a 56-year-old. Scale bars for the corresponding rows are presented in cm.*

3.7 STATISTICAL ANALYSES

Software and statistical significance. All statistical analyses were performed in IBM SPSS Statistics versions 23, 24, and 25 for Mac (IBM, Armonk, USA) for studies I, II and III/IV respectively. A statistical significance threshold of $P<0.05$ (two-tailed, equal variances not assumed) was used across all studies.

Normality. The normality of the data was determined by the Shapiro-Wilk test, histogram analysis and ensuring both the skewness and kurtosis values were within a range of ±1 for all studies. Typically, measures of anatomical and tissue volumes were normally distributed, this was also true for the myelin quantification measurements. Meanwhile, metrics regarding lesions (volume, count, fraction) and EDSS scores were non-normally distributed. Additionally, when able, we chose to graphically present the data points and allow the reader a visual grasp of the data's distribution.

Bivariate correlations: The bivariate correlations between parametric variables were calculated using Pearson correlation and Spearman's correlation for non-parametric data. The voxel-wise comparison of histological and REMyDI based myelin content was done using Pearson correlation

Group comparison. Group-level comparisons for parametric variables were compared by the independent sample t-test (equal variance not assumed) and one or more non-parametric variables by independent samples Mann–Whitney U-test (both two-tailed). Sex differences between MS participants and controls were assessed by a chi-squared test (two-tailed). Differences in age were considered using independent samples t-test (two-tailed). The lesion fraction dilation layer group differences were assessed through Mann-Whitney U-test (two-tailed, equal variance not assumed) and represented graphically by displaying the Mann-Whitney rank difference. Paired non-parametric variables were assessed by the Wilcoxon signed-rank test (two tailed). The normally distributed dilation layer periventricular myelin content group differences in Study IV were assessed by independent samples t-test (two-tailed).

Multiple comparison correction. False discovery rate correction for multiple comparisons was applied for each of the two clinical disability measurements across the corresponding baseline, longitudinal and corrected comparisons (Benjamini and Hochberg, 1995) in Study I and Study III. However, exploratory lesion fraction (Study II) and myelin mapping analyses (Study IV) were not corrected for multiple comparisons, rather the data was presented graphically to provide the reader their own opportunity to determine the bearing of the findings.

Regression analysis. Individual multiple stepwise linear regressions in Studies I, II and III with the clinical disability metrics as the dependent variable and respective MRI metrics as independent variables were accomplished by transforming the non-parametric variables, for example by $\log_{10}$ or square root transformation. Regression results are provided as the respective standardized coefficients (β).

4. RESULTS

4.1 STUDY I

Progression of cognitive impairment

Cognitive dysfunction was observed to develop in a predominantly linear manner on a group level in MS over time, as illustrated in Figure 20A. When considering the contour plot in Figure 20B, we can see that cognitive dysfunction is often coupled with physical disability measured by EDSS ($\rho=-0.47$, $P<0.001$). However, in some participants with MS, there was a sparing of cognitive functioning despite severe physical disability or vice versa. Among the six participants with an EDSS above 6.0 and an impaired cognitive index *z*-score below 0, four were imaged with spinal MRI, to reveal spinal cord lesions in three participants (75%). Changes in all neuropsychological tests over the disease duration were rather modest. SDMT had the highest proportion of abnormally low z-scores (40%), followed by ROCFT (24%), RAVLT encoding (18%), FAS (17%) and RAVLT retention (9%). The largest cognitive decline over the disease duration was observed by the ROCFT, while SDMT and RAVLT revealed more modest changes. The FAS remained relatively stable throughout the disease course.

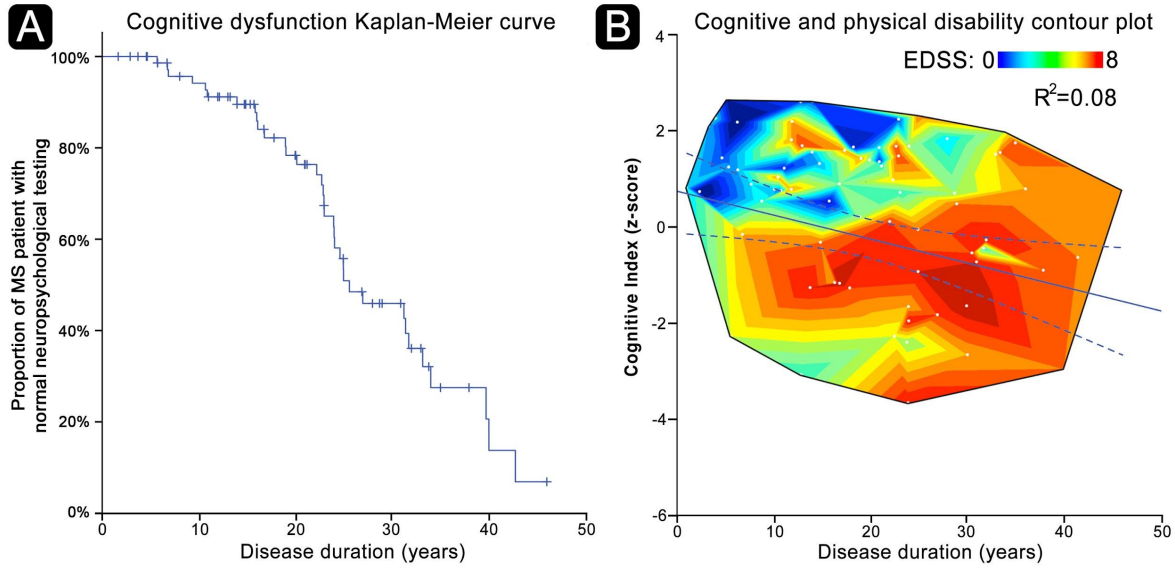

Figure 20. Progression of cognitive dysfunction in MS over the disease duration.
A. *Kaplan-Meier curve demonstrating a predominantly linear trend in the cumulative prevalence of cognitive impairment.* ***B.*** *Cognitive function (cognitive index) and physical disability (color contours) is often linked to each other but may also be decoupled, showing mainly cognitive or physical disability.*

Progression of lesion accumulation and atrophy

The neuroinflammatory and neurodegenerative progression, measured through the lesion accumulation and atrophy rates were also found to develop linearly on a group level but with large inter-individual differences. Lesion accumulation expanded, on average, at a rate of 7.2% per year. Whereas the annual grey and white matter atrophy rates were 0.70% and 1.3% respectively. The annual atrophy for the neuroanatomical volumes were: corpus callosum (2.5%), thalami (0.20%) and hippocampi (−0.56%.).

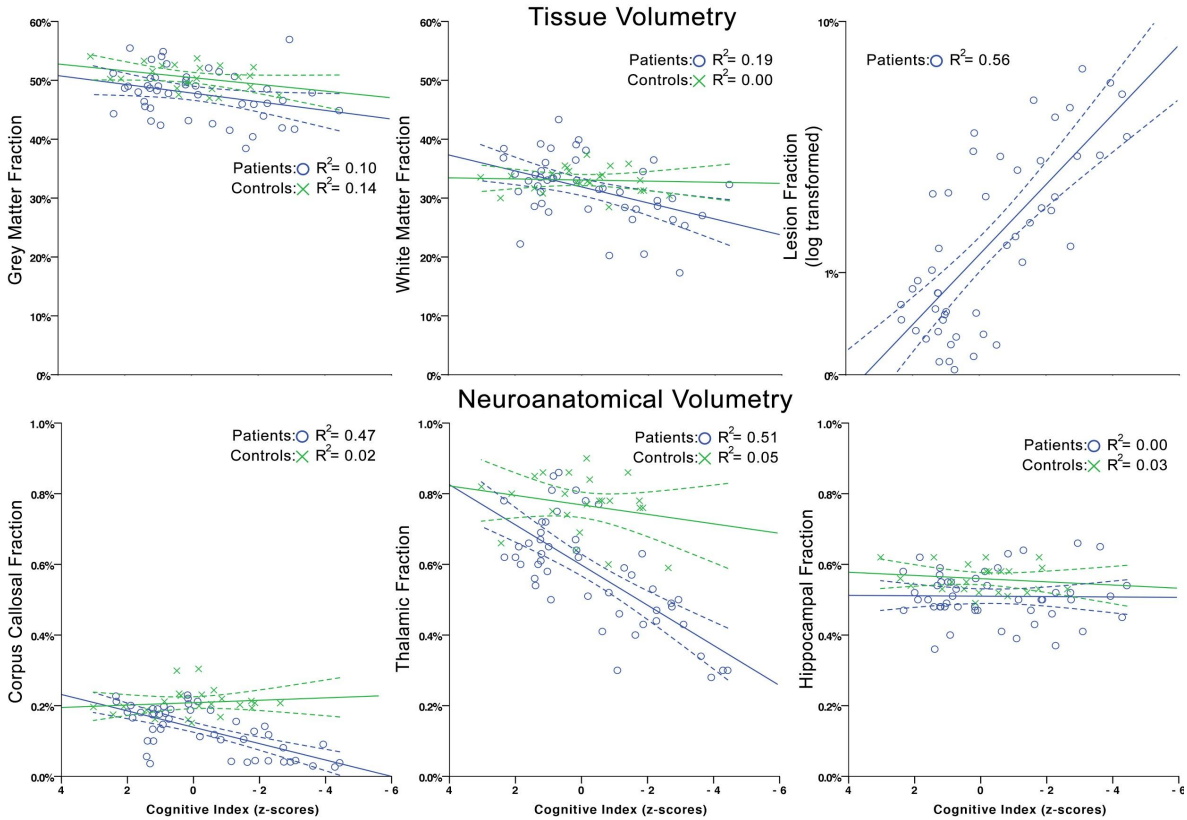

Figure 21. Neuroanatomic and tissue correlates of cognitive dysfunction. *Associations of cognitive functioning with tissue and neuroanatomical volume fractions in MS patients and controls.*

Neuroanatomical and tissue correlates of cognitive dysfunction

The cognitive index was found to correlate with imaging measurements in both MS participants and controls, illustrated in Figure 21. Cognitively impaired participants with MS had lower white matter (*29.2±5.3% vs. 34.1±4.5%, P=0.002*), corpus callosal (*0.098±0.06% vs. 0.17±0.05%, P<0.001*), thalamic (*0.50±0.13% vs. 0.66±0.13%, P<0.001*) tissue fractions and a higher lesion fraction (*2.8±2.0% vs. 1.1±1.1%, P<0.001*) compared to cognitively preserved MS participants. However, there was no difference identified in the hippocampal fraction between cognitively impaired and preserved individuals (*0.51±0.08% vs. 0.51±0.06%, P=0.67*). There was a trend for less grey matter fraction in cognitively impaired participants with MS (*46.5±4.4% vs. 49.0±3.6%, P=0.039*) but this did not survive correction for the false discovery rate. Multiple linear regression analysis showed that the cognitive index in MS was most influenced by the lesion and corpus callosal fractions and also for the SDMT and RAVLT encoding tests. However, only the lesion fraction was significant for RAVLT retention and only the corpus callosal fraction for ROCFT. FAS was also associated with the combination of hippocampal fraction alongside lesion fraction. A stepwise linear regression including only the first MRI time-point to test for a potential predictive value was highly comparable to that of the longitudinal regression results. The value of the MRI baseline brain volumetrics for the prediction of cognitive performance 8.5 years later was found for the lesion fraction (*β=-0.53, P=0.003*) and corpus callosal fraction (*β=0.42, P=0.01*). Even when accounting for the baseline cognitive performance, the lesion fraction remained as an independent predictor (*β=-0.35, P=0.008*), highlighting the influence of the lesion fraction on cognitive dysfunction.

4.2 STUDY II

Spinal cord and brain MRI results

Cervical spinal cord lesions were identified in 29 of the 35 (83%) participants with MS; in 14 of the 20 (70%) with RRMS (median 2, range 0-9 lesions) and in all 15 with SPMS (median 4, range 2-9 lesions). The SPMS participants tended to have higher cervical spinal cord lesion count (*P=0.074*). Participants with MS had a lower mean C2-C3 cross-sectional cord area relative to healthy controls, in both the grey matter (*6.8±1.5 vs. 7.70±0.94 mm^2, P=0.021*) and white matter (*52.8±9.2 vs. 58.1±4.9 mm^2, P=0.019*). However, there were no significant differences detected between RRMS and SPMS groups. There was a higher proportion of lesioned spinal cord tissue in SPMS vs. RRMS participants in the grey and white matter, mostly in the white matter (*RRMS 2.6±2.9 vs. SPMS 9.3±13.3 %, P=0.05*). Naturally, the spinal cord grey and white matter lesion fractions were strongly related to each other (ρ*=0.91, P <0.001*). Likely related to the observation that all of the MS participants with spinal cord lesions had lesion portions affecting the grey and white matter tissues, except for two of the MS participants (1 SPMS and 1 RRMS) who had solely white matter spinal cord lesions. Those diagnosed with MS also had thinner cortices versus controls (*2.33±0.12 vs. 2.41±0.07 mm, P=0.017*), and within the MS participants, there was more profound cortical thinning in those with SPMS than with RRMS (*2.26±0.10 vs. 2.40±0.10 mm, P<0.001*). There was a positive association between spinal cord grey and white matter lesion fractions and the brain white matter lesions (*r=0.39, P=0.021 and r=0.37, P=0.033*).

Lesion mapping as a function of distance from CSF

The results of the brain periventricular lesion mapping are graphically summarized in Figure 22. By applying brain periventricular CSF-proximity lesion mapping using inside-out assessment white matter MS lesions in the brain were found to more likely occur nearest the ventricular system. The gradient pattern of lesions originating nearer the CSF, was present in both disease stages and particularly more evident in those with SPMS. This is reflected in that the normalized lesion fraction percent was higher in participants diagnosed with SPMS as compared to RRMS, across nearly every periventricular layer, but highest in the two layers nearest the CSF, being layer 1 (*3.3±6.2% vs. 0.8±1.1%, P=0.002*) and layer 2 (*3.3±6.5% vs. 0.3±1.8%, P=0.004*).

The results of the cervical spinal cord and brain lesion mapping are graphically summarized in Figure 22. Through inside-out CSF-proximity mapping, spinal cord lesions were found to have a distribution closely corresponding to that of a pseudo-bell curve pattern, being skewed towards either of the two CSF-surfaces of the spinal cord. When comparing the whole lesion fraction in RRMS and SPMS participants, we identified that the bimodal inner versus outer skewness observed in the whole MS cohort was driven by RRMS participants' greater likelihood for lesion development nearer the outer subpial aspect of the cervical cord and SPMS participants' likelihood for lesion development nearer the inner aspect of the central canal. The whole lesion fraction was greater in RRMS participants relative to SPMS participants at layer

7 (*2.8±4.9% vs. 1.0±1.1%, P=0.005*), layer 8 (*3.4±2.2% vs. 0.4±1.1%, P<0.001*), layer 9 (*1.2±2.5% vs. 0.0±0.5%, P=0.002*) from the central canal CSF-surface to the subpial CSF-surface. In SPMS participants, compared to RRMS participants, lesions were mostly located in the layers nearest the central canal CSF-surface, within layer 1 (*1.6±5.1% vs. 0.0±1.1%, P=0.029*), layer 2 (*2.6±6.1% vs. 0.2±1.6%, P=0.023*), layer 3 (*2.6±5.5% vs. 0.6±2.4%, P=0.016*) and layer 4 (*2.4±3.4% vs. 0.8±2.9%, P=0.057*) from the central canal to the cord perimeter. These lesion distributions were mostly maintained when only considering the tissue specific lesion fractions within the grey and white matter. The white matter spinal cord lesion component distribution pattern was very similar for all MS participants and disease subtypes. The grey matter lesion distribution also maintained a comparable pattern, but slightly shifted more internally with a narrower distribution across fewer levels, that is likely a result of the anatomical distribution of grey matter in the spinal cord.

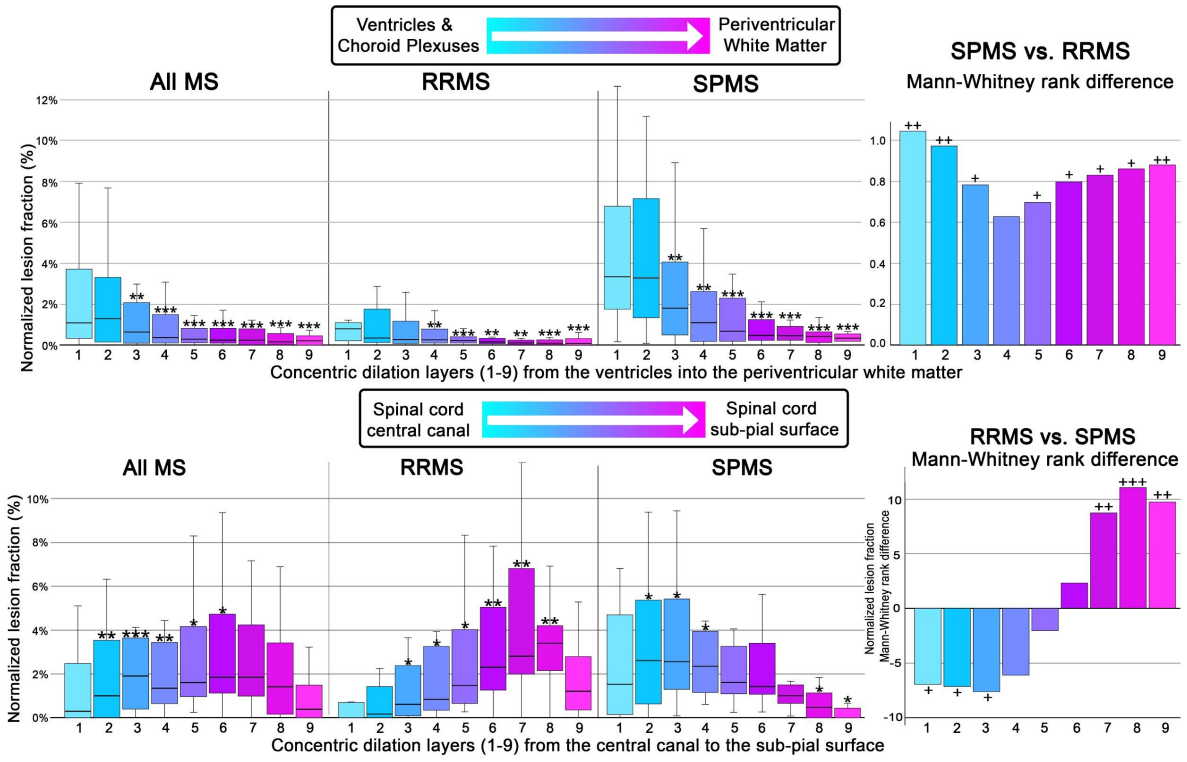

Figure 22. CSF-proximity lesion mapping. *Box-and-whisker plots presenting the normalized lesioned fractions in the respective radial dilation layers.* ***Top row: Brain.*** *Mapping the lesion fraction from the ventricular surface to the surrounding periventricular white matter.* ***Bottom row: Spinal cord.*** *Mapping the lesion fraction from the inner central canal surface to the outer sub-pial surface. Exploratory comparison of individual-level lesion fraction vs. the median of the inner-most level (*P-value < 0.05, **P-value < 0.01, ***P-value < 0.001 by Wilcoxon signed-rank test, two-tailed, equal variances not assumed).* ***Right side: Bar graphs.*** *Depict the rank difference between MS subtypes for the respective dilation layers. Exploratory comparison of RRMS vs. SPMS participants (+P-value <0.05, ++P-value < 0.01, +++P-value < 0.001, by Mann-Whitney U-test (two-tailed, equal variances not assumed).*

Clinical correlations with spinal cord and brain MRI metrics

Using stepwise linear regression it was identified that cortical thickness is the most significant (*β=-0.55, R^2=0.30, P=0.002*) contributor to physical disability (EDSS), a combined model (*R^2=0.44*) of white matter lesion fraction in the spinal cord (*β=0.44, P=0.01*) and brain (*β=0.40, P=0.02*) are the most significant contributors to fine motor skill disability (9-hole peg test), a combination of (*R^2=0.32*) cortical thickness (*β*=-0.48, *P*=0.008) and spinal cord grey matter cross-sectional area (*β=-0.37, P=0.035*) as the most significant contributors to reduced walking speed (timed 25-foot walk).

4.3 STUDY III

Ex vivo MRI-histological correlations

The REMyDI myelin quantification method correlated (*P<0.001 for all*) with both myelin-specific histological staining methods across each of the three samples: proteolipid protein-immunostaining (*r=-0.73, r=-0.63, r=-0.66*) and Luxol Fast Blue (*r=-0.66, r=-0.61, r=-0.63*). Voxel-wise correlation graphs for the three individual samples and respective staining methods are shown in Figure 23. Generally, the correlations to the axonal Bielschowsky silver staining (*r=-0.58, r=-0.48, r=-0.63; all P<0.001*) were numerically lower than the more myelin-specific staining counterparts. The histological myelin staining methods were also in agreement with one-another, proteolipid protein-immunostaining vs. Luxol Fast Blue *(r=-0.92, r=-0.93, r=0.91*). The individual quantitative maps (PD, R1 and R2) demonstrated a nonlinear relationship with myelin histology stains, indicating that additional factors influence the R1 and R2 maps and therefore are not able to, alone, sufficient to estimate the myelin content. The PD demonstrated a linear relationship but to a lesser degree than that of REMyDI.

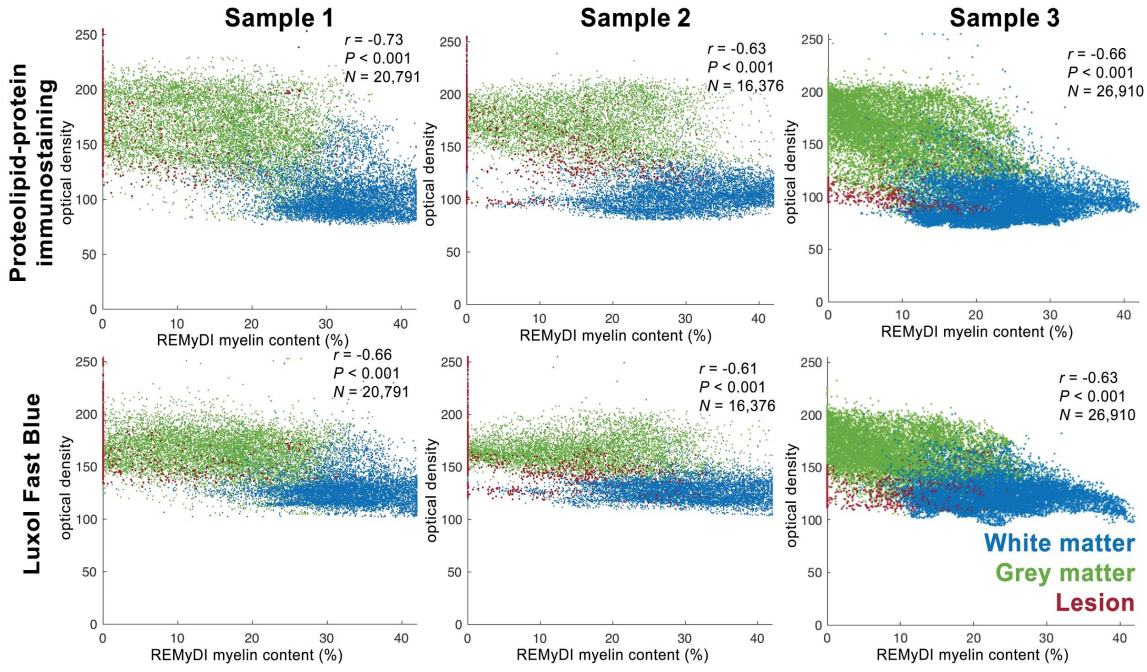

Figure 23. Voxel-wise REMyDI myelin specificity plots with myelin-specific stainings. *Three MS brain tissue samples' voxel-wise Pearson correlations of the REMyDI myelin maps with the histological stain uptake optical densities for PLP-IHC and LFB. Respective tissue voxel count (N).*

In vivo repeatability

The whole-brain REMyDI myelin fraction was found to be robust with a low overall mean coefficient of variance (CoV) at 1.2±1.5%, median 0.58% (*range 0.0-6.5%*). In the MS cohort, the mean CoV was 0.82±0.75%, median 0.68% (*range 0.0-2.6%).* In healthy controls, the overall whole-brain mean CoV was 1.4±1.8%, median 0.58% (*range 0.0-6.5%*). The overall tissue-specific myelin fractions were also found to be robust, with a mean CoV in the NAWM of 0.52±0.63%, median 0.29% (*range 0-3.0%*) and in the NAGM of 1.1±0.81%, median 0.87% (*range 0-2.9%*), respectively.

In vivo group comparison

There was no significant difference in age or sex between the MS participant and control groups. There was no significant difference between males and females in any of the conventional or REMyDI myelin quantification MRI metrics across all participants, or selectively within the control/MS subgroups. The MS participants were found to have lower myelin fractions in the whole-brain (*11.8±1.6 vs. 12.6±0.9 %, P=0.004*) and NAWM (*9.6±1.7 vs. 10.6±1.0 %, P=0.001*) compared to controls. The RRMS participants had lower whole-brain (*12.0±1.4 vs. 12.6±0.9 %, P=0.026*) and NAWM (*9.8±1.5 vs. 10.6±1.0 %, P=0.009*) myelin fractions than controls. Participants diagnosed with SPMS also had lower whole-brain brain (*11.1±2.0 vs. 12.6±0.9 %, P=0.014*) and NAWM (*8.9±2.1 vs. 10.6±1.0 %, P=0.010*) myelin fractions than controls. However, no significant differences in myelin content were observed between the MS subtypes.

In vivo clinical correlations

Physical disability, measured by EDSS (*N=70*), correlated with the whole-brain (*ρ=-0.26, P=0.032*) and NAWM (*ρ=-0.26, P=0.032*) myelin content as well as the lesion volume fraction (ρ=0.36, P=0.002) at baseline. At 2-year clinical follow-up, EDSS (*N=70*) again correlated with whole-brain (*ρ=-0.41, P<0.001*) and NAWM (*ρ=-0.41, P<0.001*) myelin content as well as the lesion volume fraction (*ρ=-0.40, P=<0.001*) and the NAWM volume fraction (*ρ=-0.41, P=0.008*). However, after correcting for baseline EDSS, only the myelin content in the whole-brain (*ρ=-0.30, P=0.013*) and NAWM (*ρ=-0.30, P=0.011*) were significantly correlated with longitudinal EDSS. Linear regression identified that the baseline EDSS was most strongly influenced by the lesion fraction, but at 2-year follow-up the whole-brain myelin fraction was identified as the strongest contributor, shown in Figure 24.

Cognitive disability, measured by SDMT, correlated with the whole-brain (*r=0.56, P<0.001*) and NAWM (*r=0.54, P<0.001*) myelin content as well as the NAWM volume fraction (*r=0.42, P=0.003*) at baseline. At 1.5-year follow-up, the NAGM myelin content tended to be correlated with SDMT scores (*r=0.38, P=0.034*), even after correcting for baseline SDMT. Stepwise linear regression identified the baseline SDMT score was most strongly related with whole-brain myelin fraction and, longitudinally, mostly associated with a combination of whole-brain and NAGM myelin fractions, shown to the right in Figure 24.

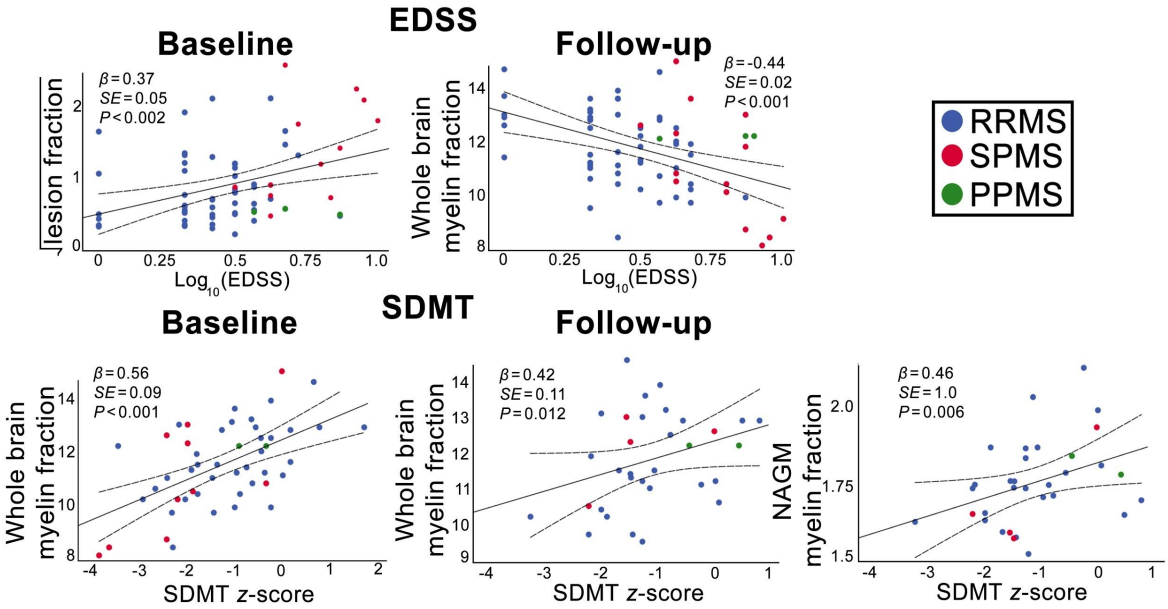

Figure 24. Relations of MRI volumetrics with clinical disability.

Linear regression of the clinical disability metrics with magnetic resonance imaging metrics. EDSS was treated as a continuous variable and was log_{10} transformed and normalized lesion fraction by the square root to become approximately normally distributed. RRMS (blue), SPMS (red) and PPMS (green). SE = standard error.

4.4 STUDY IV

Periventricular myelin mapping

The periventricular myelin mapping results and group differences are portrayed on the following page in Figure 25. As expected, all three groups (healthy controls, RRMS and PMS) demonstrated a gradient of regional myelination differences in the periventricular NAWM and WM . However, the RRMS and PMS groups had significantly lower myelin content as compared to the healthy controls in both the NAWM and WM. Additionally, not only was the myelin content lower nearest the ventricular system in RRMS and PMS participants, but the degree to which it was reduced was also greatest nearest the ventricular system. This pattern of demyelination was most pronounced nearer the ventricular system and was observed in MS participants in both the WM (including focal lesions) and diffusely in the NAWM. Myelin content in the periventricular NAWM was lowest in RRMS participants in layers 1-4 (*P<0.0001*) and in PMS participants in layers 1-3 (*P<0.0001*), relative to the myelin content in healthy controls. Meanwhile, the myelin content in the periventricular WM including lesions was lowest in RRMS participants in layers 1-7 (*P<0.0001*) and in PMS participants in layers 1-4 (*P<0.0001*), as compared to healthy controls. However, despite the fact that those with PMS tended to have lower myelin content within the periventricular NAWM and WM layers than those with RRMS, no layers between the MS subgroups had significantly different myelin content values.

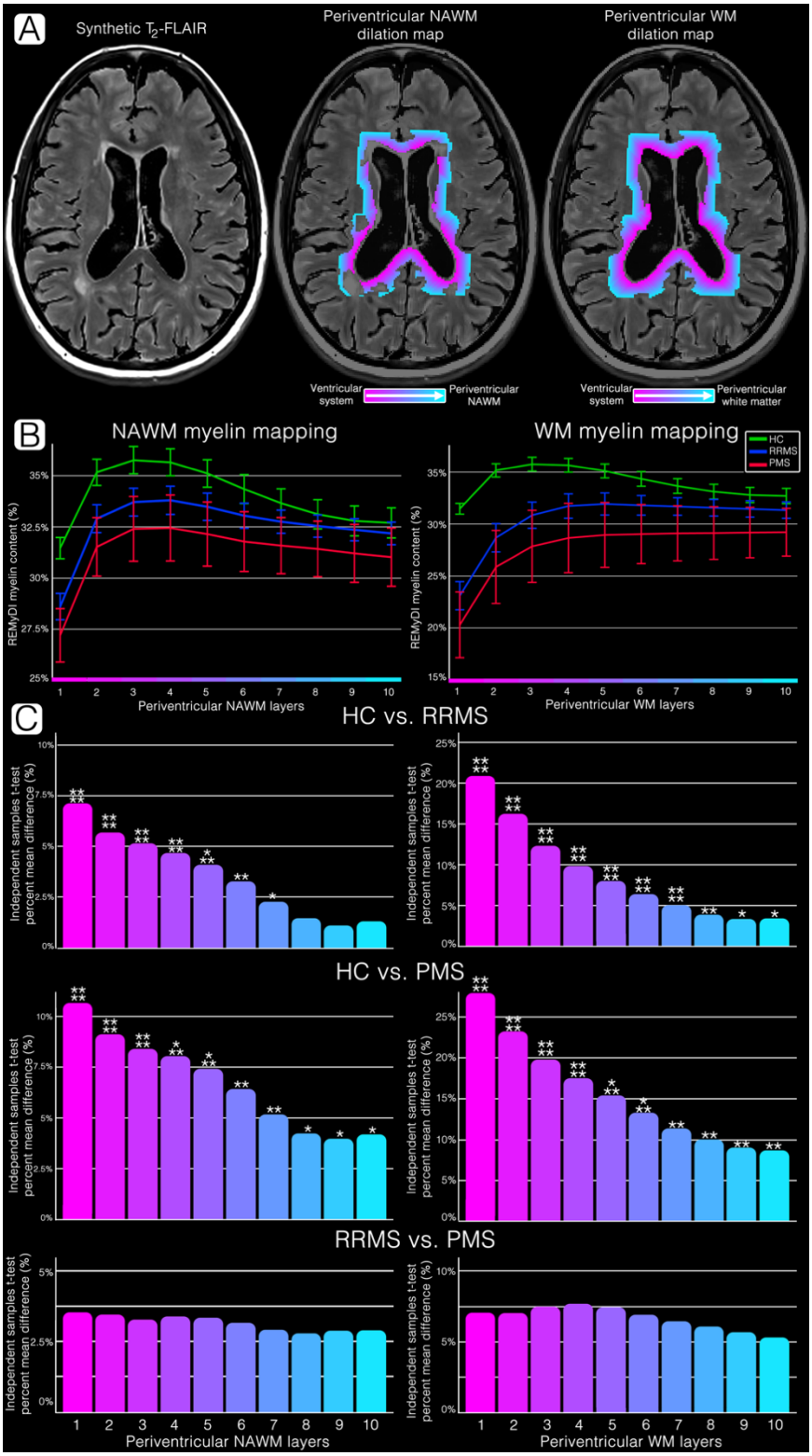

Figure 25. Periventricular myelin content mapping.

A. Representative participant. *T_2-FLAIR image alongside the corresponding NAWM and WM dilation maps (magenta to cyan) for a 34-year-old female participant with RRMS (1.3-year disease duration, EDSS score 2.0, SDMT z-score -3.0).* ***B. Myelin mapping results.*** *The mean myelin content across the periventricular NAWM and WM layers in healthy controls (green), RRMS (blue), PMS (red) participants.* ***C. Exploratory group comparisons.*** *The group-level mean percent difference of the periventricular NAWM and WM REMyDI values within the identified layer between the two respective groups by independent samples t-test, two-tailed, equal variances not assumed. *P-value <0.05, **P-value <0.01, ***P-value <0.001, ****P-value <0.0001.*

Periventricular lesion mapping

Both RRMS and PMS subgroups had greater lesion fractions nearest the ventricular system. Participants with a PMS subtype had greater median lesion fraction across all periventricular levels, with statistical significance ($P<0.05$) at layers 2, 3, 6 and 8. These periventricular lesion mapping results are in strong agreement with those of Study II.

Perilesional myelin mapping

The perilesional myelin mapping results and group differences are illustrated to the right in Figure 26. The overall pattern of perilesional myelin content seeded from the inner core of the lesion extending outwards into the extralesional NAWM is highly similar to that of a sigmoid function. The outermost perilesional layer was considered as a comparative analog for the perilesional layer with the least amount of MS pathology, which is supported by the plateauing of the myelin values in the outer NAWM layers. Paired non-parametric analysis suggests that MS pathology extends well beyond the focal demyelination within lesions and into

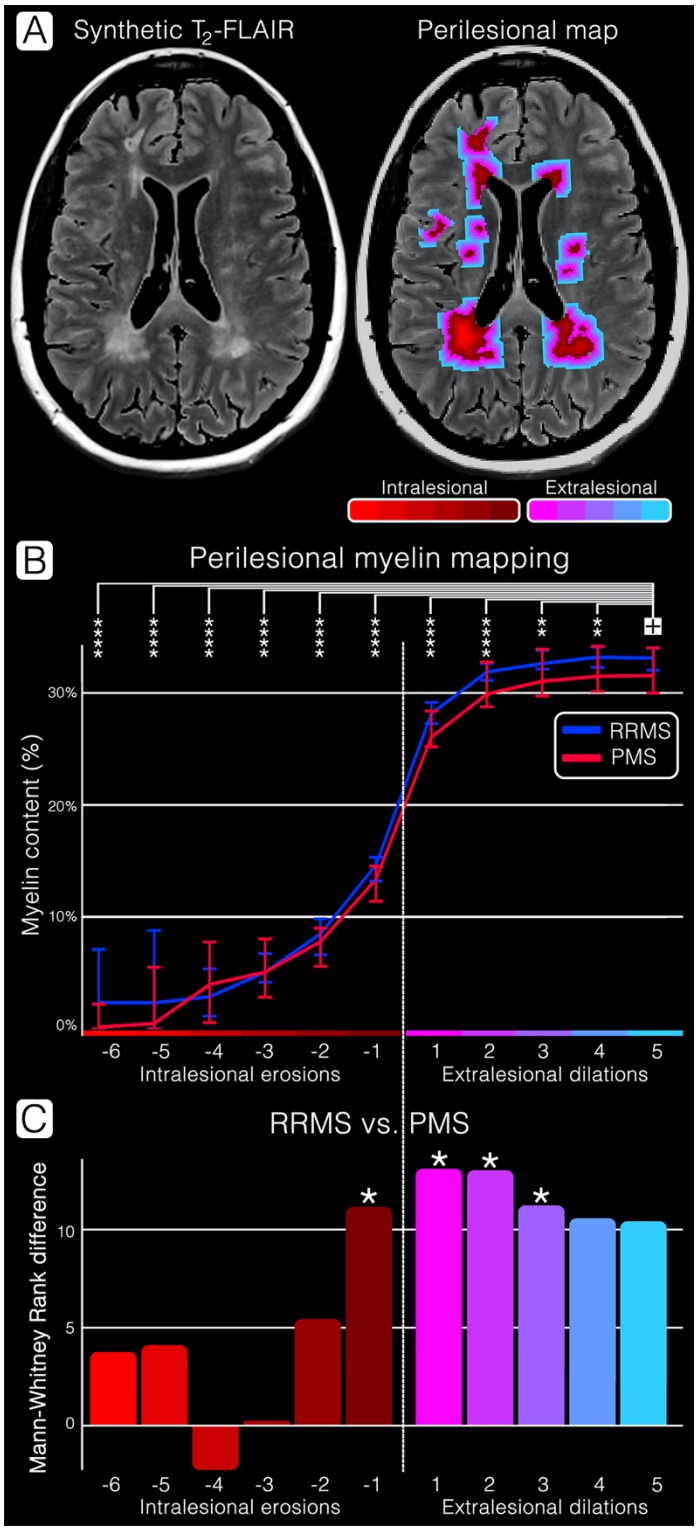

Figure 26. Perilesional myelin mapping

A. Representative participant. *T2-FLAIR image with the corresponding perilesional map for a 35-year-old female participant with RRMS (7-year disease duration, EDSS score 1, SDMT z-score -0.8).* ***B. Myelin mapping results.*** *The myelin content for the perilesional layers in RRMS (blue) and PMS (red). Paired comparisons of the myelin content with the outermost perilesional myelin content (indicated by +), by Wilcoxon signed-rank test **P-value <0.01, ****P-value <0.0001. Paired non-parametric of the myelin content in the outermost perilesional NAWM value (indicated by +) compared to the myelin content in each individual perilesional layer by Wilcoxon signed-rank test **P-value <0.01, ****P-value <0.0001.* ***C. Group comparison.*** *Exploratory group-level comparison of myelin content between MS subtypes by Mann-Whitney U-test, *P-value <0.05, two-tailed.*

the surrounding normal-appearing tissue, specifically extralesional layers 1-4. Group comparison of RRMS and PMS participants found that those layers bordering the lesion edge differed most, including intralesional layer 1 and extralesional layers 1-3, by Mann-Whitney U-test, $P<0.05$.

Clinical disability correlates of demyelination gradients

The correlational plots of the clinical disability metrics and myelin maps are displayed below in Figure 27. The metrics that were consistently associated with the periventricular NAWM myelin content were baseline SDMT scores, follow-up EDSS scores, baseline MSIS physical and psychological scores. The metrics that were consistently associated with the periventricular WM myelin content were baseline SDMT scores, baseline and follow-up EDSS scores and baseline MSIS physical. The metrics that were consistently associated with the periventricular lesion fraction were baseline and follow-up EDSS scores. Interestingly, the metrics that were consistently associated with the perilesional myelin content were baseline SDMT scores, baseline and follow-up EDSS scores, baseline MSIS physical and psychological scores; however, only with the extralesional portion of the perilesional myelin values, apart from EDSS at follow-up.

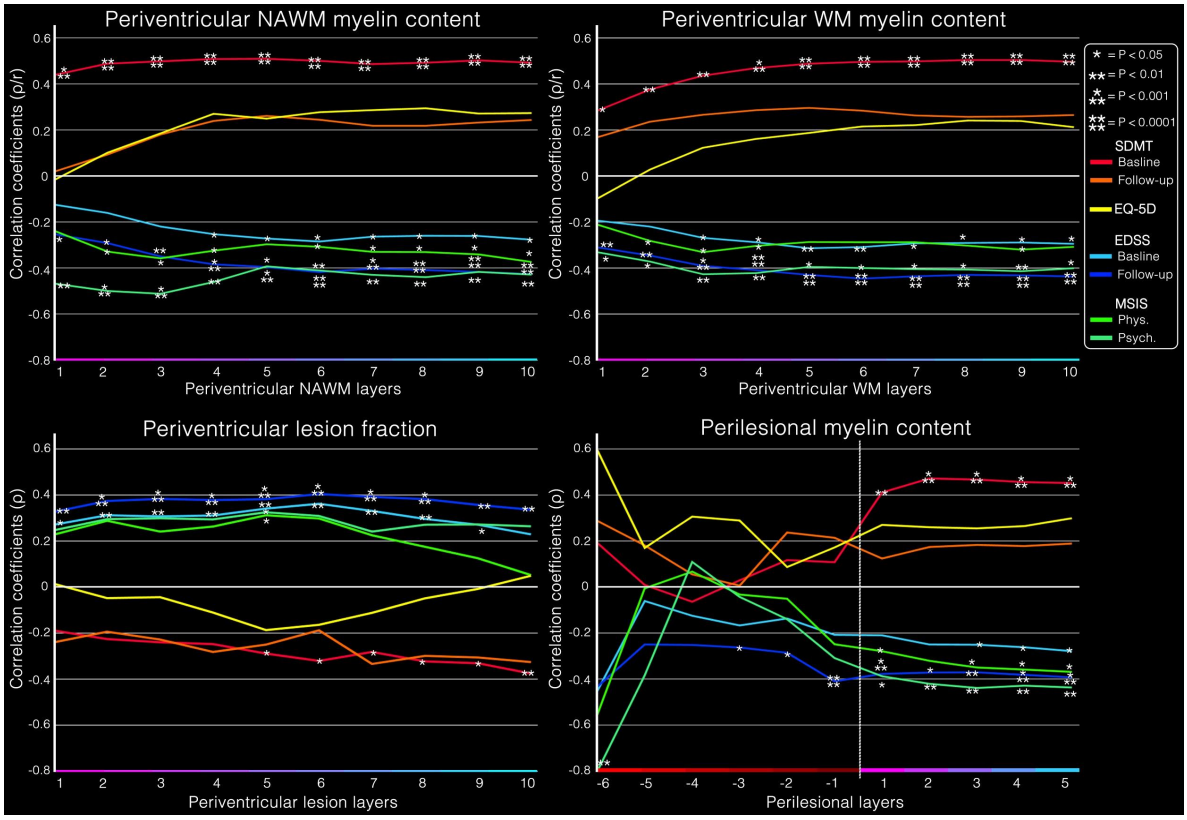

Figure 27. Myelin mapping correlations with clinical disability.
Measured by SDMT baseline (red) and follow-up (orange), EQ-5D (yellow), EDSS baseline (light blue) and follow-up (dark blue), and MSIS physical (green) and psychological (light green) with the four respective techniques.

Ex vivo myelin mapping

The *ex vivo* myelin mapping results are depicted below in Figure 28. The *ex vivo* REMyDI and histological periventricular NAWM and WM myelin mapping patterns shared visible consistency to the patterns observed *in vivo* by REMyDI for the MS participants; Presenting with a similar gradient of lower myelin content nearest the ventricular system that gradually increases and plateaus further into the parenchyma. Moreover, the sigmoid pattern of the perilesional area observed *in vivo* was also comparably represented to varying degrees in the *ex vivo* myelin mapping graphs. In total, 16 lesions (*N=7, 7, 2* respectively) were captured, the majority were periventricular (*N=9*). Interestingly, the *ex vivo* REMyDI myelin mapping patterns presented with greater dynamic variance throughout the tissues relative to the respective histological staining methodologies.

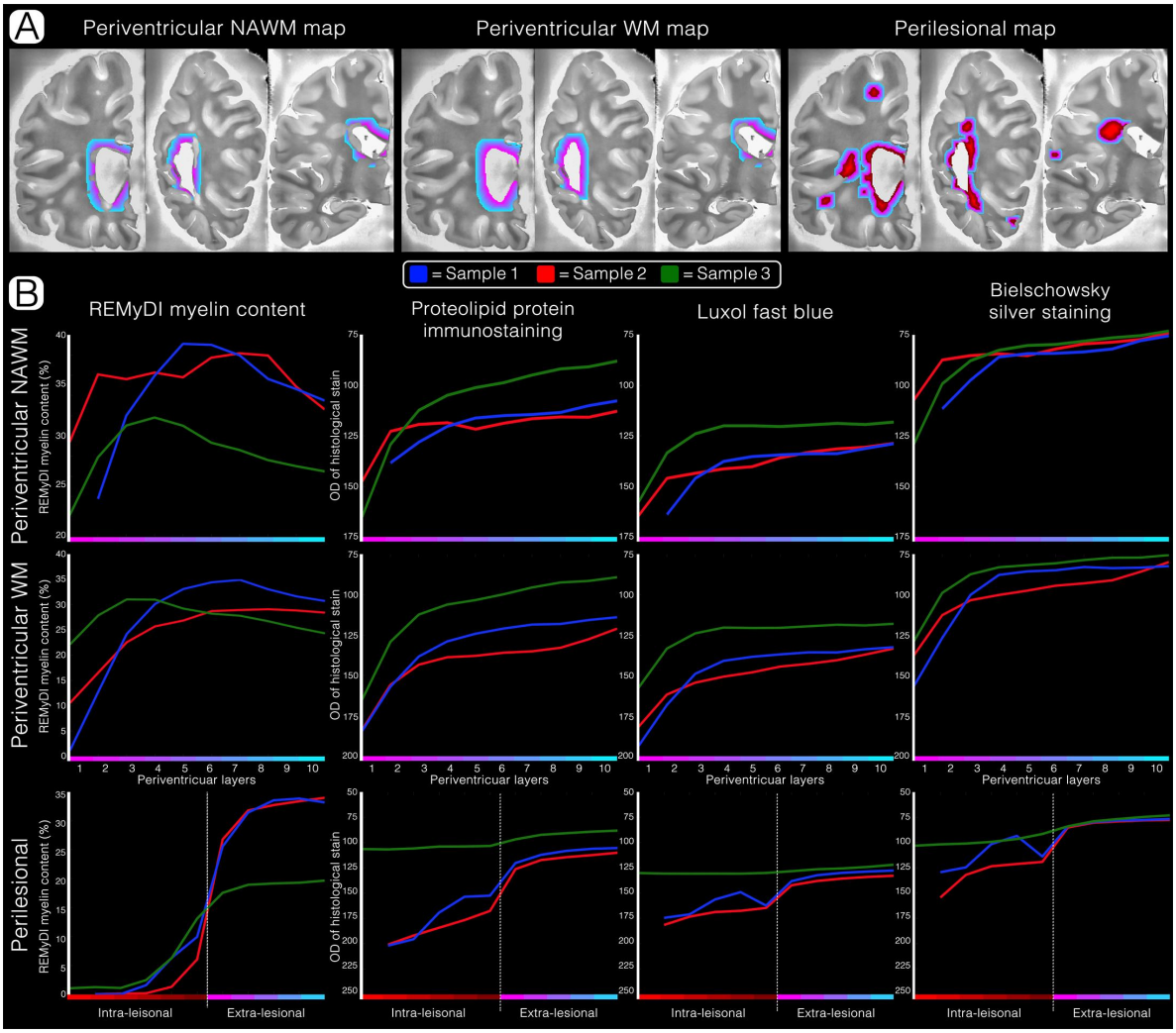

Figure 28. Ex vivo myelin mapping.

A. Segmentation maps. *Left, sample 1 in blue. Middle, sample 2 in red. Right, sample 3 in green. Mapping procedures were done the same as for the in vivo myelin mapping presented in Figures 25 and 26.* ***B. Myelin mapping results.*** *The x-axes' color bars match those of the segmentation maps.*

5. DISCUSSION

Study I

The combination of long-term neurological, neuropsychological and radiological evaluations in this study is unique compared to previous studies, which have focused on either disability monitoring or MRI follow-up, but typically lack the combination of both. The results of this study highlight the application of volumetric MRI throughout the MS disease course in relation to disability. Interestingly, some of the volumetric markers did not change much throughout the disease course and, generally, there was substantial intra-individual variability. However, when considering the association of some volumetrics with respect to cognitive functioning, there were several interesting findings. This underlines the importance of contextualizing volumetrics within the framework of an individual's clinical neurologic disability profile.

The volumetric biomarkers that were most predominantly associated with future neuropsychological functioning were the T_2 white matter lesion fraction and corpus callosal fraction. Lesions are certainly the pathological hallmark of the disease and have previously been demonstrated to contribute to disability progression. The importance of the callosal atrophy probably relates to the biological importance of the corpus callosum in connecting the two hemispheres and being essential for most bi-hemispheric functioning and communication. Moreover, it is composed of tightly bundled groupings of axons with high degrees of myelination, making it prone to MS pathology (Granberg *et al.*, 2015; Gonçalves *et al.*, 2018).

From a neuropsychological perspective, the use of a multi-faceted test battery with complementary tests provided insights into which of tests were most reflective of cognitive dysfunction in MS. Interestingly, tests that correspond to widespread functions, thus being especially vulnerable to structural and functional disconnections, were the most sensitive to capture cognitive impairment and progression. This resonates well with the aforementioned neuroanatomical findings where lesions and callosal damage likely contributes to disconnections. Another intriguing observation in this study was the preservation of cognitive functioning but pronounced physical disability in some MS participants, and *vice versa* in others. MRI has the potential to resolve this clinico-radiological paradox. For example, among the six participants with an EDSS >6.0, cognitive index *z*-score >0, four had also been imaged with spinal MRI, which revealed spinal lesions in three participants (75%). Due to physiological reasons, lesions in critical locations of the spinal cord may result in severely impeded ambulation with preserved cognitive functions. Meanwhile, cognitive impairment with relative sparing of physical abilities could be related to cortical lesions (though unable to determine at 1.5 Tesla). Notably, these notions were indeed later supported by our findings in Study II, where advanced imaging of both the brain and spinal cord was applied.

The value of applying a cognitive index as a composite measure of neuropsychological functioning in a single numeric representation seems to hold clinical value by reducing the dimensionality of the data into a meaningful metric that is more approachable to clinicians, comparable to the EDSS and composing sub-scores. It would be interesting to see if a similar

analog could be developed and integrated into the visual platform of the Swedish MS registry shown here in Figure 29, which provides visual feedback to those with MS and their caretakers, thus promoting its use and coverage.

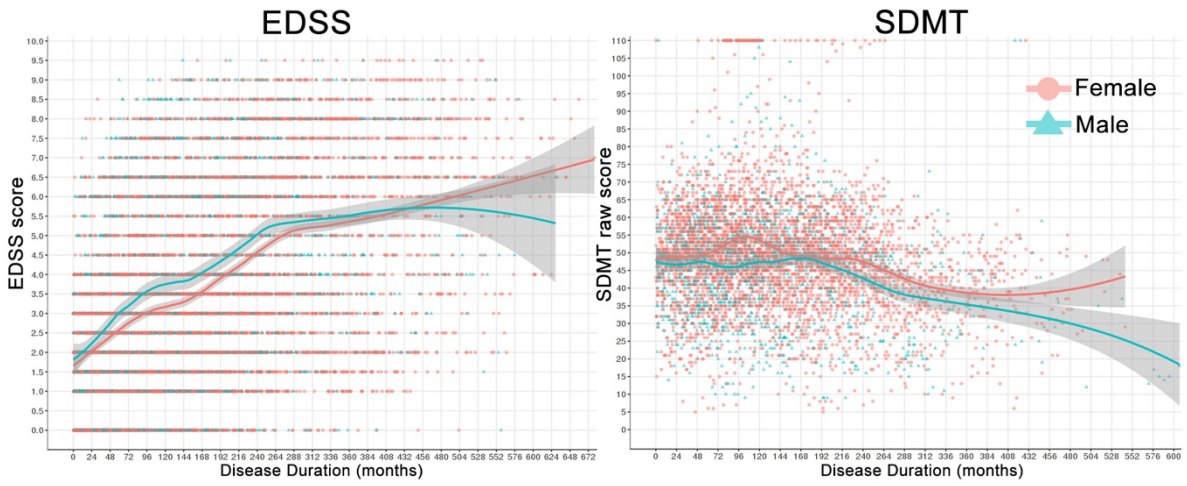

Figure 29. The progression of clinical disability in MS.
Represented by EDSS (N=10,653) and SDMT (N=5,680) scores over disease duration across all available patients at Karolinska University Hospital in Huddinge, Stockholm, Sweden according to the Swedish MS Registry. Image courtesy of Leszek Stawiarz, Swedish NEURO Registries (Dec 30th, 2020).

In terms of immediate clinical interpretation, Study I demonstrated that cognitive impairment progresses continuously in MS, accompanied by atrophy and lesion accumulation, suggesting that interventions that can effectively address these pathological processes hold importance at all disease stages, even in late stages where DMTs are typically not used today.

Study II

In this study, we applied ultra-high field strength MRI (7 T) to characterize the distribution and proportion of grey and white matter involvement of MS pathology in the brain and cervical spinal cord. Rarely has 7 T been applied to image the spinal cord in MS to date, and the combination of the two, as well as a focus of the uncharted territories of grey matter involvement (particularly in the spinal cord), provides novelty to the study. Brain and spinal cord lesion distributions were mapped based on proximity to the CSF surfaces, inspired by previous hypotheses and studies regarding the concept of a pathological gradient in MS that is related to CSF-proximity. In the brain, a periventricular gradient was seen in both RRMS and SPMS and was more pronounced in the progressive phase. In the cervical spinal cord, we observed a greater propensity of spinal cord lesions to manifest near the CSF interfaces in the subpial surface in early RRMS and around the central canal in SPMS. Thus, MS pathology was found mainly with proximity to CSF not only in the brain but also in the spinal cord.

The pathogenic cause of MS is unknown, and many of the mechanisms driving the gradient differences between subtypes remain uncertain. However, meningeal inflammation in the CSF-interface along the subpial surface has been histopathologically identified in CIS and RRMS (Frischer *et al.*, 2009; Lucchinetti *et al.*, 2011; Zurawski *et al.*, 2017), but is more typically

demonstrated in those with progressive MS (Magliozzi *et al.*, 2010; Howell *et al.*, 2011). A potential explanation may be related to the relative size of the CSF pools from which the segmentations were seeded, with the lateral ventricles of the brain being relatively much larger than that of the central canal in the spinal cord. Overall, the observations of Study II are in support of the historic outside-in theory of CSF-/ependymal-mediated inflammatory pathogenesis for MS demyelination, whereby CSF-borne immune cytotoxic factors could potentially penetrate the parenchyma to provoke focal lesion formation/expansion and produce a gradient of diffuse demyelination and/or lesion formation. An interesting side note is that enlarged perivascular spaces are more common in MS than in controls, as shown in a recent meta-analysis (Granberg *et al.*, 2020), and that the diameter of these enlarged perivascular spaces are not related to brain atrophy in MS (as may be hypothesized) but instead strongly linearly related to the T_1 and T_2 lesion volumes (data not yet published). Indeed, our PET studies have shown signs of compartmentalized inflammation with activated microglia especially in the SPMS stage of MS, potentially supporting this hypothesis (Herranz *et al.*, 2016, 2019). Further explorations along these lines of thought would require longitudinal follow-up at 7 T, ideally combined with microstructural quantitative MRI and also include monitoring of CSF flow dynamics to support the pathophysiological hypothesis. Moving forward, future studies should also include imaging of the whole spinal cord and examine the pathology of the spinal cord based on CSF-proximity using quantitative MRI metrics and *ex vivo* correlation probing the microstructural aspects of the disease.

Furthermore, this study clearly demonstrates the clinical utility of 7 T MRI, which is now clinically approved. Currently, there is only one 7 T scanner in Sweden, a national research facility in Lund. From a clinical standpoint, our findings stress the need for additional clinical ultra-high field resources in Sweden, in agreement with numerous other studies showing its clinical value also in other pathologies such as epilepsy, brain tumors, cerebrovascular diseases, and also whole-body applications (Kraff *et al.*, 2015). Certainly, 7 T MRI would not replace 1.5/3 T as the clinical workhorses but rather be applied in an application specific manner (Kraff *et al.*, 2015). A heightened sensitivity to pathology could be of particular use at the diagnostic stage of MS, aiming to even further reduce the time to diagnosis and initiation of DMT. Seeing the socio-economic disease burden of MS, where treatment and diagnostics only constitutes a small fraction of the financial burden of the disease, the case for investment in such equipment close to a large population center of patients with MS would be strategically prudent. This overall positive socio-economic aspect of such diagnostics is supported by the fact that clinical 7 T scans are indeed reimbursed by health insurance companies in the United States. This being said, such a large financial investment would likely entail nationally coordinated efforts and collaborations between regions and all leading medical and technical faculties in Sweden. It is my sincere hope that this thesis may provide a spark and contribute towards such a development in advancing patient care in Sweden.

Study III

This study aimed to systemically validate a fast quantitative myelin imaging technique intended for clinical application. First, by evaluating the specificity to myelin using two myelin-specific histological stains, but also demonstrating that the tissue specificity was weighted towards myelin rather than that of axons (which is inherently hard to disentangle seeing their spatial co-localization). Second, the variability of the technique was determined to be very low, by scan-rescan measures in both healthy volunteers and participants diagnosed with MS. Finally, the clinical utility of the myelin imaging technique was highlighted by the finding that myelin measures were more strongly related to clinical disability measures than conventional volumetric measures at the time of scanning but also to one's future physical and cognitive disability status.

The myelin specificity analyses were truly a translative collaborative effort between histopathology and radiology. Much of the effort on the histopathological side was in producing high quality and homogenous staining uptake across a whole-coronal hemispheric brain sample and also in cutting the brain tissue samples without damaging the tissue by causing micro-tears. Meanwhile, the radiological/physical complexity arose mainly in the *ex vivo* imaging scanning fixated samples at room temperature using components intended for clinical application as well as the co-registration of the MRI and histological images.

There are relatively few previous studies attempting to histologically validate myelin imaging techniques (van der Weijden et al., 2020). This is partly due to the methodological challenges mentioned above, but also due to difficulty in acquiring tissue samples and also that the field is constantly changing with more techniques that are perpetually being elaborated upon. The REMyDI MRI-based myelin imaging correspondence with histological myelin stains was moderate ($0.60 \leq r \leq 0.79$), which is comparable but slightly below previously reported correlation coefficients of other myelin imaging techniques (van der Weijden *et al.*, 2020). However, these correlations are potentially due to the stark differences in methodology. An important methodological consideration in this study was the voxel-wise comparison of REMyDI based myelin quantification with histological staining for myelin. This is, to the authors' knowledge, the first example of such analysis for myelin imaging validation. In preceding studies, manual selection of regions of interest has typically been used for MRI-histopathological correlations. Opponents would argue that the manual regions of interest approach is more favorable, due to the difficulties in registering the MRI with histological images that distort at sectioning, which is true. However, an inherent risk of bias in the manual delineation is the ability to, unblindedly choose the regions of interest with the most favorable agreement between techniques. The validation pipeline developed for this thesis may now be applied to other quantitative MRI techniques to increase our understanding of their tissue specificity and also to other diseases to heighten our understanding of their pathophysiological processes by *in vivo* monitoring.

The repeatability of a method is essential when the intent is to monitor the dynamic *in vivo* pathophysiological evolution throughout the disease course, which is certainly of key importance in chronic and dynamic disease processes such as in MS. The repeatability of REMyDI is among the best reported for myelin imaging techniques (Piredda *et al.*, 2021). Additionally, without tissue specificity and without monitoring a particular process related to the disease in question, there is no reason for applying the method. Therefore, an important consideration in terms of the clinical value of the method is whether or not these myelin measures are related to disease and disability progression, and how do they compare to more conventional metrics? The REMyDI measures were more strongly related to cognitive and physical disability as compared to conventional volumetric markers. This highlights the potential additional value of non-conventional imaging markers for clinical use. Perhaps the most promising finding is that the myelin measures were predictive of future disability, though further validations of these findings are warranted.

Study III demonstrates that REMyDI myelin imaging correlates well with myelin and provides a robust *in vivo* quantification of myelin that is related to baseline and follow-up clinical disability metrics. Beyond the detection of demyelination within lesions, there was also a reduction of myelin content in the normal-appearing tissues, highlighting the increased sensitivity to subtle/diffuse MS pathology compared to conventional MRI. The clinical application of REMyDI is also favorable due to the relatively short acquisition and image processing times as well as CE marking and FDA approval. However, an inherent drawback is that the method requires commercial licensing and that the sequence is currently 2D-based with rather thick slice thickness and gaps between slices to reduce inter-slice crosstalk. Nonetheless, REMyDI remains a promising technique to monitor the dynamic demyelination and remyelination profiles of lesions throughout the clinical course of MS and will likely prove valuable in pathophysiological monitoring. Importantly, the most promising utility of REMyDI may likely be in the benchmarking of DMTs in clinical trials for compounds claiming to have remyelination potential, such as clemastine. Furthermore, the greater the number of diagnostic tools at radiologists' disposal, specifically those that are able to probe the mechanisms of various pathology, the better. This relevancy has been evidenced most recently by the novel SARS-CoV-2 and COVID-19 pandemic, where advanced techniques will likely help our understanding of the underlying processes of the acute and long-term neurological complications of this new disease.

Study IV

In this study, we elaborated on the CSF-proximity mapping technique from Study II in combination with the myelin imaging method validated in Study III to characterize the distribution of demyelination present in the periventricular and perilesional areas of the brain in *ex vivo* MS brain tissue samples and an *in vivo* heterogeneous cohort of MS participants. Further, we correlated four common clinical measures of physical and cognitive disability in MS with the distribution of myelin content in the periventricular and perilesional regions.

We observed more pronounced demyelination in the WM nearest the ventricular system of MS participants, as compared to healthy individuals, present even when solely looking at the normal-appearing tissue. This periventricular white matter demyelination gradient and diffuse demyelination in the NAWM was similarly demonstrated in the histological stainings of the *ex vivo* samples. Additionally, when sampling from the inner lesion core to the surrounding NAWM tissue, the pattern of demyelination resembled that of a sigmoid curve, with significant demyelination diffusely extending beyond the lesion border. This diffuse extralesional demyelination was found to significantly differ between MS subtypes and was also more significantly related to physical and cognitive disability than the intralesional demyelinated content. This sigmoid pattern of perilesional myelin content was partially preserved in *ex vivo* samples, however, the abbreviated number of lesions in the samples limits the results.

Similarly, to Study II, these findings are in support of a possible CSF-borne immune cytotoxic factor-mediated pathogenic mechanism for demyelination in MS. This study most conceptually differs from Study II by additionally targeting diffuse demyelination rather than just focal lesion formation visible on MRI to a radiologist. Despite these differences, the periventricular patterns of lesion formation and diffuse white matter injury are evidently similarly linked. These periventricular patterns of demyelination have been previously demonstrated using MTR (Filippi *et al.*, 1998; Liu *et al.*, 2015; Brown *et al.*, 2017) and T_2* relaxometry at 7 T (Louapre *et al.*, 2018). However, the perilesional myelin mapping method that is uniquely applied in this work is more singularly informative. Moreover, the *ex vivo* findings that echo those of the *in vivo* patterns using both MRI-based myelin imaging and histological stainings for myelin adds accreditation to the observations.

The mechanics of immune cells migration into and pathogenic perpetuation of disease-driving mechanisms throughout the brain remain to be fully revealed. Certainly, at present technological standing, MRI cannot identify specific immune cells, but by linking the MRI-based demyelination patterns to observations made in histopathological examination, more light can be shed onto the evolution and trajectory of MS pathology. Our understanding of blood-brain barrier disruption followed by focal lesion formation predominantly mediated by T-cells around a central post-capillary venule is well described in EAE animal models. However, the blood-brain barrier may not be the only site of penetration into the CNS, nor may T-cells be the only pathological immune cell perpetuating MS pathology (Piehl, 2021). The choroid plexus has been identified as a point of immune cell entry into the brain (Vercellino *et al.*, 2008). The proposed immune activation cascade of the choroid plexus is believed to be related to an upregulation of the molecular machinery necessary for adhesion and migration of immune cells (Marques *et al.*, 2009); Thereby promoting lymphocyte access to the resident antigen-presenting cells of the choroid plexus, in turn leading to further inflammatory activation and subsequent tissue damage (Vercellino *et al.*, 2008; Martirosian *et al.*, 2016). Once the immune cells are present within the CNS, the pathological potential of these cells varies. Not all cells in and around lesions are perpetuating demyelination, and therein lies the difficulty in identifying the key pathogenic cells that do not belong. The T- and B-cells likely play a crucial role in the initiation of an autoinflammatory cascade. While T-cells may be more

readily involved in the focal inflammatory demyelination of lesions, B-cells may play a stronger role in generating an autoinflammatory cascade resulting in CSF soluble inflammatory neurotoxic factor(s) that either indirectly or directly damages myelin (Adams *et al.*, 1987; Magliozzi *et al.*, 2010; Lassmann, 2019). Our findings in Study IV again support that the readily applicable REMyDI myelin quantification method has enough sensitivity to capture varying patterns of both focal and diffuse demyelination in MS. Additionally, this shows that these myelin gradient profiles are correlated to common clinical measures of disability in MS.

General Discussion

The main goals of our research

A common theme of the discussions in these works is directly related to the goals of our research group at large and indicates the "Why?" of one's research, a concept that cannot be too often reflected upon. By wielding the sensitivity and specificity of MRI in reducing the time to diagnosis, we can help get the person with MS onto the most ideal DMT and hopefully spare their CNS from further injury. From interacting with participants diagnosed with MS, they are sometimes relieved at the point of their diagnosis, which might seem counterintuitive. However, this is due to the variability in the presentation of MS and how elusive the diagnosis can often be. The disease is so insidious that people with MS may often believe they are at fault or that something is wrong with them, that they are just "clumsy" or "forgetful", when this could not be further from the truth. It is the disease, not the person, that is causing these issues. These are symptoms, not character traits. Setting these manifestations aside, as a consequence of the disease, allows the patients their lives back, where they may now set their focus on aspects beyond the disease once they are on effective treatment.

The consideration of sensitivity versus specificity in MS diagnostics is also very intriguing because of the dynamics between one-another change throughout the MS disease course. At the time of diagnosis, the most prudent consideration is the specificity for MS pathology, currently, those fulfilling the McDonald criteria. However, when monitoring tissue destruction in the brain of someone with known MS, there is a justifiable shift towards sensitivity in monitoring demyelination or neuroaxonal degeneration. Notably, the processes associated with normal aging also cause white matter signal changes and ventricular expansion that are similarly expected to also occur in MS. Techniques with higher sensitivity to neuroinflammatory and neurodegenerative processes become more relevant throughout the disease course until specific markers can indicate a potential conversion from RRMS to SPMS that may require alternative therapeutic considerations.

The next goal is using the sensitivity of MRI to monitor these patients and ensure that the DMT chosen is the most ideal, and to also monitor for adverse effects. As technological advancements, from both a hardware and processing standpoint, further aim to extract more *in vivo* microstructural information, we can garner more information about the dynamic pathophysiological processes using MRI. Lastly, MRI measures can be applied as outcomes for benchmarking clinical trials of hopeful DMTs in MS. However, we must consider if the

more traditional measures of new/expanding lesions and volume/atrophy changes are too coarse of a measure to capture positive outcome in treatment. Additionally, are the applied MRI outcomes too far downstream from the DMT intervention? Seemingly, the most direct linkage between MRI specificity and treatment outcome is that of therapies targeting remyelination. Whereby, the applied MRI sequence can directly visualize and measure the intended outcome, as opposed to indirectly gauging an effect of the intended mechanism of action for the DMT. Take for example a DMT that aims to limit lymphocyte influx into the brain, which is intimately connected with the formation of focal lesions, where a treatment effect on the accumulation of new T_2-lesions is a straightforward interpretation. In contrast, MRI atrophy metrics remain an indirect measure of the combined effect of several simultaneous and related disease processes, making results more difficult to interpret.

Clinical implementation of quantitative MRI

The implementation of quantitative MRI metrics of MS pathology into clinical practice has several obstacles to overcome. The confidence in the methodologies must also be well demonstrated before clinical application. Certainly, much of the aforementioned analyses are necessary when applying for CE marking and FDA approval. Not only are these validation considerations important for the MRI protocol but also any imaging analysis and processing methods. Here, we chose to use the SyMRI application of REMyDI for myelin quantification because the sequence and processing suite are already clinically approved, meaning we could apply them in a clinical setting alongside our standardized MS MRI protocol. Importantly, the implementation of other quantitative MRI analysis in the clinic can, partially, be facilitated by similar extensive validation. Inevitably, however, the process of obtaining regulatory approvals and clinically worthy implementation tools entails considerable financial backing. Thus, there is a fundamental financial nature to be considered in the process of clinical introduction that is often left unmentioned in scientific texts, as some of those values are perceived to be in contradiction with one another. Therefore, formal CE marking and FDA approval are typically the final hurdles left un-surpassed by these advanced MRI methods. Where they are instead left to be applied solely in a research setting.

Time is a key aspect not only in the diagnosis of MS patients but also in treatment monitoring and the interpretation of the MRI reads by the neuroradiologist. Therefore, one of the features that require essential development when considering the clinical application is the processing time and computational power necessary to produce the final image/volume and the complexity in reading/interpreting the output. A highly computationally intense processing method may likely be too demanding for clinics and may require substantial investment in an institution's computational processing network beforehand. Interpretation of multiple non-intuitive metrics may leave the reader hesitant for further inquiry. Additionally, the data needs to not only be produced and analyzed with a formally organized approach but needs an accompanying streamlined aesthetically presented user interface. This would be to lessen the interpretational burden for the clinicians and allow for better appreciation of the patients' current and former status. The programming necessary for this step involves substantial time investment.

One of the more interesting observations of MRI in MS is the degree of discrepancy between what has been developed and used in MS research compared to what is currently used in clinical practice. Certainly, the flexibility and acceptance of the clinical audience must be well-considered. There exists a natural and healthy skepticism about the incorporation of unproven methodologies in a formal clinical setting, especially when the methods are for-profit based and not made freely available. This is an equitable consideration. Medical practices and guidelines are purposefully regulated at higher levels. One cannot develop a technique and claim its validity without rigorous safety and efficacy assessments. The choices of the research community must be held to the highest of ethical standards and not do research the easy and fast way, but the correct way. Cherry-picking results and forcing through studies must be avoided in these critical analyses, because it is selfish to do so when the true benefactors are the patients. However, the rigidity of the clinical community cannot be left unaccountable in this discussion. Simply consider the long-reigning dogma of MS as a white matter disease despite decades-old histopathological evidence of the disease (Lumsden, 1970), followed by numerous examples of *in vivo* evidence at 3 T (Kidd *et al.*, 1999) and more resoundingly identified at 7 T near a decade prior (Mainero *et al.*, 2009). It took nearly two decades for the surmounting evidence to be considered and warrant inclusion into the MRI diagnostic criteria from juxtacortical to juxtacortical/cortical. It is unlikely that quantitative microstructural MRI methods would be incorporated into the McDonald criteria. Nonetheless, the kinship of supportive relations between the clinic and research communities needs to be further advanced to best suit the patients' needs. Through the collaborative driven effort between clinicians and researchers, those affected by MS will benefit.

6. CONCLUSIONS

The MRI quantification of MS pathology is a field that is continuously progressing, predicated on both the great clinical need and the opportunity for MRI to address these needs. The patients must come first. Our obligation, as a field, in applying MRI in MS is to i. reduce the time to diagnosis; ii. provide more sensitive treatment monitoring; iii. shed light on the pathological processes in MS and their evolution; and iv. facilitate the benchmarking and development of future therapeutic strategies in MS. Altogether, these goals aim to foremost benefit patients and spare them from this sometimes horrendously debilitating disease. The current standing of clinical MRI monitoring in MS must progress for the direct benefit of those with MS. Quantitative *in vivo* MRI biomarkers have begun demonstrating strong potential for a prominent future role in clinics. This is particularly evident in MS, where MRI is applied so prolifically and has already become so key to the diagnosis. However, there remain important aspects to address moving forward; in the development, validation and understanding of these tools and in the incorporation of these measures into clinical practice. With patients in mind, we stride forth and continue these efforts.

7. FUTURE ASPECTS

Further studies should aim to expand upon the findings of the present studies. This is most ideally done through standardized longitudinal MRI follow-up in order to monitor the evolving relationship between the clinical metrics in parallel to changes in the MRI metrics. This would be important when aiming to study the dynamic effects of demyelination versus remyelination over time in MS. Ideally, further development could also aim to involve more patients of the various MS subtypes to study the differences in underlying demyelinating pathology *in vivo* between the different clinical phenotypes, which would be especially interesting with regards to PPMS that remains a distinct clinical subtype. In conjunction with clinical values, 'myelin content profiles' based on patterns of demyelination as assessed by MRI could be studied longitudinally to assess if it can add predictive information in terms of identifying patients that are likely to convert from RIS or CIS to clinically definite MS, or from RRMS to SPMS. Developing a method specific reference myelin atlas based on age and sex could facilitate the detection of even more subtle demyelination in normal-appearing tissue on an individual level. The complexity of imaging the process of demyelination is a difficult one because, effectively, it is quantifying something that is absent. Thus, a myelin atlas would provide direct comparison to healthy individuals. Comparing myelin content across different anatomical structures would hold informative value, particularly in the spinal cord, cortex and subcortical grey matter regions where demyelination may be especially difficult to identify. Importantly, myelin loss does not occur only in MS, there are other disorders that entail a demyelinating pathological component, including neuromyelitis optica, acute disseminated encephalomyelitis, MOG-antibody disease, leukodystrophies and developmental disorders. Myelin imaging may also hold potential value for imaging diseases where demyelination may occur via indirect pathophysiology, such as for dementia disorders, movement disorders, stroke and malignancies.

Moving forward, an emphasis on the development and validation of quantitative MRI techniques demonstrating increased microstructural tissue sensitivity and specificity can allow for better interpretation and understanding of the MRI signal changes associated with pathophysiological changes. Acquisition of intact tissue samples of the brain and spinal cord to be scanned potentially, *in situ*, to be compared with histological measures would also be valuable. Ideally, there would be several tissue samples from donors diagnosed with various neurodegenerative disorders. Additionally, the chosen MRI measures should be comprehensible and acquired at multiple field strengths (1.5/3/7/9.4 T) and at both clinically comparable resolution and the maximally possible resolution to further bridge the gap between MRI and microscopy. Potential corresponding candidate histological analysis for discerning pathological biomarkers include: proteolipid immunohistochemistry for lipids; Luxol Fast Blue for lipids; Turnbull staining for iron distribution; Bielschowsky silver stain for axons; immunohistochemistry labeling of synapses by synaptophysin (SVP-38), haematoxylin and eosin; anti-CD20 immunohistochemistry for B cells; anti-CD4/CD8 immunohistochemistry for T cells; anti-aquaporin-4 immunohistochemistry as a glymphatic

system marker; and immunohistochemistry labeling of hyperphosphorylated tau, β-amyloid and α-synuclein for disease specific markers.

Additionally, the concurrent multi-modal application of advanced quantitative MRI imaging alongside additional imaging modalities in conjunction with clinical, imaging, immunologic, or pathologic metrics can expand the definition of disease activity. Myelin imaging techniques (MacKay and Laule, 2016, Ouellette *et al.*, 2020*a*), high field diffusion-weighted imaging (De Santis *et al.*, 2019; Yu *et al.*, 2019) and magnetization transfer (Filippi *et al.*, 1998; Kearney *et al.*, 2014; Liu *et al.*, 2015; Brown *et al.*, 2017, 2019) have shown promise to assess the microstructural dynamics of tissue damage in MS. Molecular imaging of activated microglia/macrophages by ^{11}C-PBR28 in conjunction with 7 T MRI captured increased immune activity in the cortex and white matter of MS patients (Herranz *et al.*, 2016). Comparative analysis of the various tissue specificities demonstrated by different advanced quantitative MRI methodologies may also provide better insight for clinical implementation and help to weigh the numerous options. While there have been some very well-done meta-analyses in the field of myelin imaging (Piredda *et al.*, 2021), the techniques are rapidly evolving and more are being developed. Instead, more direct comparative evidence can be gathered from the acquisition of numerous myelin imaging techniques on several different whole-sample brain tissue sections. Naturally, this approach should be done in conjunction with other advanced quantitative imaging methodologies, ideal candidates would include: advanced diffusion-weighted imaging techniques (NODDI and CHARMED) and quantitative T_2* imaging. Moreover, the *ex vivo* histopathological analyses should not be limited to querying the pathological dynamics in MS, but also other diseases including Alzheimer's disease (AD), amyotrophic lateral sclerosis (ALS), Parkinsonian syndromes, and also more novel diseases such as the neurological manifestations of COVID-19 (Klironomos *et al.*, 2020).

Bringing together multiple fields is truly key in the understanding MS. There is a great opportunity in combining lifestyle, environmental and genetic factors in MS registry-based studies. Combining neuroimaging biomarkers with CSF/blood-borne biomarkers can link the observed neuroimaging and molecular medicine definitions of disease activity to better characterize the pathophysiological processes driving the chronic inflammation found in MS. Neurofilament light chain has shown sensitivity to neurodegeneration and has been found to discern treatment effects in MS (Delcoigne *et al.*, 2020), but remains unspecific to MS (Lassmann, 2019). Myelin basic protein found in the CSF is also very interesting to compare with measures of myelin imaging, particularly in monitoring those with disease progression and an increase of myelin basic protein without lesion formation, potentially indicating diffuse demyelination as the culprit. CSF-borne markers of axonal (Neurofilament light chain) and synaptic integrity (Bsn, bassoon, presynaptic cytomatrix protein) would be ideal candidates for comparison with advanced diffusion metrics (NODDI and CHARMED). On a final note, MRI has proved to be of immense importance for elucidating pathogenetic mechanisms and drug development in MS in the past. With this thesis, my aim has been to demonstrate how MRI can play a similar role also in the future, in turn translating into better care of our patients and improving their long-term outcomes.

8. ACKNOWLEDGEMENTS

I wish to thank everyone who contributed to the works found in this thesis. In particular, I would like to distinguish:

To my main supervisor, Dr. **Tobias Granberg**, thank you for everything. You saw potential in me and have since continuously and sincerely fostered my advancement with great patience. From our first mirrored image meeting to choosing to be roommates the following day. Through the late night Neuromancer google sheet whiteboard nights fueled by Five Guys and the early mornings stuck on the Tobin. Thank you for trusting me to be your first Ph.D. student. For bringing out the best in me and always leading by example with an incomparable work ethic and quality. Thank you for your friendship and thank you for introducing Asia, Adeline and I to Swedish culture and traditions. Thank you for your dedication, responding to emails at 2:00 the morning, always being there, and even letting me stay with you and Alexandra when I first arrived in Sweden when Felix was only a week old. Thank you for your guidance in my writing and for dampening my Donald-isms. Always helping me accel, you have helped me see the forest through the trees, how to observe the future goals of our efforts and the dedication needed. Thank you for being my supervisor, mentor and friend.

To professor **Fredrik Piehl**, my supervisor, for your guidance in manuscript crafting. Your expertise in MS pathology has certainly facilitated my understanding and has been woven into my works. My understanding of disease-modulatory therapies in MS is a result of your written works, lectures and conversations with me. Thank you, for your guidance in supporting my lecturing in courses and the opportunity to advance my understanding of MS.

To professor **Caterina Mainero**, my supervisor and first primary investigator, for providing me with the opportunity to enter this field and facilitating my understanding of practices at the forefront of MS research. You believed in me and encouraged the initiation of my own study. Your guidance allowed me to be comprehensively involved from beginning to end. Your insight of topics on the forefront of MS research has shaped not only this thesis but the field. Thank you for nurturing my early development by opening the door to MRI research in MS.

To professor **Maria Kristoffersen-Wiberg**, my supervisor, for your steadfast support. You have always made the time for commentary and expertise throughout the doctoral process and manuscript refinement. You have always taken the time for and been present at each of my doctoral events despite your numerous clinical and academic duties.

To Dr. **Michael Plattén**, my fellow PhD student and co-author, for your friendship, expertise and comradery. You are wholly involved across my studies and our collaborations. You are always the first to provide commentary and edits, which is even more remarkable as you've already provided so much input during each Sunday and week-night scanning session. You have always been very willing to contribute and gracious with your time, despite simultaneously working clinically. Your above and beyond assistance and hard work is greatly appreciated. Your future is very bright, and I am eagerly looking forward to seeing it unfold.

To Dr. **Gabriel Mangeat,** my co-author and climbing coach, for your trainings and teachings as I initially replaced your role in Boston. Then continuously working closely throughout our collaborations on both of our PhD projects. Your expertise has truly been invaluable. Your crafting of visual elements has greatly inspired my own. You are one of the most talented individuals I know, and I am thankful for your instruction. Last but not least, thank you for teaching me to follow my feet on the wall.

To my Martinos Center colleagues, Dr. **Elena Herranz**, Dr. **Andrada Treaba**, Dr**. Celine Louapre**, Dr. **Valeria Barletta**, Dr. **Sindhuja T. Govindarajan** and **Ambica Mehndiratta**. who patiently taught me the foundational principles of MRI research in MS. This was my first job, where I matured (somewhat) during my time with you all and there are too many positive experiences to list. Thank you all for so much.

To my fellow Ph.D. students Dr. **Yngve Forslin** and Dr. **Henrik Sjöström**, who have now completed their studies and, by doing so, continued to raise the bar in contributions to the field. Your advice throughout the doctoral process has been very consequential to my studies.

To professor **Sten Fredrikson**, for your guidance in the neuropsychological aspects of MS, the history of MS and the evolution of the pathogenic theories.

To my clinical research colleague, **Roya Shams**, who has raised the standard of organization within our research group, brought expertise in the subtle nuisances of MRI scanning while simultaneously helping me practicing Swedish and smiling through all the pictures of Adeline.

My fellow group members Dr. **Åsa Bergendal,** Dr. **Sara Shams**, Dr. **Mana Shams**, Dr. **Carmen Cananau**, and Dr. **Farouk Hashim**, for your ever ready and willing presence in providing commentary and support throughout my studies and presentations.

I would also like to acknowledge my co-authors and collaborators for their invaluable contributions, support and mentoring throughout my journey thus far:

Our MS genetic epidemiology collaborators here at Karolinska Institutet Dr. **Ingrid Kockum**, Dr. **Alexandra Gyllenberg**, Dr. **Ali Manouchehrinia**, and Dr. **Thomas Moridi**, our ongoing ambitious collaborations have compelling potential and exemplify the power of collaborative vision. Thank you for the opportunity to be involved.

Our collaborators at Brigham and Women's Hospital led by Dr. **Rohit Bakshi**, with Dr. **Shahamat Tauhid**, Dr. **Fawad Yousuf,** for your guidance in collaborative projects and partnership on the editorial board of the Journal of Neuroimaging.

Our preclinical and clinical collaborators in research combating COVID-19 Dr. **Johan Lundberg** and Dr. **Jonathan Al-Saadi** for your sincere exemplary dedication to your craft during such an important and historical time. The last several months have been both dizzying and inspiring. Especially your guidance in working with preclinical animal models, the opportunity to expand my understanding of thorax MRI, the red room power sessions, and the middle of the night MAX burger runs.

Our clinical collaborators in research combating COVID-19 Dr**. Benjamin V. Ineichen**, Dr. **Stefanos Kli**r**onomos**, Dr**. Antonios Tzortzakakis**, and Dr. **Jesper Almqvist**. Your efforts in rapidly producing high-quality works while also working clinically have been beyond remarkable and inspiring during this important time.

Our clinical collaborators Dr. **Björn Evertsson** and Dr. **Alexander Juto** for your influential and eager study proposals probing the treatment dynamics of MS pathology.

MRI nurses **Soroush Sohrabian**, **Mansour Haghgou**, **Mikael Hasselberg, Maria Andersson, Kerstin Eriksson,** and **Karin Telin,** for all of your dedication in scanning patients and being available for questions. Thank you for your expertise in advising MRI protocols and troubleshooting everything from radio malfunctions to scanner restarts.

Our collaborators at NeuroPoly led by Dr. **Julien Cohen Adad** with Dr. **Atef Badji**, Dr. **Benjamin De Leener,** Dr. **Charley Gros**, Dr. **Sara Dupont** for your remarkable support in using SCT, our ongoing exciting collaborations and the opportunity to speak about our studies.

Our collaborators at Synthetic MRI led by Dr. **Marcel Warntjes,** for your swift support in working SyMRI and contributions to the study projects. Your continued development of the SyMRI platform is inspiring and provided the foundation of this work.

Our collaborators in clinical geriatrics Dr. **Eric Westman** and Dr**. Daniel Ferreira** for your collaborative support and your leading contributions in organizing imaging cognitive impairment network and imaging seminar series.

Our collaborators at the Swedish NEURO Registries, Dr. **Jan Hillert** and Dr. **Leszek Stawiarz**, your dedicated efforts in producing the MS registry are truly remarkable and a leading collaborative example in the world of MS registry-based research.

Our collaborators in histopathology at Invicro, Dr. **Howard Dobson** and Dr. **Ildiko Polyak** for your imagination and expertise exemplified by your efforts in supporting our goal of whole-tissue histopathological analysis. This translational collaboration was one of the most unique learning experiences of my studies.

Importantly, I would like to take this opportunity to thank my half-time committee of Dr. **Anne-Marie Landtblom**, Dr. **Magnus Kaijser**, and Dr. **Anna Falk Delgado**, for your time, and considerations given at my halftime review. They have since allowed me to remain on course and have influenced my studies and efforts in the present work.

Importantly, I would like to take this opportunity to thank study **participants, donors, and** their family members, for their time and effort, without which this research would not be possible. It is for them that our efforts continue. This research was made possible by the funds of the **MultipleMS EU Horizon 2020** grant, **COMBAT-MS** Patient-Centered Outcomes Research Institute grant, the **Swedish Society for Medical Research**, the **Christer Lindgren and Eva Fredholm Foundation**, **Karolinska Institutet** and **Stockholms Läns Landsting** through an ALF grant.

In particular, I would like to honor those who have profoundly affected my life at large:

My parents **Russ** and **Susan Ouellette**. Mom, you sat with me during long nights at the kitchen table and worked with me over summers to foster my curiosity. You met with my teachers pleading with them not to give up on me. Your bookshelves are filled with books about the successful parenting of overactive children. You pushed me to stake the advanced biology course I was interested in but was out of my recommended track. You are and always will be the most wonderful Mom, DMIL Grandma and are so very missed each and every day. Dad, through example and dedication you have provided me with my work ethic, taking pride in what I do and how I do it. Your personal sacrifices have provided me with each of the opportunities at hand. While only in month 5 of becoming a father myself, my appreciation for your selflessness over the decades as a Dad, DFIL and now Grandpa, grows each day.

My wife **Asia Ouellette,** you are an amazing life partner, best friend and mother. You have simultaneously proofed my manuscripts, been an amazing mom and incredibly supportive throughout everything. You moved here to Stockholm, we've gotten married and grown our family in five short years. Our journey has been an amazing one, and it is the direct result of you and your adventurous spirit, dragging me out of my hermit's solitude. You've kept our family upright. We've been on many adventures, but our best is yet to come.

Our daughter **Adeline Claire Ouellette**, you are amazing. You are so strong and so smart. Watching you grow and learn so fast, soon you will, no doubt, be teaching your parents a great deal. Your mother and I are so thankful and proud of all that you are. You are the inspiration that so many cherish. We love you. Forever and always little Buglet.

9. REFERENCES

Absinta M, Sati P, Gaitán MI, Maggi P, Cortese ICM, Filippi M, et al. Seven-tesla phase imaging of acute multiple sclerosis lesions: A new window into the inflammatory process. Ann Neurol 2013; 74: 669–78.

Adams CWM, Abdulla YH, Torres EM, Poston RN. Periventricular lesions in multiple sclerosis: Their perivenous origin and relationship to granular ependymitis. Neuropathol Appl Neurobiol 1987; 13: 141–52.

Ahlgren C, Odén A, Lycke J. High nationwide incidence of multiple sclerosis in Sweden. PLoS One 2014; 9: e108599.

Akaishi T, Takahashi T, Fujihara K, Misu T, Mugikura S, Abe M, et al. Number of MRI T1-hypointensity corrected by T2/FLAIR lesion volume indicates clinical severity in patients with multiple sclerosis. PloS One 2020; 15: e0231225.

Almqvist J, Granberg T, Tzortzakakis A, Klironomos S, Kollia E, Öhberg C, et al. Neurological manifestations of coronavirus infections - a systematic review. Ann Clin Transl Neurol 2020; 7: 2057–71.

Ambarki K, Lindqvist T, Wåhlin A, Petterson E, Warntjes MJB, Birgander R, et al. Evaluation of Automatic Measurement of the Intracranial Volume Based on Quantitative MR Imaging. Am J Neuroradiol 2012; 33: 1951–6.

Arshad M, Stanley JA, Raz N. Test-retest reliability and concurrent validity of in vivo myelin content indices: Myelin water fraction and calibrated T_1 w/T_2 w image ratio: Test-Retest Reliability and Concurrent Validity of in Vivo Myelin Content Indices. Hum Brain Mapp 2017; 38: 1780–90.

Ascherio A, Munger KL, Lennette ET, Spiegelman D, Hernán MA, Olek MJ, et al. Epstein-Barr Virus Antibodies and Risk of Multiple Sclerosis: A Prospective Study. JAMA 2001; 286: 3083.

Ashburner J, Friston KJ. Unified segmentation. NeuroImage 2005; 26: 839–51.

Assaf Y, Basser PJ. Composite hindered and restricted model of diffusion (CHARMED) MR imaging of the human brain. NeuroImage 2005; 27: 48–58.

Bakshi R, Thompson AJ, Rocca MA, Pelletier D, Dousset V, Barkhof F, et al. MRI in multiple sclerosis: current status and future prospects. Lancet Neurol 2008; 7: 615–25.

Balestroni G, Bertolotti G. [EuroQol-5D (EQ-5D): an instrument for measuring quality of life]. Monaldi Arch Chest Dis Arch Monaldi Mal Torace 2012; 78: 155–9.

Barkhof F. The clinico-radiological paradox in multiple sclerosis revisited. Curr Opin Neurol 2002; 15: 239–45.

Barragán-Martínez C, Speck-Hernández CA, Montoya-Ortiz G, Mantilla RD, Anaya J-M, Rojas-Villarraga A. Organic Solvents as Risk Factor for Autoimmune Diseases: A Systematic Review and Meta-Analysis. PLOS ONE 2012; 7: e51506.

Barry RL, Vannesjo SJ, By S, Gore JC, Smith SA. Spinal cord MRI at 7T. NeuroImage 2018; 168: 437–51.

Benjamini Y, Hochberg Y. Controlling the False Discovery Rate: A Practical and Powerful Approach to Multiple Testing. J R Stat Soc Ser B Methodol 1995; 57: 289–300.

Berg J, Lindgren P, Fredrikson S, Kobelt G. Costs and quality of life of multiple sclerosis in Sweden. Eur J Health Econ 2006; 7: 75–85.

Birkl C, Langkammer C, Golob-Schwarzl N, Leoni M, Haybaeck J, Goessler W, et al. Effects of formalin fixation and temperature on MR relaxation times in the human brain: Formalin fixation MR relaxation mechanisms. NMR Biomed 2016; 29: 458–65.

Bodini B, Veronese M, García-Lorenzo D, Battaglini M, Poirion E, Chardain A, et al. Dynamic Imaging of Individual Remyelination Profiles in Multiple Sclerosis. Ann Neurol 2016; 79: 726–38.

Brown JWL, Chowdhury A, Kanber B, Prados Carrasco F, Eshaghi A, Sudre CH, et al. Magnetisation transfer ratio abnormalities in primary and secondary progressive multiple sclerosis. Mult Scler 2020; 26: 679–87.

Brown JWL, Pardini M, Brownlee WJ, Fernando K, Samson RS, Prados Carrasco F, et al. An abnormal periventricular magnetization transfer ratio gradient occurs early in multiple sclerosis. Brain J Neurol 2017; 140: 387–98.

Brownlee WJ, Hardy TA, Fazekas F, Miller DH. Diagnosis of multiple sclerosis: progress and challenges. The Lancet 2017; 389: 1336–46.

Brück W, Gold R, Lund BT, Oreja-Guevara C, Prat A, Spencer CM, et al. Therapeutic Decisions in Multiple Sclerosis: Moving Beyond Efficacy. JAMA Neurol 2013; 70: 1315–24.

Burks JS, DeVald BL, Jankovsky LD, Gerdes JC. Two coronaviruses isolated from central nervous system tissue of two multiple sclerosis patients. Science 1980; 209: 933–4.

Calabrese M, Reynolds R, Magliozzi R, Castellaro M, Morra A, Scalfari A, et al. Regional Distribution and Evolution of Gray Matter Damage in Different Populations of Multiple Sclerosis Patients. PLoS One 2015; 10: e0135428.

Challoner PB, Smith KT, Parker JD, MacLeod DL, Coulter SN, Rose TM, et al. Plaque-associated expression of human herpesvirus 6 in multiple sclerosis. Proc Natl Acad Sci 1995; 92: 7440–4.

Cifelli A, Arridge M, Jezzard P, Esiri MM, Palace J, Matthews PM. Thalamic neurodegeneration in multiple sclerosis. Ann Neurol 2002; 52: 650–3.

Cohen-Adad J, Polimeni JR, Helmer KG, Benner T, McNab JA, Wald LL, et al. T2* mapping and B0 orientation-dependence at 7T reveal cyto- and myeloarchitecture organization of the human cortex. NeuroImage 2012; 60: 1006–14.

Compston A, Coles A. Multiple sclerosis. The Lancet 2008; 372: 1502–17.

Connor JR, Menzies SL. Relationship of iron to oligondendrocytes and myelination. Glia 1996; 17: 83–93.

Cristallo A, Gambaro F, Biamonti G, Ferrante P, Battaglia M, Cereda PM. Human coronavirus polyadenylated RNA sequences in cerebrospinal fluid from multiple sclerosis patients. New Microbiol 1997; 20: 105–14.

Dal-Bianco A, Grabner G, Kronnerwetter C, Weber M, Höftberger R, Berger T, et al. Slow expansion of multiple sclerosis iron rim lesions: pathology and 7 T magnetic resonance imaging. Acta Neuropathol (Berl) 2017; 133: 25–42.

Dawson J. The histology of disseminated sclerosis. The Lancet 1916; 187: 1090–1.

De Leener B, Fonov VS, Collins DL, Callot V, Stikov N, Cohen-Adad J. PAM50: Unbiased multimodal template of the brainstem and spinal cord aligned with the ICBM152 space. NeuroImage 2018; 165: 170–9.

De Leener B, Kadoury S, Cohen-Adad J. Robust, accurate and fast automatic segmentation of the spinal cord. NeuroImage 2014; 98: 528–36.

De Leener B, Lévy S, Dupont SM, Fonov VS, Stikov N, Louis Collins D, et al. SCT: Spinal Cord Toolbox, an open-source software for processing spinal cord MRI data. NeuroImage 2017; 145: 24–43.

De Santis S, Granberg T, Ouellette R, Treaba CA, Herranz E, Fan Q, et al. Evidence of early microstructural white matter abnormalities in multiple sclerosis from multi-shell diffusion MRI. NeuroImage Clin 2019; 22: 101699.

Delcoigne B, Manouchehrinia A, Barro C, Benkert P, Michalak Z, Kappos L, et al. Blood neurofilament light levels segregate treatment effects in multiple sclerosis. Neurology 2020

Deoni SCL, Rutt BK, Arun T, Pierpaoli C, Jones DK. Gleaning multicomponent T_1 and T_2 information from steady-state imaging data. Magn Reson Med 2008; 60: 1372–87.

Deppe M, Krämer J, Tenberge J-G, Marinell J, Schwindt W, Deppe K, et al. Early silent microstructural degeneration and atrophy of the thalamocortical network in multiple sclerosis. Hum Brain Mapp 2016; 37: 1866–79.

Dupont SM, De Leener B, Taso M, Le Troter A, Nadeau S, Stikov N, et al. Fully-integrated framework for the segmentation and registration of the spinal cord white and gray matter. NeuroImage 2017; 150: 358–72.

Dutta R, Trapp BD. Mechanisms of neuronal dysfunction and degeneration in multiple sclerosis. Prog Neurobiol 2011; 93: 1–12.

Dwyer MG, Bergsland N, Ramasamy DP, Jakimovski D, Weinstock-Guttman B, Zivadinov R. Atrophied Brain Lesion Volume: A New Imaging Biomarker in Multiple Sclerosis. J Neuroimaging Off J Am Soc Neuroimaging 2018; 28: 490–5.

Esiri MM, Gay D. Immunological and neuropathological significance of the Virchow-Robin space. J Neurol Sci 1990; 100: 3–8.

Fedorov A, Beichel R, Kalpathy-Cramer J, Finet J, Fillion-Robin J-C, Pujol S, et al. 3D Slicer as an image computing platform for the Quantitative Imaging Network. Magn Reson Imaging 2012; 30: 1323–41.

Filippi M, Bar-Or A, Piehl F, Preziosa P, Solari A, Vukusic S, et al. Multiple sclerosis. Nat Rev Dis Primer 2018; 4: 1–27.

Filippi M, Brück W, Chard D, Fazekas F, Geurts JJG, Enzinger C, et al. Association between pathological and MRI findings in multiple sclerosis. Lancet Neurol 2019; 18: 198–210.

Filippi M, Rocca MA, Barkhof F, Brück W, Chen JT, Comi G, et al. Association between pathological and MRI findings in multiple sclerosis. Lancet Neurol 2012; 11: 349–60.

Filippi M, Rocca MA, Ciccarelli O, De Stefano N, Evangelou N, Kappos L, et al. MRI criteria for the diagnosis of multiple sclerosis: MAGNIMS consensus guidelines. Lancet Neurol 2016; 15: 292–303.

Filippi M, Rocca MA, Martino G, Horsfield MA, Comi G. Magnetization transfer changes in the normal appearing white matter precede the appearance of enhancing lesions in patients with multiple sclerosis. Ann Neurol 1998; 43: 809–14.

Fischl B. FreeSurfer. NeuroImage 2012; 62: 774–81.

Fisniku LK, Brex PA, Altmann DR, Miszkiel KA, Benton CE, Lanyon R, et al. Disability and T2 MRI lesions: a 20-year follow-up of patients with relapse onset of multiple sclerosis. Brain 2008; 131: 808–17.

Fog T. The topography of plaques in multiple sclerosis with special reference to cerebral plaques. Acta Neurol Scand Suppl 1965; 15: 1–161.

Forn C, Belloch V, Bustamante JC, Garbin G, Parcet-Ibars MA, Sanjuan A, et al. A symbol digit modalities test version suitable for functional MRI studies. Neurosci Lett 2009; 456: 11–4.

Frischer JM, Bramow S, Dal-Bianco A, Lucchinetti CF, Rauschka H, Schmidbauer M, et al. The relation between inflammation and neurodegeneration in multiple sclerosis brains. Brain 2009; 132: 1175–89.

Giovannoni G, Turner B, Gnanapavan S, Offiah C, Schmierer K, Marta M. Is it time to target no evident disease activity (NEDA) in multiple sclerosis? Mult Scler Relat Disord 2015; 4: 329–33.

Girard OM, Prevost VH, Varma G, Cozzone PJ, Alsop DC, Duhamel G. Magnetization transfer from inhomogeneously broadened lines (ihMT): Experimental optimization of saturation parameters for human brain imaging at 1.5 Tesla: Optimizing Saturation Parameters for ihMT Brain Imaging at 1.5T. Magn Reson Med 2015; 73: 2111–21.

Glasser MF, Van Essen DC. Mapping Human Cortical Areas In Vivo Based on Myelin Content as Revealed by T1- and T2-Weighted MRI. J Neurosci 2011; 31: 11597–616.

Gonçalves LI, Dos Passos GR, Conzatti LP, Burger JLP, Tomasi GH, Zandoná MÉ, et al. Correlation between the corpus callosum index and brain atrophy, lesion load, and cognitive dysfunction in multiple sclerosis. Mult Scler Relat Disord 2018; 20: 154–8.

Goodin DS, Reder AT, Ebers GC, Cutter G, Kremenchutzky M, Oger J, et al. A randomized cohort study 21 years after the start of the pivotal IFNβ-1b trial. 2012: 8.

Granberg T, Bergendal G, Shams S, Aspelin P, Kristoffersen-Wiberg M, Fredrikson S, et al. MRI-Defined Corpus Callosal Atrophy in Multiple Sclerosis: A Comparison of Volumetric Measurements, Corpus Callosum Area and Index: Corpus Callosum Area, a Time-Effective Biomarker in MS. J Neuroimaging 2015; 25: 996–1001.

Granberg T, Fan Q, Treaba CA, Ouellette R, Herranz E, Mangeat G, et al. In vivo characterization of cortical and white matter neuroaxonal pathology in early multiple sclerosis. Brain 2017; 140: 2912–26.

Granberg T, Martola J, Kristoffersen-Wiberg M, Aspelin P, Fredrikson S. Radiologically isolated syndrome – incidental magnetic resonance imaging findings suggestive of multiple sclerosis, a systematic review. Mult Scler J 2013; 19: 271–80.

Granberg T, Moridi T, Brand JS, Neumann S, Hlavica M, Piehl F, et al. Enlarged perivascular spaces in multiple sclerosis on magnetic resonance imaging: a systematic review and meta-analysis. J Neurol 2020; 267: 3199–212.

Granberg T, Uppman M, Hashim F, Cananau C, Nordin LE, Shams S, et al. Clinical Feasibility of Synthetic MRI in Multiple Sclerosis: A Diagnostic and Volumetric Validation Study. Am J Neuroradiol 2016; 37: 1023–9.

Green AJ, Gelfand JM, Cree BA, Bevan C, Boscardin WJ, Mei F, et al. Clemastine fumarate as a remyelinating therapy for multiple sclerosis (ReBUILD): a randomised, controlled, double-blind, crossover trial. The Lancet 2017; 390: 2481–9.

Greve DN, Fischl B. Accurate and robust brain image alignment using boundary-based registration. NeuroImage 2009; 48: 63–72.

Gros C, De Leener B, Dupont SM, Martin AR, Fehlings MG, Bakshi R, et al. Automatic spinal cord localization, robust to MRI contrasts using global curve optimization. Med Image Anal 2018; 44: 215–27.

Haacke EM, Liu S, Buch S, Zheng W, Wu D, Ye Y. Quantitative susceptibility mapping: current status and future directions. Magn Reson Imaging 2015; 33: 1–25.

Hagemeier J, Heininen-Brown M, Gabelic T, Guttuso T, Silvestri N, Lichter D, et al. Phase White Matter Signal Abnormalities in Patients with Clinically Isolated Syndrome and Other Neurologic Disorders. Am J Neuroradiol 2014; 35: 1916–23.

Hagiwara A, Hori M, Yokoyama K, Takemura MY, Andica C, Kumamaru KK, et al. Utility of a Multiparametric Quantitative MRI Model That Assesses Myelin and Edema for Evaluating Plaques, Periplaque White Matter, and Normal-Appearing White Matter in Patients with Multiple Sclerosis: A Feasibility Study. Am J Neuroradiol 2017; 38: 237–42.

Hagiwara A, Warntjes M, Hori M, Andica C, Nakazawa M, Kumamaru KK, et al. SyMRI of the Brain: Rapid Quantification of Relaxation Rates and Proton Density, With Synthetic MRI, Automatic Brain Segmentation, and Myelin Measurement. Invest Radiol 2017; 52: 647–57.

Hauser SL, Bar-Or A, Comi G, Giovannoni G, Hartung H-P, Hemmer B, et al. Ocrelizumab versus Interferon Beta-1a in Relapsing Multiple Sclerosis. N Engl J Med 2017; 376: 221–34.

Hawellek DJ, Hipp JF, Lewis CM, Corbetta M, Engel AK. Increased functional connectivity indicates the severity of cognitive impairment in multiple sclerosis. Proc Natl Acad Sci 2011; 108: 19066–71.

Hedström AK, Åkerstedt T, Hillert J, Olsson T, Alfredsson L. Shift work at young age is associated with increased risk for multiple sclerosis. Ann Neurol 2011; 70: 733–41.

Hedström AK, Åkerstedt T, Olsson T, Alfredsson L. Shift work influences multiple sclerosis risk. Mult Scler 2015; 21: 1195–9.

Hedström AK, Bäärnhielm M, Olsson T, Alfredsson L. Exposure to environmental tobacco smoke is associated with increased risk for multiple sclerosis. Mult Scler Houndmills Basingstoke Engl 2011; 17: 788–93.

Hedström AK, Sundqvist E, Bäärnhielm M, Nordin N, Hillert J, Kockum I, et al. Smoking and two human leukocyte antigen genes interact to increase the risk for multiple sclerosis. Brain 2011; 134: 653–64.

Herranz E, Giannì C, Louapre C, Treaba CA, Govindarajan ST, Ouellette R, et al. Neuroinflammatory component of gray matter pathology in multiple sclerosis: Inflammation in GM in MS. Ann Neurol 2016; 80: 776–90.

Herranz E, Louapre C, Treaba CA, Govindarajan ST, Ouellette R, Mangeat G, et al. Profiles of cortical inflammation in multiple sclerosis by ^{11} C-PBR28 MR-PET and 7 Tesla imaging. Mult Scler J 2019: 135245851986732.

Hobart J, Lamping D, Fitzpatrick R, Riazi A, Thompson A. The Multiple Sclerosis Impact Scale (MSIS-29) A new patient-based outcome measure. Brain 2001; 124: 962–73.

Hovanec DL, Flanagan TD. Detection of antibodies to human coronaviruses 229E and OC43 in the sera of multiple sclerosis patients and normal subjects. Infect Immun 1983; 41: 426–9.

Howell OW, Reeves CA, Nicholas R, Carassiti D, Radotra B, Gentleman SM, et al. Meningeal inflammation is widespread and linked to cortical pathology in multiple sclerosis. Brain 2011; 134: 2755–71.

IMSGC. Multiple sclerosis genomic map implicates peripheral immune cells and microglia in susceptibility. Science 2019; 365: eaav7188.

Ineichen BV, Moridi T, Granberg T, Piehl F. Rituximab treatment for multiple sclerosis. Mult Scler J 2020; 26: 137–52.

Jenkinson M, Beckmann CF, Behrens TEJ, Woolrich MW, Smith SM. FSL. NeuroImage 2012; 62: 782–90.

Kappos L, Wolinsky JS, Giovannoni G, Arnold DL, Wang Q, Bernasconi C, et al. Contribution of Relapse-Independent Progression vs Relapse-Associated Worsening to Overall Confirmed Disability Accumulation in Typical Relapsing Multiple Sclerosis in a Pooled Analysis of 2 Randomized Clinical Trials. JAMA Neurology 2020; 77: 1.

Katsavos S, Coles A. Alemtuzumab as Treatment for Multiple Sclerosis. Cold Spring Harb Perspect Med 2018; 8.

Kearney H, Miller DH, Ciccarelli O. Spinal cord MRI in multiple sclerosis—diagnostic, prognostic and clinical value. Nat Rev Neurol 2015; 11: 327–38.

Kearney H, Yiannakas MC, Samson RS, Wheeler-Kingshott CAM, Ciccarelli O, Miller DH. Investigation of magnetization transfer ratio-derived pial and subpial abnormalities in the multiple sclerosis spinal cord. Brain 2014; 137: 2456–68.

Khodanovich MY, Sorokina IV, Glazacheva VY, Akulov AE, Nemirovich-Danchenko NM, Romashchenko AV, et al. Histological validation of fast macromolecular proton fraction mapping as a quantitative myelin imaging method in the cuprizone demyelination model. Sci Rep 2017; 7: 46686.

Kidd D, Barkhof F, McConnell R, Algra PR, Allen IV, Revesz T. Cortical lesions in multiple sclerosis. Brain 1999; 122: 17–26.

Kilsdonk ID, Lopez-Soriano A, Kuijer JPA, de Graaf WL, Castelijns JA, Polman CH, et al. Morphological features of MS lesions on FLAIR* at 7 T and their relation to patient characteristics. J Neurol 2014; 261: 1356–64.

Kister I, Bacon TE, Chamot E, Salter AR, Cutter GR, Kalina JT, et al. Natural History of Multiple Sclerosis Symptoms. Int J MS Care 2013; 15: 146–56.

Klaver R, Popescu V, Voorn P, Galis-de Graaf Y, van der Valk P, de Vries HE, et al. Neuronal and Axonal Loss in Normal-Appearing Gray Matter and Subpial Lesions in Multiple Sclerosis. J Neuropathol Exp Neurol 2015; 74: 453–8.

Klironomos S, Tzortzakakis A, Kits A, Öhberg C, Kollia E, Ahoromazdae A, et al. Nervous System Involvement in Coronavirus Disease 2019: Results from a Retrospective Consecutive Neuroimaging Cohort. Radiology 2020; 297: E324–34.

Koch-Henriksen N, Sørensen PS. The changing demographic pattern of multiple sclerosis epidemiology. Lancet Neurol 2010; 9: 520–32.

Kolind S, Matthews L, Johansen-Berg H, Leite MI, Williams SCR, Deoni S, et al. Myelin water imaging reflects clinical variability in multiple sclerosis. NeuroImage 2012; 60: 263–70.

Kolind S, Seddigh A, Combes A, Russell-Schulz B, Tam R, Yogendrakumar V, et al. Brain and cord myelin water imaging: a progressive multiple sclerosis biomarker. NeuroImage Clin 2015; 9: 574–80.

Kraff O, Fischer A, Nagel AM, Mönninghoff C, Ladd ME. MRI at 7 tesla and above: Demonstrated and potential capabilities. J Magn Reson Imaging 2015; 41: 13–33.

Kronlage M, Pitarokoili K, Schwarz D, Godel T, Heiland S, Yoon M-S, et al. Diffusion Tensor Imaging in Chronic Inflammatory Demyelinating Polyneuropathy: Diagnostic Accuracy and Correlation With Electrophysiology. Invest Radiol 2017; 52: 701–7.

Kurtzke JF. Rating neurologic impairment in multiple sclerosis: An expanded disability status scale (EDSS). Neurology 1983; 33: 1444.

Langdon D, Amato M, Boringa J, Brochet B, Foley F, Fredrikson S, et al. Recommendations for a Brief International Cognitive Assessment for Multiple Sclerosis (BICAMS). Mult Scler J 2012; 18: 891–8.

Langkammer C, Krebs N, Goessler W, Scheurer E, Ebner F, Yen K, et al. Quantitative MR Imaging of Brain Iron: A Postmortem Validation Study. Radiology 2010; 257: 455–62.

Lassmann H. Multiple Sclerosis Pathology. Cold Spring Harb Perspect Med 2018; 8.

Lassmann H. Pathogenic Mechanisms Associated With Different Clinical Courses of Multiple Sclerosis. Front Immunol 2018; 9: 3116.

Lassmann H, Bradl M. Multiple sclerosis: experimental models and reality. Acta Neuropathol (Berl) 2017; 133: 223–44.

Laule C, Moore GRW. Myelin water imaging to detect demyelination and remyelination and its validation in pathology. Brain Pathol 2018; 28: 750–64.

Levesque IR, Giacomini PS, Narayanan S, Ribeiro LT, Sled JG, Arnold DL, et al. Quantitative magnetization transfer and myelin water imaging of the evolution of acute multiple sclerosis lesions. Magn Reson Med 2010; 63: 633–40.

Lezak MD, Howieson DB, Bigler ED, Tranel D. Neuropsychological Assessment. Oxford, New York: Oxford University Press; 2012.

Li R, Bar-Or A. The Multiple Roles of B Cells in Multiple Sclerosis and Their Implications in Multiple Sclerosis Therapies. Cold Spring Harb Perspect Med 2019; 9: a029108.

Li W, Wu B, Liu C. Quantitative susceptibility mapping of human brain reflects spatial variation in tissue composition. NeuroImage 2011; 55: 1645–56.

Liu Z, Pardini M, Yaldizli Ö, Sethi V, Muhlert N, Wheeler-Kingshott CAM, et al. Magnetization transfer ratio measures in normal-appearing white matter show periventricular gradient abnormalities in multiple sclerosis. Brain 2015; 138: 1239–46.

Louapre C, Collongues N, Stankoff B, Giannesini C, Papeix C, Bensa C, et al. Clinical Characteristics and Outcomes in Patients With Coronavirus Disease 2019 and Multiple Sclerosis. JAMA Neurol 2020; 77: 1079–88.

Louapre C, Govindarajan ST, Giannì C, Madigan N, Sloane JA, Treaba CA, et al. Heterogeneous pathological processes account for thalamic degeneration in multiple sclerosis: Insights from 7 T imaging. Mult Scler J 2018; 24: 1433–44.

Lublin FD, Reingold SC, Cohen JA, Cutter GR, Sørensen PS, Thompson AJ, et al. Defining the clinical course of multiple sclerosis: the 2013 revisions. Neurology 2014; 83: 278–86.

Lucchinetti CF, Popescu BFG, Bunyan RF, Moll NM, Roemer SF, Lassmann H, et al. Inflammatory Cortical Demyelination in Early Multiple Sclerosis. N Engl J Med 2011; 365: 2188–97.

Lumsden CE. The pathology of multiple sclerosis. North-Holland, Amsterdam; 1970

Mackay A, Whittall K, Adler J, Li D, Paty D, Graeb D. In vivo visualization of myelin water in brain by magnetic resonance. Magn Reson Med 1994; 31: 673–7.

MacKay AL, Laule C. Magnetic Resonance of Myelin Water: An in vivo Marker for Myelin. Brain Plast 2016; 2: 71–91.

Magliozzi R, Howell OW, Reeves C, Roncaroli F, Nicholas R, Serafini B, et al. A Gradient of neuronal loss and meningeal inflammation in multiple sclerosis. Ann Neurol 2010; 68: 477–93.

MAGNIMS. MAGNIMS consensus guidelines on the use of MRI in multiple sclerosis—establishing disease prognosis and monitoring patients: Evidence-based guidelines. Nat Rev Neurol 2015; 11: 597–606.

MAGNIMS, Enzinger C, Barkhof F, Ciccarelli O, Filippi M, Kappos L, et al. Nonconventional MRI and microstructural cerebral changes in multiple sclerosis. Nat Rev Neurol 2015; 11: 676–86.

MAGNIMS, Rovira À, Wattjes MP, Tintoré M, Tur C, Yousry TA, et al. MAGNIMS consensus guidelines on the use of MRI in multiple sclerosis—clinical implementation in the diagnostic process: Evidence-based guidelines. Nat Rev Neurol 2015; 11: 471–82.

Mahad DH, Trapp BD, Lassmann H. Pathological mechanisms in progressive multiple sclerosis. Lancet Neurol 2015; 14: 183–93.

Mainero C, Benner T, Radding A, van der Kouwe A, Jensen R, Rosen BR, et al. In vivo imaging of cortical pathology in multiple sclerosis using ultra-high field MRI. Neurology 2009; 73: 941–8.

Mainero C, Louapre C, Govindarajan ST, Giannì C, Nielsen AS, Cohen-Adad J, et al. A gradient in cortical pathology in multiple sclerosis by in vivo quantitative 7 T imaging. Brain 2015; 138: 932–45.

Marburg O. Die sogenannte ‘akute multiple Sklerose’ (Encephalomyelitis periaxialis scleroticans). Jahrb Psychiatr Neurol 1906; 27: 211–312.

Marques F, Sousa JC, Coppola G, Geschwind DH, Sousa N, Palha JA, et al. The choroid plexus response to a repeated peripheral inflammatory stimulus. BMC Neurosci 2009; 10: 135.

Martirosian V, Julian A, Neman J. Chapter 7 - The Role of the Choroid Plexus in the Pathogenesis of Multiple Sclerosis. In: Neman J, Chen TC, editor(s). The Choroid Plexus and Cerebrospinal Fluid. San Diego: Academic Press; 2016. p. 103–27

McDonald WI, Compston A, Edan G, Goodkin D, Hartung H-P, Lublin FD, et al. Recommended diagnostic criteria for multiple sclerosis: Guidelines from the international panel on the diagnosis of multiple sclerosis. Ann Neurol 2001; 50: 121–7.

McRobbie DW, Moore EA, Graves MJ, Prince MR. MRI: From Picture to proton. Second. United States of America: Cambridge University Press, New York; 2006

Mei F, Fancy SPJ, Shen Y-AA, Niu J, Zhao C, Presley B, et al. Micropillar arrays as a high-throughput screening platform for therapeutics in multiple sclerosis. Nat Med 2014; 20: 954–60.

Mentis A-FA, Dardiotis E, Grigoriadis N, Petinaki E, Hadjigeorgiou GM. Viruses and Multiple Sclerosis: From Mechanisms and Pathways to Translational Research Opportunities. Mol Neurobiol 2017; 54: 3911–23.

Munger KL, Bentzen J, Laursen B, Stenager E, Koch-Henriksen N, Sørensen TIA, et al. Childhood body mass index and multiple sclerosis risk: a long-term cohort study. Mult Scler Houndmills Basingstoke Engl 2013; 19: 1323–9.

Naganawa S, Koshikawa T, Nakamura T, Kawai H, Fukatsu H, Ishigaki T, et al. Comparison of flow artifacts between 2D-FLAIR and 3D-FLAIR sequences at 3 T. Eur Radiol 2004; 14: 1901–8.

NAIMS, Sati P, Oh J, Constable RT, Evangelou N, Guttmann CRG, et al. The central vein sign and its clinical evaluation for the diagnosis of multiple sclerosis: a consensus statement from the North American Imaging in Multiple Sclerosis Cooperative. Nat Rev Neurol 2016; 12: 714–22.

Nakamura K, Chen JT, Ontaneda D, Fox RJ, Trapp BD. T1-/T2-weighted ratio differs in demyelinated cortex in multiple sclerosis: T1-/T2-Weighted Ratio in MS. Ann Neurol 2017; 82: 635–9.

O’Gorman C, Lucas R, Taylor B. Environmental risk factors for multiple sclerosis: a review with a focus on molecular mechanisms. Int J Mol Sci 2012; 13: 11718–52.

Oh J, Zackowski K, Chen M, Newsome S, Saidha S, Smith SA, et al. Multiparametric MRI correlates of sensorimotor function in the spinal cord in multiple sclerosis. Mult Scler J 2013; 19: 427–35.

Olsson T, Barcellos LF, Alfredsson L. Interactions between genetic, lifestyle and environmental risk factors for multiple sclerosis. Nat Rev Neurol 2017; 13: 25–36.

Oshio K, Feinberg DA. GRASE (Gradient-and Spin-Echo) imaging: A novel fast MRI technique. Magn Reson Med 1991; 20: 344–9.

Ouellette R, Bergendal Å, Shams S, Martola J, Mainero C, Kristoffersen Wiberg M, et al. Lesion accumulation is predictive of long-term cognitive decline in multiple sclerosis. Mult Scler Relat Disord 2018; 21: 110–6.

Ouellette R, Mangeat G, Polyak I, Warntjes M, Forslin Y, Bergendal Å, et al. Validation of rapid magnetic resonance myelin imaging in multiple sclerosis. Ann Neurol 2020

Ouellette R, Treaba CA, Granberg T, Herranz E, Barletta V, Mehndiratta A, et al. 7 T imaging reveals a gradient in spinal cord lesion distribution in multiple sclerosis. Brain J Neurol 2020

de Paula Faria D, Copray S, Sijbesma JWA, Willemsen ATM, Buchpiguel CA, Dierckx RAJO, et al. PET imaging of focal demyelination and remyelination in a rat model of multiple sclerosis: comparison of [11C]MeDAS, [11C]CIC and [11C]PIB. Eur J Nucl Med Mol Imaging 2014; 41: 995–1003.

Piehl F. Current and emerging disease modulatory therapies and treatment targets for multiple sclerosis. J Intern Med 2021

Piredda GF, Hilbert T, Thiran J-P, Kober T. Probing myelin content of the human brain with MRI: A review. Magn Reson Med 2021; 85: 627–52.

Polman CH, Reingold SC, Banwell B, Clanet M, Cohen JA, Filippi M, et al. Diagnostic criteria for multiple sclerosis: 2010 Revisions to the McDonald criteria. Ann Neurol 2011; 69: 292–302.

Polman CH, Reingold SC, Edan G, Filippi M, Hartung H-P, Kappos L, et al. Diagnostic criteria for multiple sclerosis: 2005 revisions to the "McDonald Criteria". Ann Neurol 2005; 58: 840–6.

Poser CM, Paty DW, Scheinberg L, McDonald WI, Davis FA, Ebers GC, et al. New diagnostic criteria for multiple sclerosis: Guidelines for research protocols. Ann Neurol 1983; 13: 227–31.

Prasloski T, Rauscher A, MacKay AL, Hodgson M, Vavasour IM, Laule C, et al. Rapid whole cerebrum myelin water imaging using a 3D GRASE sequence. NeuroImage 2012; 63: 533–9.

Prineas JW, Barnard RO, Kwon EE, Sharer LR, Cho E-S. Multiple sclerosis: Remyelination of nascent lesions: Remyelination of nascent lesions. Ann Neurol 1993; 33: 137–51.

Reich DS, Lucchinetti CF, Calabresi PA. Multiple Sclerosis. N Engl J Med 2018; 378: 169–80.

Reuter M, Schmansky NJ, Rosas HD, Fischl B. Within-subject template estimation for unbiased longitudinal image analysis. NeuroImage 2012; 61: 1402–18.

Righart R, Biberacher V, Jonkman LE, Klaver R, Schmidt P, Buck D, et al. Cortical pathology in multiple sclerosis detected by the T1/T2-weighted ratio from routine magnetic resonance imaging: Cortical Pathology in MS. Ann Neurol 2017; 82: 519–29.

Rocca MA, Comi G, Filippi M. The Role of T1-Weighted Derived Measures of Neurodegeneration for Assessing Disability Progression in Multiple Sclerosis. Front Neurol 2017; 8: 433.

Rovira À, Barkhof F. Multiple Sclerosis and Variants. In: Barkhof F, Jager R, Thurnher M, Rovira Cañellas A, editor(s). Clinical Neuroradiology. Cham: Springer International Publishing; 2018. p. 1–41

Sailer M, Fischl B, Salat D, Tempelmann C, Schönfeld MA, Busa E, et al. Focal thinning of the cerebral cortex in multiple sclerosis. Brain 2003; 126: 1734–44.

Schumacher GA, Beebe G, Kibler RF, Kurland LT, Kurtzke JF, Mcdowell F, et al. Problems of the experimental trials of therapy in multiple sclerosis: report by the panel on the evaluation of experimental trials of therapy in multiple sclerosis. Ann N Y Acad Sci 1965; 122: 552–68.

Shin M-S, Park S-Y, Park S-R, Seol S-H, Kwon JS. Clinical and empirical applications of the Rey–Osterrieth Complex Figure Test. Nat Protoc 2006; 1: 892.

Sigalovsky IS, Fischl B, Melcher JR. Mapping an intrinsic MR property of gray matter in auditory cortex of living humans: A possible marker for primary cortex and hemispheric differences. NeuroImage 2006; 32: 1524–37.

Simon JH, Li D, Traboulsee A, Coyle PK, Arnold DL, Barkhof F, et al. Standardized MR Imaging Protocol for Multiple Sclerosis: Consortium of MS Centers Consensus Guidelines. Am J Neuroradiol 2006; 27: 455–61.

Simpson S, Blizzard L, Otahal P, Mei IV der, Taylor B. Latitude is significantly associated with the prevalence of multiple sclerosis: a meta-analysis. J Neurol Neurosurg Psychiatry 2011; 82: 1132–41.

Sormani MP, De Rossi N, Schiavetti I, Carmisciano L, Cordioli C, Moiola L, et al. Disease Modifying Therapies and COVID-19 Severity in Multiple Sclerosis [Internet]. Rochester, NY: Social Science Research Network; 2020 [cited 2020 Dec 9] Available from: https://papers.ssrn.com/abstract=3631244

Stankoff B, Freeman L, Aigrot M-S, Chardain A, Dollé F, Williams A, et al. Imaging central nervous system myelin by positron emission tomography in multiple sclerosis using [methyl-11C]-2-(4′-methylaminophenyl)- 6-hydroxybenzothiazole. Ann Neurol 2011; 69: 673–80.

Stewart JN, Mounir S, Talbot PJ. Human coronavirus gene expression in the brains of multiple sclerosis patients. Virology 1992; 191: 502–5.

Thompson AJ, Banwell BL, Barkhof F, Carroll WM, Coetzee T, Comi G, et al. Diagnosis of multiple sclerosis: 2017 revisions of the McDonald criteria. Lancet Neurol 2018; 17: 162–73.

Toschi N, De Santis S, Granberg T, Ouellette R, Treaba CA, Herranz E, et al. Evidence for Progressive Microstructural Damage in Early Multiple Sclerosis by Multi-Shell Diffusion Magnetic Resonance Imaging. Neuroscience 2019; 403: 27–34.

Treaba CA, Granberg TE, Sormani MP, Herranz E, Ouellette RA, Louapre C, et al. Longitudinal Characterization of Cortical Lesion Development and Evolution in Multiple Sclerosis with 7.0-T MRI. Radiology 2019; 291: 740–9.

Tu T-W, Williams RA, Lescher JD, Jikaria N, Turtzo LC, Frank JA. Radiological–pathological correlation of diffusion tensor and magnetization transfer imaging in a closed head traumatic brain injury model. Ann Neurol 2016; 79: 907–20.

Tustison NJ, Cook PA, Klein A, Song G, Das SR, Duda JT, et al. Large-scale evaluation of ANTs and FreeSurfer cortical thickness measurements. NeuroImage 2014; 99: 166–79.

Vågberg M, Axelsson M, Birgander R, Burman J, Cananau C, Forslin Y, et al. Guidelines for the use of magnetic resonance imaging in diagnosing and monitoring the treatment of multiple sclerosis: recommendations of the Swedish Multiple Sclerosis Association and the Swedish Neuroradiological Society. Acta Neurol Scand 2017; 135: 17–24.

Van Obberghen E, Mchinda S, le Troter A, Prevost VH, Viout P, Guye M, et al. Evaluation of the Sensitivity of Inhomogeneous Magnetization Transfer (ihMT) MRI for Multiple Sclerosis. Am J Neuroradiol 2018; 39: 634–41.

Vavasour IM, Laule C, Li DKB, Traboulsee AL, MacKay AL. Is the magnetization transfer ratio a marker for myelin in multiple sclerosis? J Magn Reson Imaging 2011; 33: 710–8.

Vercellino M, Votta B, Condello C, Piacentino C, Romagnolo A, Merola A, et al. Involvement of the choroid plexus in multiple sclerosis autoimmune inflammation: A neuropathological study. J Neuroimmunol 2008; 199: 133–41.

van der Walt S, Schönberger JL, Nunez-Iglesias J, Boulogne F, Warner JD, Yager N, et al. scikit-image: image processing in Python. PeerJ 2014; 2: e453.

Wang F, Dong Z, Tian Q, Liao C, Fan Q, Hoge WS, et al. In vivo human whole-brain Connectom diffusion MRI dataset at 760 μm isotropic resolution [Internet]. Neuroscience; 2020 [cited 2020 Dec 4] Available from: http://biorxiv.org/lookup/doi/10.1101/2020.10.05.327395

Wang Y, Liu T. Quantitative susceptibility mapping (QSM): Decoding MRI data for a tissue magnetic biomarker. Magn Reson Med 2015; 73: 82–101.

Warntjes JBM, Leinhard OD, West J, Lundberg P. Rapid magnetic resonance quantification on the brain: Optimization for clinical usage. Magn Reson Med 2008; 60: 320–9.

Warntjes JBM, Persson A, Berge J, Zech W. Myelin Detection Using Rapid Quantitative MR Imaging Correlated to Macroscopically Registered Luxol Fast Blue–Stained Brain Specimens. Am J Neuroradiol 2017; 38: 1096–102.

Warntjes M, Engström M, Tisell A, Lundberg P. Modeling the Presence of Myelin and Edema in the Brain Based on Multi-Parametric Quantitative MRI. Front Neurol 2016; 7: 16.

van der Weijden CWJ, García DV, Borra RJH, Thurner P, Meilof JF, van Laar P-J, et al. Myelin quantification with MRI: A systematic review of accuracy and reproducibility. NeuroImage 2020: 117561.

Westerlind H, Ramanujam R, Uvehag D, Kuja-Halkola R, Boman M, Bottai M, et al. Modest familial risks for multiple sclerosis: a registry-based study of the population of Sweden. Brain J Neurol 2014; 137: 770–8.

Winklewski PJ, Sabisz A, Naumczyk P, Jodzio K, Szurowska E, Szarmach A. Understanding the Physiopathology Behind Axial and Radial Diffusivity Changes-What Do We Know? Front Neurol 2018; 9: 92.

Yarnykh VL. Fast macromolecular proton fraction mapping from a single off-resonance magnetization transfer measurement. Magn Reson Med 2012; 68: 166–78.

Yarnykh VL, Bowen JD, Samsonov A, Repovic P, Mayadev A, Qian P, et al. Fast Whole-Brain Three-dimensional Macromolecular Proton Fraction Mapping in Multiple Sclerosis. Radiology 2015; 274: 210–20.

Yu F, Fan Q, Tian Q, Ngamsombat C, Machado N, Bireley JD, et al. Imaging G-Ratio in Multiple Sclerosis Using High-Gradient Diffusion MRI and Macromolecular Tissue Volume. Am J Neuroradiol 2019; 40: 1871–7.

Yushkevich PA, Piven J, Hazlett HC, Smith RG, Ho S, Gee JC, et al. User-guided 3D active contour segmentation of anatomical structures: Significantly improved efficiency and reliability. NeuroImage 2006; 31: 1116–28.

Zhang H, Schneider T, Wheeler-Kingshott CA, Alexander DC. NODDI: Practical in vivo neurite orientation dispersion and density imaging of the human brain. NeuroImage 2012; 61: 1000–16.

Zhao W, Cohen-Adad J, Polimeni JR, Keil B, Guerin B, Setsompop K, et al. Nineteen-channel receive array and four-channel transmit array coil for cervical spinal cord imaging at 7T: RF Coil for Spinal Cord MRI at 7T. Magn Reson Med 2014; 72: spcone-spcone.

Zurawski J, Lassmann H, Bakshi R. Use of Magnetic Resonance Imaging to Visualize Leptomeningeal Inflammation in Patients With Multiple Sclerosis: A Review. JAMA Neurol 2017; 74: 100–9.